Tubulin-binding dibenz[*c*,*e*]oxepines: Part 2.[1] Structural variation and biological evaluation as tumour vasculature disrupting agents

Steven B. Rossington, John A. Hadfield, Steven D. Shnyder, Timothy W. Wallace and Kaye J. Williams

5,7-Dihydro-3,9,10,11-tetramethoxybenz[*c*,*e*]oxepin-4-ol **1**, prepared from a dibenzyl ether precursor *via* Pd-catalysed intramolecular direct arylation, possesses broad-spectrum *in vitro* cytotoxicity towards various tumour cell lines, and induces vascular shutdown, necrosis and growth delay in tumour xenografts in mice at sub-toxic doses. The biological properties of **1** and related compounds can be attributed to their ability to inhibit microtubule assembly at the micromolar level, by binding reversibly to the same site of the tubulin αβ-heterodimer as colchicine **2** and the allocolchinol, *N*-acetylcolchinol **4**.

Keywords: Dibenz[*c*,*e*]oxepine; Iintramolecular direct arylation; Tubulin targeting; Tumour growth inhibition; Vascular shutdown; Colchicinoid

1. Introduction

As the conduit for oxygen, nutrients and waste products, the vascular system that supports a tumour is a rational target for anticancer therapy. Two strategies have emerged for the clinical exploitation of this principle,[2] the first being the use of angiogenesis inhibitors, which target growth factors so as to prevent the formation of new vasculature.[3] The pioneering example of this approach is the monoclonal antibody bevacizumab (Avastin).[4] The second strategy is to employ vascular disrupting agents (VDAs) to attack newly-formed tumour vasculature, which is structurally flawed by excessive branching, uneven diameter, shunts, *etc*., and more sensitive than normal host vasculature to small molecules that perturb the morphology and functionality (migration, adhesion, proliferation) of the nascent endothelial cells.[5] Microtubules play a prominent role in maintaining the physical structure of these cells, and most VDAs are tubulin-binding agents that undermine tubulin-microtubule dynamics at sub-micromolar concentrations.

In seeking new structures for screening as VDAs, we identified the dibenz[*c*,*e*]oxepinol **1** as a potent inhibitor of microtubule assembly and a possible lead in this context.[1] A crystallographic analysis of the dibenz[*c*,*e*]oxepine nucleus[6] led us to conclude that it was well equipped to serve in this capacity by virtue of its ability to match, in both degree and sense, the conformational helicity of colchicine **2**, which is crucial to the latter's ability to bind to tubulin,[7] and by analogy with *N*-acetylcolchinol methyl ether (NCME) **3**, whose binding to tubulin is strong but rapidly reversible, *i.e.* compatible with drug-like pharmacokinetics.[8] Indeed the parent phenol *N*-acetylcolchinol (NAC) **4** was developed as a VDA in the form of the phosphate prodrug ZD6126 **5**, although the project was curtailed following the observation of adverse cardiac events in phase I clinical trials.[9,10] Various alternative structures have progressed to clinical trials as VDAs,[11] the best known being combretastatin A-4 (CA-4) **6** which, as the phosphate prodrug **7** (CA-4P; fosbretabulin; Zybrestat), has featured in human trials as a single agent[12] and in combinations with cytotoxic agents (paclitaxel, carboplatin), radiotherapy, or the antiangiogenic agent, bevacizumab.[13] Other stilbenes in development include combretastatin A-1 (CA-1) **8**, in the form of the prodrug **9** (OXi4503),[14] and AVE8062 **10** (ombrabulin).[15] The benzofuran **11** (BNC105),[16] the diketopiperazine **12** (plinabulin),[17] the pyrimidine **13**[18] and the chromene **14** (crolibulin)[19] have also progressed to clinical trials. Despite their structural diversity, all of these candidate VDAs bind to tubulin at, or close to, the same site as colchicine **2**, which is located at the interface of the two subunits of the α,β-tubulin heterodimer.[20]

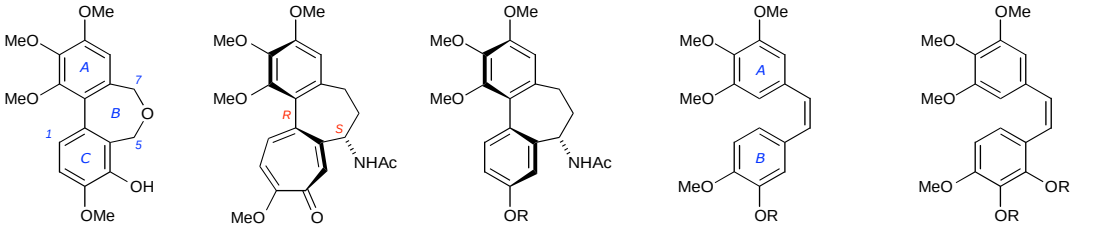

1 | **2** | **3** R = Me *NCME*, **4** R = H *NAC*, **5** R = PO_3H_2 | **6** R = H *CA-4*, **7** R = PO_3Na_2 | **8** R = H *CA-1*, **9** R = PO_3Na_2

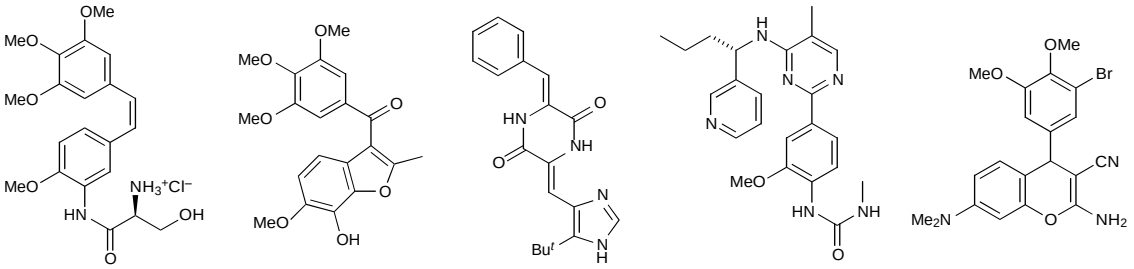

10 *AVE8062* | **11** *BNC105* | **12** *NPI-2358* | **13** *CYT997* | **14** *EPC2407*

While the colchicine binding site of tubulin can accommodate a range of structures, it is not an ideal target for therapeutics. Agents that inhibit microtubule assembly by binding to this site are associated with dose-limiting cardiac events (ischemia, infarction, ventricular tachycardia),[21] and this has been attributed to cell-cycle arrest in the endothelial cells of the myocardium.[22] Zybrestat **7** shows neurotoxic and cardiac effects (prolonged QT interval), and clinical trial protocols include measures to counteract hypertension and cardiac ischemia.[13a,23] Prolonged QT interval is also observed with OXi4503 **9**[14] and CYT997 **13**.[18a] Cardiotoxicity is thus a generic issue with tubulin-targeting VDAs, highlighting the need for finely-balanced therapeutics that are not compromised by this problem.[24]

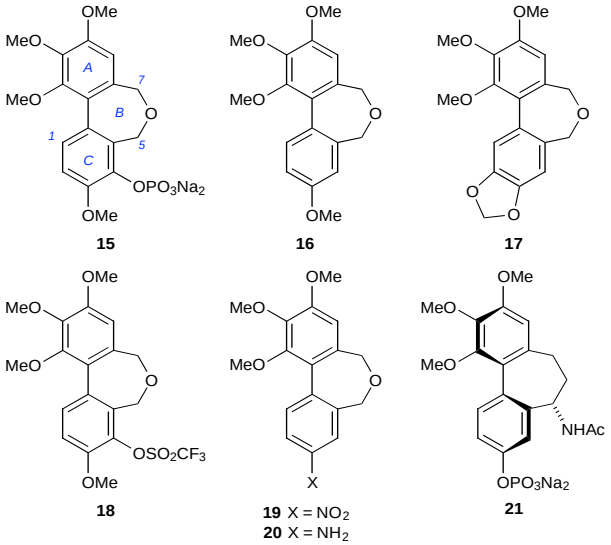

15 | **16** | **17** | **18** | **19** X = NO_2, **20** X = NH_2 | **21**

The dibenz[*c*,*e*]oxepine pharmacophore is easily accessible[1,25] and potentially tunable with respect to binding, metabolic and transport characteristics.[26] In this paper we describe new routes to the lead structure **1** and its biological evaluation as a VDA, along with the analogues **15**–**20**. The results show that in human tumour xenografts in mice, the prodrugs **15** (derived from **1**) and **21** (from the clinically tested VDA **5**) are similar in their ability to induce necrosis, and that **1** inhibits tumour growth *in vivo*.

2. Results and discussion

2.1. Synthesis of materials

Our original route to the key structure **1**, based on a conventional Ullmann biaryl synthesis,[1] was improved by switching to iodoarene cross-coupling partners (Scheme 1). The C-ring precursor **23** was conveniently prepared by direct iodination of *o*-vanillin mesylate **22** using iodine and periodic acid,[27] and the same method provided the A-ring precursor **24** from 3,4,5-trimethoxybenzaldehyde. The outcome of the Ullmann coupling of **23** and **24** was strongly dependent on the reaction conditions, but guided by the painstaking analysis of this type of reaction by Brown and coworkers,[28] we obtained acceptable yields of **25** using a solvent-free 3:1 mixture of the two components, a 5-fold excess of Cu powder, and careful control of the reaction time and temperature. Ring-closure of the diol **26** to **27** was induced with aq. HBr, and the methanesulfonyl protecting group was cleanly removed from **27**, to give **1**, using a modified version of Carreira's method.[29]

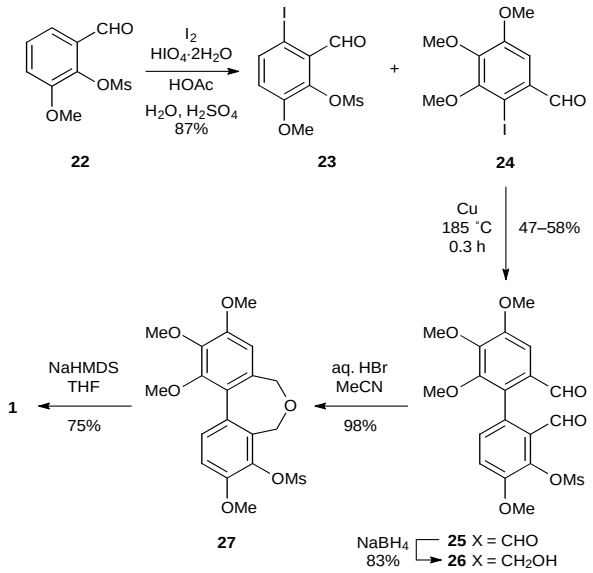

Scheme 1. Improved Ullmann cross-coupling route to **1**.

We also developed a potentially more versatile approach to **1** featuring a Pd-catalysed intramolecular direct arylation (IDA) reaction as the cyclisation step. This strategy called for the

construction of a dibenzyl ether bearing the latent A- and C-ring substituents of the target compound, together with a single halogen atom to mediate the metalation step. To prepare such a precursor for **1**, the MOM-protected aldehyde **29** was reduced to the alcohol **30**, which was then alkylated using 3,4,5-trimethoxybenzyl bromide **31** (Scheme 2). The resulting ether **32** was subjected to the IDA cyclisation conditions first described by Fagnou and coworkers[30,31] and adapted by us for the preparation of dibenz[*c*,*e*]azepines.[32] Chromatography of the product gave the desired heterocycle **34** in moderate yield, confirming that this is a viable approach to dibenz[*c*,*e*]oxepines. Subsequent removal of the MOM group from **34** using aq. HCl completed the new route to the target **1**.

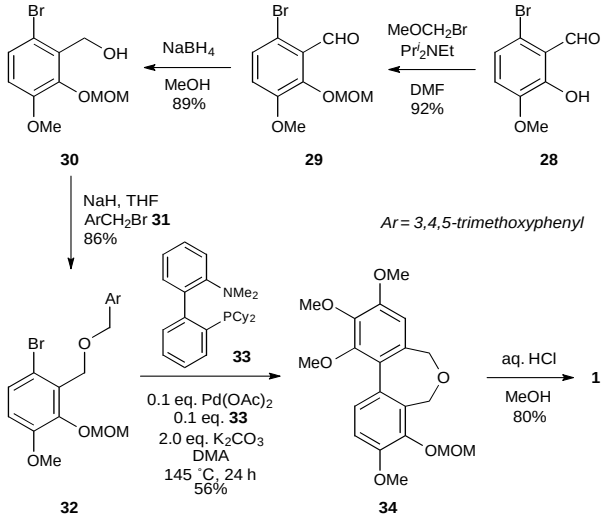

Scheme 2. Intramolecular direct arylation route to **1**.

In seeking a water-soluble version of the dibenzoxepinol **1**, we used a conventional reaction sequence[33] to prepare the disodium phosphate **15** *via* the intermediates **35** and **36**. Mixing the dihydrogen phosphate **36** with two molar equivalents of freshly prepared sodium methoxide in methanol, followed by evaporation and drying *in vacuo*, provided the disodium salt **15** as white powder. Although essentially homogeneous by ^{1}H, ^{13}C and ^{31}P NMR spectroscopy, this material proved to be hygroscopic, and microanalytical samples always retained small amounts of water and methanol.

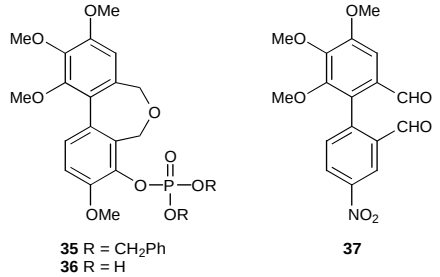

35 R = CH_2Ph
36 R = H

37

The dibenzoxepinol **1** was also converted into the derived triflate **18** by conventional means. The amine **20** was acquired in three steps from the biaryl dialdehyde **37**, which proved accessible *via* an Ullmann cross-coupling reaction. Subsequent reduction and cyclisation gave the nitro compound **19**, which was transformed into the amine **20** by catalytic hydrogenation.

2.2. Biological evaluation

2.2.1. 1. Inhibition of microtubule assembly and in vitro antiproliferative activity

Dibenzoxepines were routinely screened for their ability to inhibit microtubule assembly[34,35] and for growth inhibitory activity (IC_{50}) against the K562 human chronic myelogenous leukaemia cell line.[36] Both of these assays are routinely used for evaluating test compounds and provide a useful comparison with benchmarks such as colchicine **2** and CA-4 **6**. The results (Table 1) show that the ability of the phenolic compound **1** to inhibit microtubule assembly is matched by the phosphate **15** (entry 6), with the latter also showing sub-nanomolar IC_{50} values in the K562 assay. The activity shown by the triflate **18** (entry 9) is also noteworthy, and is consistent with prodrug behaviour.

Table 1. Activities (IC_{50}) of compounds in the microtubule assembly and K562 *in vitro* cytotoxicity assays.

Entry	Compound	Tubulin assembly IC_{50} μM[a,b]	K562 assay IC_{50} nM[c,d]
1[e]	**1**	2.2	34
2	**2**	2.0	19
3	**3**	0.7[f]	–[g]
4	**6**	1.3	1.0
5	**7**	0.9	0.72
6	**15**	1.4	0.23
7	**16**	7.4	110
8	**17**	>10	85
9	**18**	15	0.25
10	**19**	>10	16
11	**20**	>10	10

[a]Concentration required for 50% inhibition of tubulin assembly.

[b]Entries in this column are corrected for variations in the value for **6**, which was used as a reference for assay batches.

[c]Concentration that inhibits the growth of K562 cell line by 50% after incubation for 5 days. Each drug concentration was tested in triplicate, and the standard error of each value is <10%.

[d]Entries in this column are normalised to the value for **6**, which varied over the range 1.2–3.0 between batches.

[e]Values from ref. 1.

[f]Value from ref. 37.

[g]Not determined.

2.2.2. 2. In vitro *screening against NCI-60 cell lines*

The dibenzoxepines **1** and **15**–**17** were evaluated in the US National Cancer Institute (NCI) anticancer drug screen against the NCI-60 panel of human tumour cell lines.[38,39] The sixty cell lines of this panel are organised by disease type, and test data relating to both the levels and the patterns of activity across the panel can be instructive. Some of the results of the NCI-60 five-dose assay of the dibenzoxepines are shown in Table 2. Compounds **1** and **16** reach similar levels in their inhibitory effects, each with more than twenty instances in which the GI_{50} value is below 100 nM, whereas **15** and **17** register this level only with the MDA-MB-435 (melanoma) cell line.

Table 2. *In vitro* cell growth inhibition data for various dibenzoxepines against the NCI-60 panel of human cancer cell lines.

		Cell growth inhibition (GI_{50}, μM)[a,b,c]			
Panel	*Cell line*	**1**	**15**	**16**	**17**
Leukaemia	CCRF-CEM	0.04	0.29	0.08	0.35
	HL-60(TB)	0.03	0.32	0.04	0.39
	K-562	0.04	0.28	0.04	0.21
	MOLT-4	0.06	0.40	0.09	0.47
	SR	0.04	0.19	0.04	0.17
Non-small cell lung	NCI-H522	0.04	0.30	0.28	0.39
Colon	HCT-116	0.32	0.43	0.05	0.37
	HCT-15	0.08	0.44	0.08	0.48
	KM12	0.05	0.30	0.05	0.36
	SW-620	0.05	0.40	0.05	0.40
CNS	SF-268	[illegible]	[illegible]	[illegible]	[illegible]
	SF-295	0.27	0.32	0.06	0.33
	SF-539	0.05	0.33	0.16	0.35
	SNB-19	0.14	0.51	0.98	0.68
	SNB-75	0.07	0.54	0.09	0.46
	U251	0.30	0.48	0.10	0.48
Melanoma	LOXIMVI	0.08	0.66	0.21	0.87
	M14	0.05	0.27	0.05	0.23
	MALME-3M	*ND*	2.51	>100	>100
	MDA-MB-435	0.03	0.04	0.03	0.05
	SK-MEL-2	0.26	5.37	0.10	0.56
	SK-MEL-28	1.58	0.89	0.08	*ND*
	SK-MEL-5	0.04	0.26	0.03	0.21
	UACC-62	1.00	5.50	0.08	0.79
Ovarian	NCI/ADR-RES	0.05	0.28	0.07	0.36
	OVCAR-3	0.21	0.28	0.05	0.25
	SK-OV-3	[illegible]	0.40	0.13	0.47
Renal	RXF393	0.04	0.21	0.08	0.20
Prostate	DU-145	0.06	0.39	0.18	0.37
Breast	BT-549	0.26	2.24	0.20	0.54
	HS578T	0.04	0.24	0.24	0.43
	MCF7	0.07	0.40	0.04	0.40
	MDA-MB-468	0.22	1.15	0.03	0.17

[a]GI_{50}: concentration required for 50% cell growth inhibition.

[b]Only the cell-lines featuring one GI_{50} value below 100 nM are included in this table; see *Supplementary Material* for the full data set.

[c]Shading is applied to values below 100 nM; *ND* = not determined.

The results with the human colorectal tumour cell line HCT-15, which is known to express multidrug resistance protein (P-glycoprotein),[40] implies that the inhibitory properties of **1** and **16** are not unduly affected by this efflux pump, which can undermine the effects of tubulin-targeting anticancer agents.[41] The NCI-60 mean GI_{50} values for **1** and **16** are similar (*ca.* 0.3 μM), which compares to 0.04 μM for NCME **3**.

The NCI-60 screening results from the dibenzoxepines **1** and **15**–**17**, together with the public data for the colchicinoids **2**–**4** and the stilbenes **6** and **7**, were analysed using the matrix COMPARE algorithm.[42] In this type of analysis, the activity profile of a 'seed' compound against the NCI-60 cell lines can be compared to that of any 'target' compound in the same database, with the COMPARE algorithm being used to generate a series of correlation coefficients (Table 3). Compounds that exert their inhibitory effects by similar mechanisms of action can produce similar patterns of differential antiproliferative data, and the coefficients within the dibenzoxepine matrix (Table 3a) provide a reasonable case for the mechanistic correlation of this group of compounds, the borderline case being **16**. However, the extent to which this correlation is based on interaction with tubulin remains unclear, as is illustrated by the second section of results obtained with **2**–**4**, **6** and **7** (Table 3b). Matrix COMPARE coefficients (*r* values) less than 0.6 are of questionable significance,[43,44] and there is considerable variation in the coefficient values across the whole matrix, ranging from notable homology (**2** with **3**; **3** with **6**; **6** with **7**) to almost complete disparity with *N*-acetylcolchinol **4**, which in turn shows a modest correlation with **16**. Taken together, these results provide a reminder that the relationship between cytotoxicity (or cytostaticity) and the ability to shutdown vasculature remains obscure.

Using the standard COMPARE protocol, the antiproliferative activity profiles of **1** and **15**–**17** were compared with those of the NCI standard agents collection of anticancer agents.[45] This analysis, which can be used to identify the cellular targets of antitumour agents,[44,46] was extended to include compounds **2**–**4**, **6** and **7** as the seeds (Table 3c). The observed correlation of **15** with maytansine and vincristine, which are known to target microtubule formation,[47] provides further evidence that, as intended, the biological target of the dibenzoxepines is tubulin.

Table 3. Results of COMPARE analyses involving the dibenzoxepines **1** and **15**–**17**. (a) Matrix COMPARE data for the dibenzoxepines. (b) Standard COMPARE data for colchicinoids **2**–**4** and stilbenes **6** and **7**. (c) Correlations from a standard COMPARE analysis of dibenzoxepines with the NCI standard agent database.[a,b]

	Target vector	Seed vector **1**	**15**	**16**	**17**	**2**	**3**	**4**	**6**	**7**
a	**1**		0.81	0.84	0.79					
	15	0.81		0.66	0.73					
	16	0.84	0.66		0.86					
	17	0.79	0.73	0.87						
b	**2** colchicine	0.50	0.50	0.53	0.52		0.74	0.22	0.51	0.49
	3 NCME	0.43	0.48	0.42	0.45	0.74		0.02	0.71	0.58
	4 NAC	0.44	0.33	0.62	0.45	0.22	0.02		–0.01	0.12
	6 CA-4	0.40	0.43	0.31	0.31	0.51	0.71	–0.01		0.77
	7 CA-4P	0.58	0.53	0.40	0.38	0.49	0.58	0.12	0.77	
c	maytansine	0.51	0.56	0.54	0.56	0.76	0.87	0.47	0.67	0.45
	vincristine	0.57	0.62	0.53	0.56	0.78	0.81	0.41	0.58	0.50
	paclitaxel	0.51	0.45	0.49	0.60	0.54	0.36	0.49	–	–
	rhizoxin	0.43	0.45	0.45	0.52	0.74	0.83	0.38	0.64	0.59
	vinblastine	0.43	0.50	0.47	0.48	0.75	0.89	0.29	0.64	0.44

[a]Matrix (*r*) values are Pearson's correlation coefficients,[38] based on a comparison of the NCI GI_{50} mean graphs for each compound; see *Supplementary Material* for full search parameters and results.

[b]Shading is arbitrarily applied to *r* values ≥0.55. NCI descriptors: **2**, NSC 757; **3**, NSC 51046; **4**, NSC 51045; **6**, 613729; **7**, NSC 645646; maytansine, NSC 153858; vincristine, NSC 67574; paclitaxel, NSC 125973; rhizoxin, NSC 332598; vinblastine, NSC 49842.

2.2.3. 3. In vivo *antivascular effects of 15*

Given its close structural analogy and progress to clinical trials, we selected the erstwhile drug candidate **5**,[9,48] in the form of its disodium salt **21**, as a benchmark for assessing the ability of **15** to function as a VDA at levels beneath the maximum tolerated dose (MTD). In a side-by-side single-dose study, seven groups of athymic nude mice (n=3 per group) bearing subcutaneous DLD-1 human colon adenocarcinoma xenografts were used to assess the effects of treatment with the test compounds **15** and **21** on the functional vasculature in tumours. Once an established tumour vascular network was in place, mice were treated with a single intravenous dose (400 mg/kg) of **15** or **21** (three groups per compound). The results (Figure 1) provided a clear demonstration of the vascular shutdown induced by both compounds, peaking *ca.* one hour after the administration of the compound. This state persisted throughout the 24-h study period for **21**, whereas for **15** some recovery of vasculature was evident from 4 h post dose.

The extent of tumour necrosis (Figure 2) was only seen to be different to the control at 24 hours post dose for both compounds, which is consistent with the time delay expected for necrosis to occur following loss of blood supply to the tumour cells. The ability of the dibenzoxepine **15** to target experimental tumours is clearly evident, and parallels that of the related allocolchinol **21**.

Representative images from the functional vasculature and necrosis studies are provided in Figures 3 and 4 respectively.

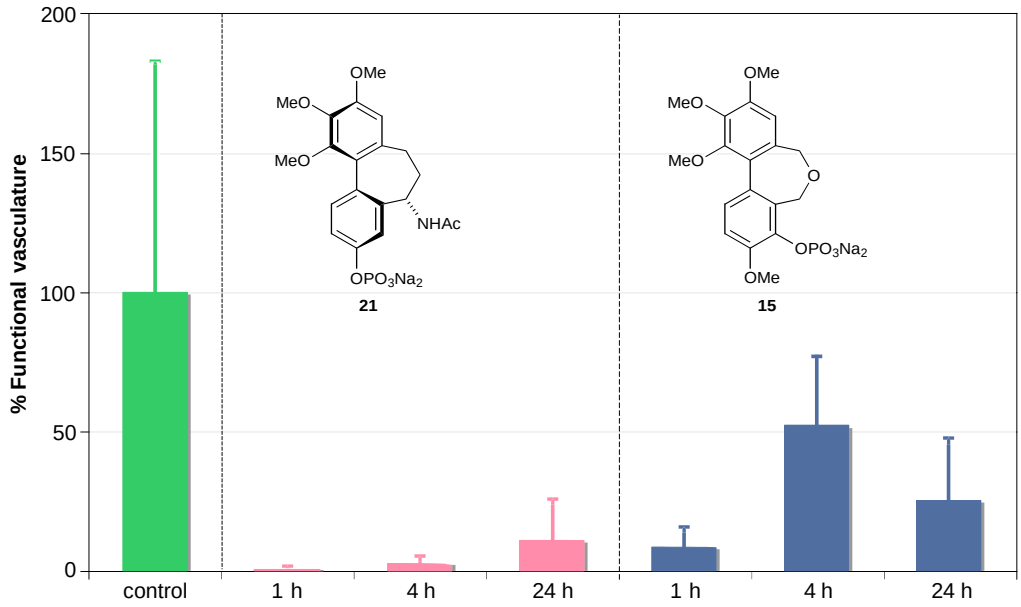

Figure 1. Chart showing the time-dependent vascular shutdown of DLD-1 human colon adenocarcinoma xenografts in mice following a single intravenous dose (400 mg/kg) of **15** or **21** (mean ± SEM).

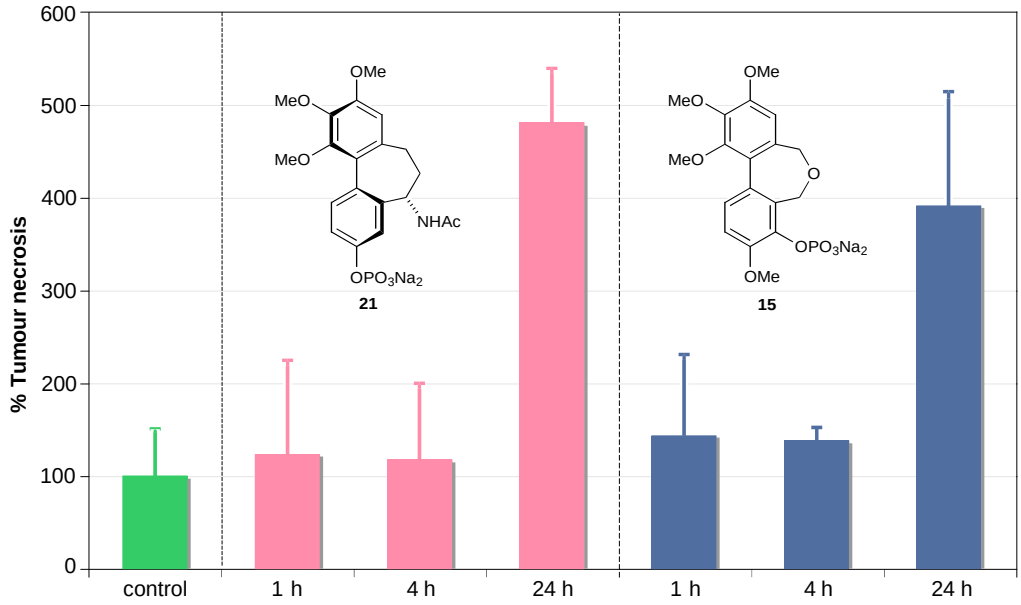

Figure 2. Chart showing the quantification of tumour necrosis in DLD-1 human colon adenocarcinoma xenografts in mice following a single intravenous dose (400 mg/kg) of **15** or **21** (mean ± SD).

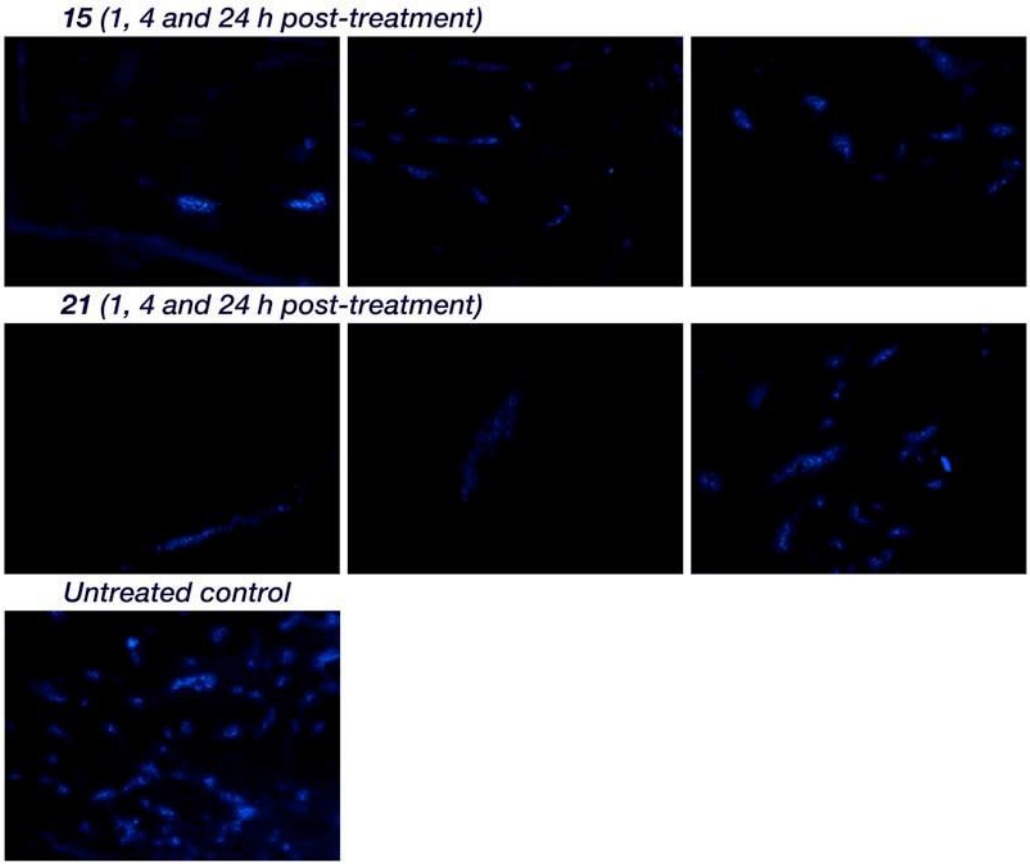

Figure 3. Representative images of DLD-1 human colon adenocarcinoma xenografts showing remaining functional vasculature using Hoechst 33342 staining, following a single intravenous dose of **15** or **21** at 400 mg kg^{-1} at 1, 4 and 24 h post dose.

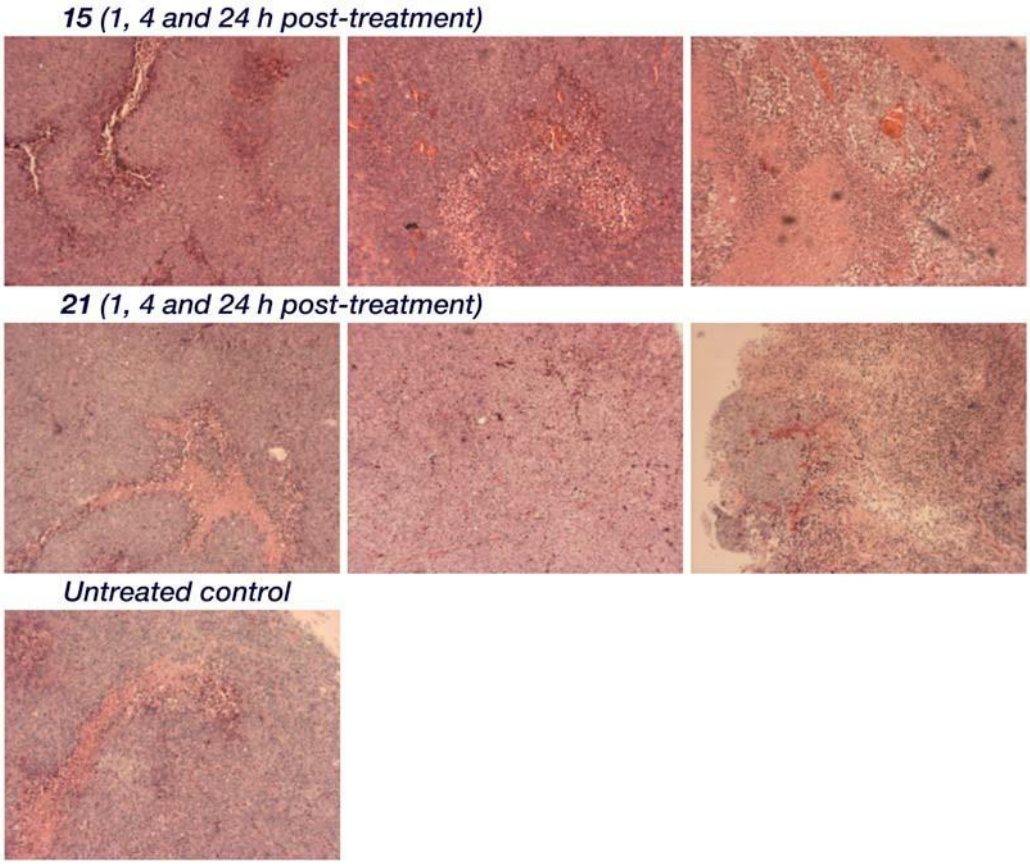

Figure 4. Representative images of haematoxylin- and eosin-stained DLD-1 human colon adenocarcinoma xenografts following a single intravenous dose of **15** or **21** at 400 mg kg^{-1} at 1, 4 and 24 h post dose.

2.2.4. 4. In vivo *antitumour effects of 1*

The potential of the benz[*c*,*e*]oxepine series as a source of *in vivo* antitumour agents was investigated using benzoxepinol **1** in a two-dose study with mice bearing subcutaneous Calu-6 lung tumour xenografts. Calu-6 is well vascularised and has been used previously to study VDAs.[49] Guidelines for the MTDs of various dibenzoxepines in mice were obtained by monitoring the effects of a single exposure on body weight over two weeks, and a limit of 270 mg/kg was set for **1** (Figure 5a). The antitumour properties of **1** were then monitored in a 10-day study of mice with implanted Calu-6 xenografts. Doses of one-quarter or one-half of the nominal MTD on days 1 and 5 had approximately the same inhibiting effect on tumour growth for 24 h, with regrowth then resuming at the original rate (Figure 5b). The dibenzoxepine **1** was thus demonstrated to be carcinostatic, inducing a growth delay in the experimental tumours at one-quarter of the nominal MTD, and was well tolerated in tumour-bearing mice.

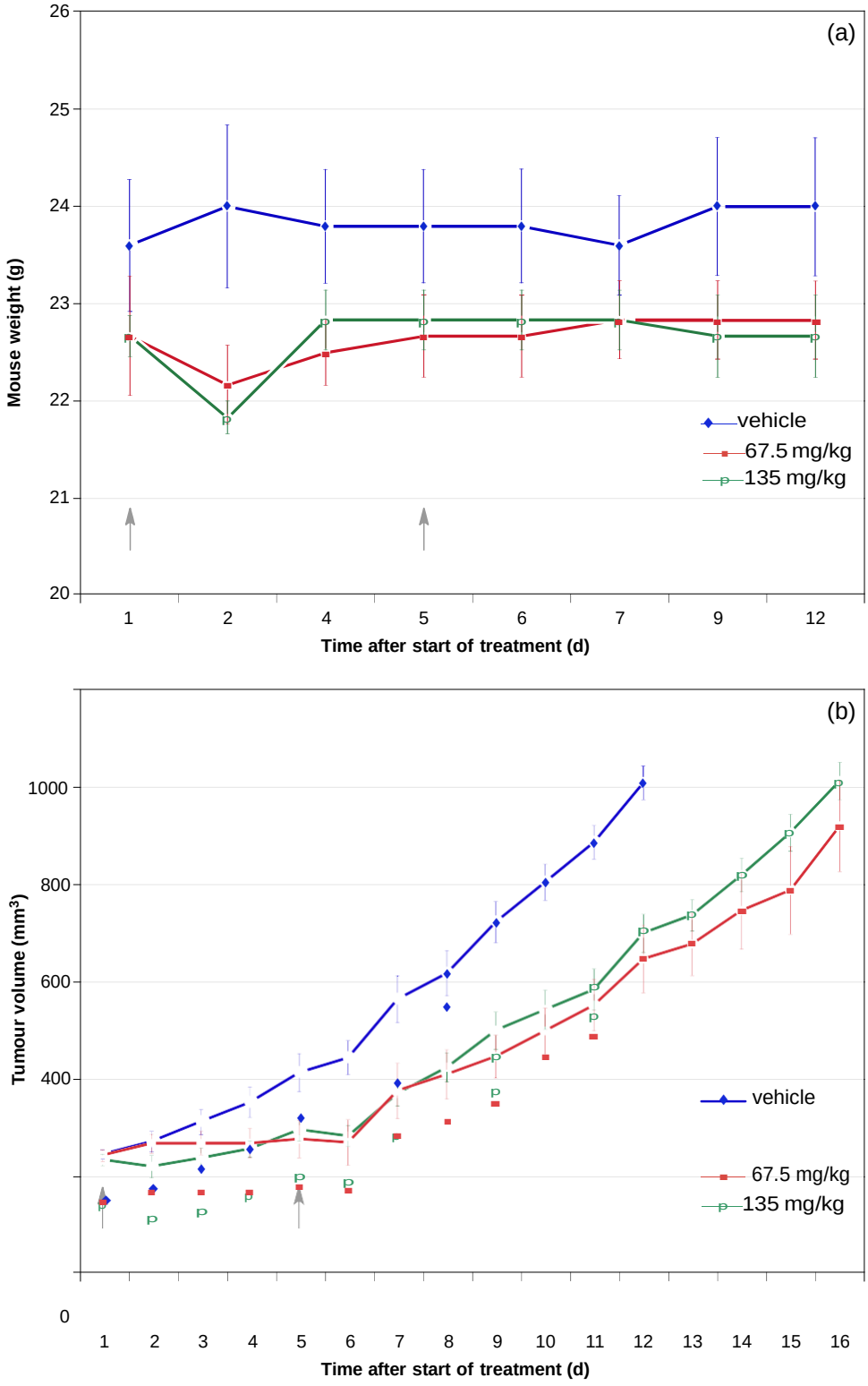

Figure 5. The dibenzoxepine **1** is well tolerated in tumour-bearing mice and induces a highly significant growth delay in subcutaneous Calu-6 lung tumour xenografts. (a) shows average mouse weight, (b) shows average tumour volume (n=5 control, n=6 treated mice per group). Arrows indicate administration of **1** at the noted dosages. The doses 67.5 mg/kg and 135 mg/kg equate to 0.25 and 0.5 MTD respectively. Compound **1** was dosed in 5% DMSO in peanut oil.

2.2.5. 5. Mechanistic considerations

The tubulin-binding capability of the dibenzoxepine **1** is consistent with its structural analogy with colchicine. The 1SA0 crystal structure provides a detailed picture of the interaction of *N*-deacetyl-*N*-(2-mercaptoacetyl)colchicine (DAMA-colchicine) **38** with the interchain boundary of the αβ-tubulin heterodimer,[20] which accounts for the disruptive effect of colchicinoids on the finely-poised dynamics of this interface. We speculate that, while chemically distinct from colchicine **2** and the combretastatins such as **6**, the dibenzoxepine **1** binds to the αβ-tubulin heterodimer at the same location and in a similar manner.[1] Our mechanistic model for this interaction, shown in Figure 6a, assumes the favourable locations of H-bond donor and acceptor sites ***a*** and ***b*** that can anchor the C-ring of the β-tubulin-bound ligand to the nearby α-tubulin. It is generally assumed that β -Cys241 provides colchicinoids with the third anchor **c**, although the case for this being solely through H-bonding is less compelling, as the trimethoxy motif is not indispensible.[50]

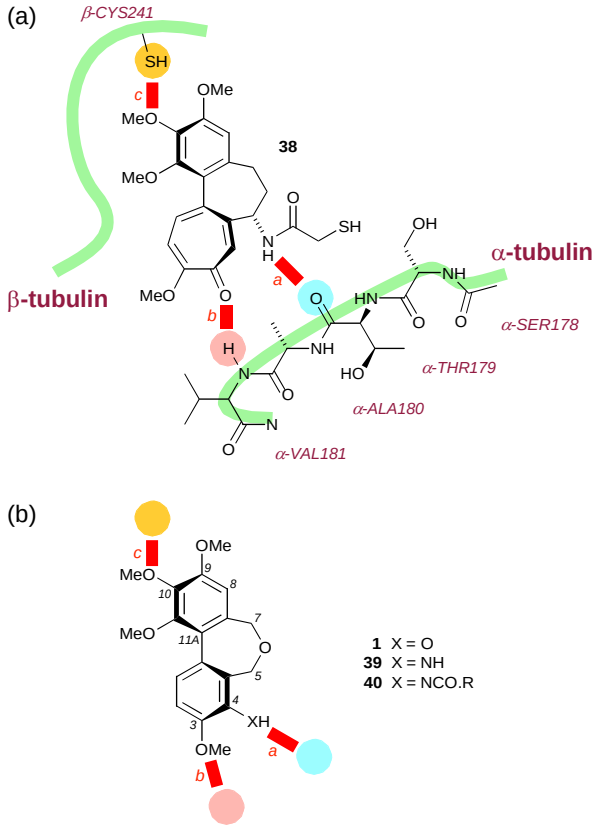

Figure 6. Depictions of (a) the supposed binding interactions within (or leading to) the DAMA-colchicine:αβ-tubulin:RB3 (1SA0) crystal structure (ref. 24a) and (b) the proposed analogy of **1** and **39**.

Conformational analysis of **1** using the methodology of Blundell *et al.*[51] gave a detailed view of its dynamic 3D-structure in dilute aqueous solution (Figure 7a). Overlaying the resulting conformers of **1**, in which the biaryl axis is free to assume the tubulin-binding (a*R*) configuration, and the bound colchicinoid **38** in 1SA0 (Figure 7b) indicates that the C(3) methoxy group of **1** coincides with the carbonyl oxygen of the (distorted) tropolone ring. In an alternative comparison (Figure 7c), conformers of **1** and a model of combretastatin A-4 **6** were overlaid with the X-ray structure of colchicine **3**.[52] This provides further support for the idea of a distinctive binding motif of **1**, in which the C(4) hydroxy group can function as an H-bond donor in the domain normally occupied by the amide NH of the colchicinoid.

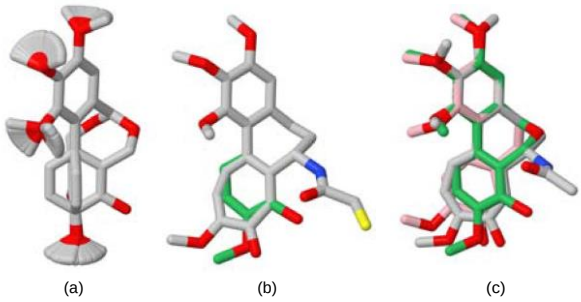

Figure 7. Calculated and crystallographic models overlaid on atoms C(11A), C(8) and C(10) of **1**. (a) The dynamic 3D-structure of **1** in aqueous solution. Carbon atoms are shown in grey and oxygen in red. (b) The bound conformation of **38** from 1SA0 (residue 701, carbon atoms in grey) and the closest matching preferred solution conformer of **1** (carbon atoms in green) aligned in the same pose. (c) The crystal structure of **3** (carbon atoms in grey) with the closest matching solution conformer of **1** (carbon atoms in green) and model of **6** (carbon atoms in pink) aligned in the same pose. N atoms are shown in blue and O in red; H are omitted for clarity.

The mechanistic model represented in Figure 6 should extend to the amine **39**, which also bears a C(4)-substituent suited to the role of the H-bond donor in anchor **a**, capable of binding to the residue Thr179 located on the α-tubulin chain (Figure 6b). On the same basis, and by analogy with ombrabulin **10**, we speculate that a range of amides **40** derived from **39** may be potent tubulin binding agents, and hence potential VDAs.

3. Conclusions

In seeking new vascular disrupting agents, we evaluated the accessibility and biological properties of a series of substituted dibenz[*c*,*e*]oxepines, identifying candidate compounds by their ability to inhibit the growth of experimental tumour cell lines *in vitro*. The most potent of the compounds studied was the benzoxepinol **1**, which in the NCI-60 anticancer drug screen manifested broad-spectrum antiproliferative activity whose profile (COMPARE analysis) indicated tubulin as the biological target. The results of *in vivo* studies confirm that the disodium phosphate prodrug **15**, derived from **1**, induces vascular shutdown and necrosis in DLD-1 human colon adenocarcinoma xenografts to an extent approaching that displayed by *N*-acetylcolchinol **4**, a structurally related allocolchicine derivative and recent drug candidate. The phenol **1** has also been shown to inhibit the growth of Calu-6 lung tumour xenografts in mice at a dose of one-quarter of the nominal MTD.

On the basis of the tubulin binding model shown in Figure 6, the large body of SAR data available for colchicinoids, and the characteristics of the compounds that we have prepared to date, we propose that the dibenz[*c*,*e*]oxepine pharmacophore offers a series of colchicinoid analogues with tunable tubulin binding characteristics. Exploitation of the IDA strategy (Scheme 2) should allow rapid access to new VDAs with design features that would prove difficult to achieve by the modification of natural colchicinoids. Amides of the form **40** are proposed as a focus for further development in this context.

4. Experimental section

4.1. *Chemistry*

Melting points were determined using Kofler hot-stage, Buchi 512 or Stuart Scientific SMP10 equipment and are uncorrected. Unless otherwise indicated, IR spectra were recorded for neat thin films using Perkin-Elmer 1710FT or Nicolet Nexus 670/870 spectrometers. NMR spectra were measured using a Bruker Avance III 400 spectrometer and are calibrated by reference to signals from the solvent ($CDCl_3$ at 77.16 ppm and CD_3OD at 49.00 ppm for ^{13}C spectra; residual protium in $CDCl_3$ at 7.26 ppm, CD_3OD at 3.31 ppm and D_2O at 4.79 ppm for ^{1}H spectra).[53] Chemical shifts for ^{19}F and ^{31}P spectra are quoted relative to $CFCl_3$ and 85% H_3PO_4 at 0 ppm respectively. Coupling constants (*J* values) are given in Hz; multiplicities are given as singlet (s), doublet (d), triplet (t), quartet (C), quintet (qn) or multiplet (m). NMR spectra were assigned with the aid of COSY, HMBC, HMQC and DEPT spectra where appropriate. Low-resolution mass spectra were recorded on a Micromass Trio 2000 instrument using the electrospray ionisation method; data for peaks of intensity <20% of that of the base peak are omitted. High-resolution (accurate mass) data were recorded using a Thermo Finnigan MAT95XP instrument. Elemental analyses were carried out by the University of Manchester microanalytical service.

Starting materials and solvents were routinely purified by conventional techniques.[54] Reactions were routinely carried out in a nitrogen atmosphere. Tetrahydrofuran (THF) was dried immediately prior to use, by distillation from sodium-benzophenone ketyl under nitrogen. Organic solutions were dried using anhydrous $MgSO_4$ and concentrated by rotary evaporation under reduced pressure. Analytical thin layer chromatography (TLC) was carried out using Macherey-Nagel Polygram SIL G/UV_{254} plates and the chromatograms were routinely visualised using UV light (254 nm). Preparative column (flash) chromatography was carried out on 60H silica gel (Merck 9385) using the flash technique.[55] Compositions of solvent mixtures are quoted as ratios of volume. 'Petroleum' refers to a light petroleum fraction, b.p. 60–80 ˚C, unless otherwise stated. 'Ether' refers to diethyl ether. Details of the preparations of **19** and **20** are provided in *Supplementary Material*.

4.1.1. 1. Improved Ullmann route to 5,7-dihydro-3,9,10,11-tetramethoxybenz[c,e]oxepin-4-ol 1

4.1.1.1. 1. 2-Formyl-6-methoxyphenyl methanesulfonate (22)[56]

Methanesulfonyl chloride (17.76 g, 155 mmol, 12.0 mL) was added to a solution of *o*-vanillin (21.60 g, 142 mmol) in dichloromethane (200 mL) at 0 °C. The mixture was left to stir for 5 min, then triethylamine (17.42 g, 172.2 mmol, 24.0 mL) was added dropwise, keeping the internal temperature at 0–5 °C. The mixture was stirred for a further 1 h at 0–5 ˚C and then at room temperature for a further 0.5 h. The precipitate was collected on a Buchner funnel and rinsed with dichloromethane (80 mL). The filtrate was washed with water (120 mL), aq. HCl (1 M; 2 x 70 mL), saturated sodium hydrogen carbonate (120 mL) and brine (120 mL). Drying and evaporation under reduced pressure gave the crude mesylate **22** (32.0 g, 98%) as a pale yellow oil which rapidly solidified. Crystallisation from ethanol (*ca.* 1 mL/g) gave colourless prisms (two crops, total 26.11 g, 80%), m.p. 78–80 ˚C (lit.[56] 79–80 ˚C); δ_H (400 MHz, $CDCl_3$) 3.36 (3 H, s, SO_2Me), 3.95 (3 H, s, OMe), 7.26 (1 H, dd, *J* 8.2, 1.6 Hz, 5-H), 7.38 (1 H, apparent dt, *J ca.* 8, 0.7 Hz, 4-H), 7.53 (1 H, dd, *J* 7.8, 1.6 Hz, 3-H) and 10.33 (1 H, d, *J* 0.7 Hz, CHO); δ_C (100 MHz, $CDCl_3$) 39.5, 56.6, 118.3, 120.5, 128.2, 131.3, 140.3, 152.2 and 188.4; R_f 0.35 (EtOAc - hexane, 1:1); R_f 0.57 (EtOAc - toluene, 1:9, three elutions).

4.1.1.2. 3-Iodo-2-formyl-6-methoxyphenyl methanesulfonate (23)

To apply the iodination procedure described,[27] the aldehyde **22** (2.763 g, 12.0 mol) was dissolved in a warm solvent mixture (60 mL; from acetic acid - water - conc. sulfuric acid 100 : 10 : 3 v/v/v). Iodine (1.28 g, 5.04 mmol) was added, followed by periodic acid dihydrate (602 mg, 2.64 mmol). The flask was closed with a balloon to retain vapours and the mixture was stirred at 60–65 ˚C for 24 h, after which time the dark mixture had become a clear red solution. With continued stirring, the mixture was diluted with water (50 mL), decolourised by the portionwise addition of solid $Na_2S_2O_5$ (total 500 mg), and poured into water (100 mL). The resulting yellow precipitate was collected, washed with water and dried at the pump, giving the crude *title compound* **23** (3.71 g, 87%) which was crystallised from ethanol (10 mL) and dried *in vacuo*, giving pale yellow prismatic needles (3.19 g, 75%), m.p. 102–104 ˚C (Found: C, 30.56; H, 2.48; I, 35.81; S, 8.87. $C_9H_9IO_5S$ requires C, 30.35; H, 2.55; I, 35.63; S, 9.00%); ν_{max}/cm^{-1} 3094, 3045, 3020, 3010, 2941, 2912, 2887, 2841, 1702, 1588, 1563, 1467, 1437, 1390, 1361, 1325, 1293, 1277, 1218, 1181, 1162, 1120, 1059, 971, 877, 822, 791, 707; δ_H (400 MHz, $CDCl_3$) 10.05 (1 H, s, CHO), 7.86 (1 H, d, *J* 8.8 Hz, 4-H), 6.94 (1 H, d, *J* 8.8 Hz, 5-H), 3.93 (3 H, s, OMe), 3.38 (3 H, s, SMe); δ_C (100 MHz, $CDCl_3$) 40.0 (CH_3), 56.8 (CH_3), 85.3 (C), 118.6 (CH), 130.4 (C), 138.9 (C), 139.7 (CH), 153.4 (C), 192.0 (CH); *m/z* (ES$^+$) 411 (67%), 379 (*M*Na$^+$, 100), 374 (*M*H_2O^+, 73), 357 (*M*H$^+$, 18); R_f 0.26 (EtOAc - toluene, 1:9) [**22** has R_f 0.20 under the same conditions].

4.1.1.3. 2-Iodo-3,4,5-trimethoxybenzaldehyde (24)

To apply the iodination procedure described,[27] 3,4,5-trimethoxybenzaldehyde (58.86 g, 0.30 mol) was dissolved by warming in a mixture of acetic acid (700 mL) and 2 M sulfuric acid (70 mL). Iodine (32.00 g, 126 mmol) was added, followed by periodic acid dihydrate (15.04 g, 66 mmol). The flask was closed with a septum cap to retain vapours and the mixture was stirred for 4 h at 60–65 ˚C, during which the colour changed from opaque purple to clear orange-brown. The stirred mixture was treated dropwise with a solution made by dissolving $Na_2S_2O_5$ (14.5 g, 76 mmol) in water (50 mL) and then poured into water (2.0 L). The precipitated solid was collected on a Büchner funnel, rinsed with water, dried on the filter and then *in vacuo*, giving the aldehyde **24** (76.69 g, 79%) as a cream solid, m.p. 67–68 ˚C [lit.[25d] 67 ˚C (cyclohexane)]; δ_H (400 MHz, $CDCl_3$) 10.04 (1 H, s, CHO), 7.34 (1 H, s, 6-H), 3.96 (3 H, s, OMe), 3.91 (3 H, s, OMe), 3.90 (3 H, s, OMe); δ_C (100 MHz, $CDCl_3$) 56.4 (CH_3), 61.2 (CH_3), 61.3 (CH_3), 91.7 (C), 108.7 (CH), 130.7 (C), 147.9 (C), 153.1 (C), 154.1 (C), 195.4 (CH); R_f 0.20 (EtOAc - hexane, 1:4).

4.1.1.4. 2,6'-Diformyl-4,2',3',4'-tetramethoxybiphenyl-3-yl methanesulfonate (25)

The mesylate **23** (3.56 g, 10.0 mmol) and aldehyde **24** (9.66 g, 30.0 mmol) were placed in a 100 mL round-bottomed flask and

the mixture was melted by gentle heating with a hot-air gun. Dendritic copper powder (Aldrich 357456; 20.33 g, 0.32 mol) was mixed into the melt using a spatula, and the flask was then heated in a Woods metal bath at 185 ˚C for 20 min. The reaction mixture was then allowed to cool and extracted with EtOAc (100 mL). The resulting suspension was filtered through a pad of Celite, rinsing with EtOAc, and the filtrate concentrated. Chromatography of the residue over silica gel (elution with EtOAc - hexane, gradient 1:2 to 1:1) yielded 4,4',5,5',6,6'-hexamethoxy-1,1'-biphenyl-2,2'-dicarboxaldehyde[1] followed by the *title compound* **25** (2.00 g, 47%), which formed colourless prisms, m.p. 132 ˚C (EtOH) [lit.[1] 131–132 ˚C (EtOAc)]; δ_H (400 MHz, $CDCl_3$) 10.18 (1 H, s, 2-CHO), 9.63 (1 H, s, 6'-CHO), 7.36 (1 H, s, 5'-H), 7.26 (1 H, d, *J* 8.5 Hz, 6-H), 7.15 (1 H, d, *J* 8.5 Hz, 5-H), 4.03 (3 H, s, OMe), 3.98 (3 H, s, OMe), 3.57 (3 H, s, OMe), 3.43 (3 H, s, SMe); δ_C (100 MHz, $CDCl_3$) 40.0 (CH_3), 56.3 (CH_3), 56.6 (CH_3), 60.9 (CH_3), 61.2 (CH_3), 105.9 (CH), 116.4 (CH), 127.3 (C), 129.7 (C), 130.3 (C), 130.7 (C), 132.1 (CH), 139.5 (C), 147.3 (C), 150.8 (C), 152.3 (C), 153.8 (C), 189.0 (CH), 190.2 (CH); R_f 0.20 (EtOAc - hexane, 2:1), 0.30 (ether). These data are in full accord with those published earlier.[1] In a small-scale version of this procedure, the mesylate **23** (356 mg, 1.0 mmol) gave the dialdehyde **25** (246 mg, 58%) as a colourless solid.

4.1.1.5. 2,6'-Bis(hydroxymethyl)-4,2',3',4'-tetramethoxybiphenyl-3-yl methanesulfonate (26)

Sodium borohydride (1.25 g, 33.0 mmol) was added portionwise to a stirred suspension of the dialdehyde **25** (6.37 g, 15.0 mmol) in MeOH (90 mL) at room temperature. The mixture, which became clear and warm, was stirred for a further 1 h and then diluted with water (120 mL). The bulk of the MeOH was removed by rotary evaporation and the residue was extracted with EtOAc (3 x 90 mL). The combined extracts were washed with brine (90 mL), dried and evaporated. Crystallisation of the residue from EtOAc (20 mL) gave a semi-solid mass that was broken up using ether (10 mL), collected on a filter, rinsed with EtOAc - ether (1:1) and dried *in vacuo*, giving the *title compound* **26** (4.54 g, 71%) as a white solid, m.p. 124–125 ˚C (EtOAc); R_f (EtOAc - hexane 2:1) 0.18. Concentration and trituration of the residue with EtOAc - ether (1:3) gave a further 0.80 g (12%) of the product, which was identical (^{1}H-NMR, ^{13}C-NMR) to material prepared previously.[1]

4.1.1.6. 5,7-Dihydro-3,9,10,11-tetramethoxybenz[c,e]oxepin-4-yl methanesulfonate (27)

To a solution of **26** (4.285 g, 10.0 mmol) in acetonitrile (50 mL) was added 48% aq. hydrobromic acid (2.5 mL, 22 mmol) and the solution was stirred at 50–55 ˚C for 1 h. Water (50 mL) and dichloromethane (40 mL) were added, the layers were separated and the aqueous layer was extracted with dichloromethane (40 mL). The extracts were combined, washed with brine (40 mL), dried and concentrated, giving the *title compound* **27** (4.035 g, 98%) as a colourless crystalline solid, m.p. 158–161 ˚C (MeOH), identical (TLC, ^{1}H-NMR, ^{13}C-NMR) to an authentic sample.[1]

4.1.1.7. 5,7-Dihydro-3,9,10,11-tetramethoxybenz[c,e]oxepin-4-ol (1)

A solution of **27** (2.265 g, 5.52 mmol) in THF (35 mL) at 0 ˚C under N_2 was treated dropwise with 2 M sodium hexamethyldisilazide in THF (5.0 mL, 10.0 mmol).[29] After 5 min the solution was cautiously diluted with 2 M aqueous hydrochloric acid (12 mL) at 0 ˚C, further diluted with water (20 mL) and extracted with EtOAc (3 x 30 mL). The combined organic extracts were washed with brine (40 mL), dried and evaporated. The resulting beige solid was dissolved in dichloromethane and the solution filtered through a short column of flash silica (h 4 cm, d 3 cm), eluting with dichloromethane. The eluate gave the title compound **1** (1.37 g, 75%) as a colourless solid, identical (TLC, ^{1}H-NMR, ^{13}C-NMR) to an authentic sample.[1]

4.1.2. 2. Intramolecular direct arylation route to 1

4.1.2.1. 1. 6-Bromo-3-methoxy-2-(methoxymethoxy)benzaldehyde (29)

To a stirred solution of 6-bromo-2-hydroxy-3-methoxybenzaldehyde **28**[57] (4.67 g, 20.2 mmol) and diisopropylethylamine (4.90 mL, 3.64 g, 28.1 mmol) in DMF (40 mL) at 0 ˚C was added dropwise bromomethyl methyl ether (2.00 mL, 3.062 g, 24.5 mmol). After stirring at 0 ˚C for 10 min and then at room temperature for 1 h, the mixture was poured into rapidly stirring water (200 mL). The precipitate was collected on a filter, washed with water (3 x 40 mL) and dried *in vacuo*. To remove polar impurities, a solution of the crude product (5.28 g) in dichloromethane was filtered through a plug of silica gel (3 cm diameter, 6 cm depth), eluting with dichloromethane. Evaporation of the eluate provided the *title compound* **29** (5.10 g, 92%) as a cream solid, m.p. 69–71 ˚C (EtOH) (Found: C, 43.29; H, 3.92; Br, 29.13. $C_{10}H_{11}BrO_4$ requires C, 43.66; H, 4.03; Br, 29.05%); ν_{max}/cm^{-1} 2944, 2835, 1701, 1573, 1464, 1433, 1301, 1258, 1157, 1064, 951; δ_H (400 MHz, $CDCl_3$) 10.37 (1 H, d, *J* 0.5 Hz, CHO), 7.36 (1 H, dd, *J* 8.8, 0.5 Hz, 5-H), 6.96 (1 H, d, *J* 8.8 Hz, 5-H), 5.17 (2 H, s, OCH_2O), 3.87 (3 H, s, ArOMe), 3.55 (3 H, s, CH_2OMe); δ_C (100 MHz, $CDCl_3$) 56.4 (CH_3), 58.1 (CH_3), 100.1 (CH_2), 113.2 (C), 117.4 (CH), 129.2 (C), 129.8 (CH), 148.9 (C), 152.5 (C), 190.8 (CH); *m/z* (ES^+) 340/338 (MNa$_2$H$_2$O , 100%), 299/297 (MNa , 80); R_f 0.27 (EtOAc - hexane, 1:3).

4.1.2.2. 2. (6-Bromo-3-methoxy-2-(methoxymethoxy)phenyl)methanol (30)

A stirred solution of the aldehyde **29** (4.125 g, 15.0 mmol) in MeOH (75 mL) at room temperature was treated portionwise with sodium borohydride (0.76 g, 20 mmol). The solution was stirred for a further 2 h and then poured into water (200 mL). The mixture was extracted with dichloromethane (3 x 30 mL) and the extract dried and concentrated. Removal of the final traces of solvent *in vacuo* gave the *title compound* **30** (3.714 g, 89%) as a colourless oil which slowly solidified. The analytical sample had m.p. 60–62 ˚C (EtOAc - hexane, 1:4) (Found: C, 43.56; H, 4.67; Br, 28.73. $C_{10}H_{13}BrO_4$ requires C, 43.34; H, 4.73; Br, 28.83%); ν_{max}/cm^{-1} 3457, 2941, 2837, 1576, 1465, 1437, 1399, 1298, 1269, 1231, 1197, 1159, 1071, 1011, 960, 924, 799; δ_H (400 MHz, $CDCl_3$) 7.31 (1 H, d, *J* 8.8 Hz, 4-H), 6.77 (1 H, d, *J* 8.8 Hz, 5-H), 5.09 (2 H, s, OCH_2O), 4.81 (2 H, s, $ArCH_2O$), 3.83 (3 H, s, ArOMe), 3.59 (3 H, s, CH_2OMe); δ_C (100 MHz, $CDCl_3$) 56.1 (CH_3), 57.8 (CH_3), 60.0 (CH_2), 99.6 (CH_2), 113.2 (CH), 115.4 (C), 128.8 (CH), 134.9 (C), 146.2 (C), 151.8

(C); *m/z* (ES^+) 301/299 (MNa^+, 100%); R_f 0.18 (EtOAc - hexane, 1:2).

4.1.2.3. 3. 5-Bromomethyl-1,2,3-trimethoxybenzene (31)[58]

To a stirred solution of 3,4,5-trimethoxybenzyl alcohol (10.0 g, 50.5 mmol) in dry dichloromethane (150 mL) under N_2 at –5 ˚C was added dropwise a solution of phosphorus tribromide (3.50 mL, 10.1 g, 37.2 mmol) in dichloromethane (10 mL). After stirring at –5 ˚C for 45 min, the mixture was poured on to ice (200 g), neutralised with sat. aq. $NaHCO_3$ (120 mL), and the organic layer was separated. The aqueous phase was extracted with dichloromethane (2 x 20 mL) and the combined organic phases were washed with brine (30 mL), dried and concentrated to obtain the *title compound* **31** (13.0 g, 99%) as a colourless solid, m.p. 76–78 ˚C (hexane) [lit.[58b] 86–87 ˚C (petroleum)]; δ_H (400 MHz, $CDCl_3$) 6.61 (2 H, s, 4-H and 6-H), 4.54 (2 H, s, CH_2Br), 3.86 (6 H, s, 1-OMe and 3-OMe), 3.84 (3 H, s, 2-OMe) (in accord with published data[43]); δ_C (100 MHz, $CDCl_3$) 34.4, 56.2, 61.0, 106.2, 133.3, 138.2, 153.4.

4.1.2.4. 4. 1-Bromo-4-methoxy-3-(methoxymethoxy)-2-(((3,4,5-trimethoxyphenyl) methoxy)methyl)benzene (32)

To a stirred suspension of sodium hydride (60% dispersion in mineral oil; 750 mg, 18.75 mmol) in THF (45 mL) under N_2 at room temperature was added dropwise a solution of the alcohol **30** (2.08 g, 7.5 mmol) in THF (9 mL). After stirring at room temperature for 1.5 h, the mixture was treated dropwise with a solution of the bromide **31** (2.35 g, 9.0 mmol) in THF (9 mL) and the stirred mixture was heated at 45 ˚C for 2.5 h. It was then poured into water (180 mL) and extracted with dichloromethane (3 x 60 mL). The combined organic phases were washed with water (90 mL) and brine (90 mL), dried and evaporated. Chromatography of the residue over silica gel (elution with EtOAc - hexane, 1:3) gave the *title compound* **32** (2.95 g, 86%) as a colourless viscous oil (Found: $M+Na^+$, 479.0678; $C_{20}H_{25}BrO_7Na$ requires 479.0681); ν_{max}/cm^{-1} 2939, 2838, 1592, 1505, 1463, 1422, 1397, 1355, 1330, 1273, 1234, 1152, 1128, 1101, 1072, 1008, 957, 829, 805, 780, 691; δ_H (400 MHz, $CDCl_3$) 7.30 (1 H, d, *J* 8.8 Hz, 5-H), 6.77 (1 H, d, *J* 8.8 Hz, 6-H), 6.65 (2 H, s, 2'-H, 6'-H), 5.10 (2 H, s, OCH_2O), 4.72 (2 H, s, OCH_2), 4.55 (2 H, s, CH_2O), 3.86 (6 H, s, ArO*Me*), 3.822 (3 H, s, ArO*Me*), 3.818 (3 H, s, ArO*Me*), 3.52 (3 H, s, CH_2O*Me*); δ_C (100 MHz, $CDCl_3$) 56.0 (CH_3), 56.1 (2 x CH_3), 57.7 (CH_3), 60.8 (CH_3), 66.7 (CH_2), 72.9 (CH_2), 99.6 (CH_2), 104.8 (2 x CH), 113.5 (CH), 116.7 (CBr), 128.4 (CH), 131.6 (C), 134.2 (C), 137.3 (C), 146.3 (C), 151.9 (C), 153.2 (2 x C); *m/z* (ES^+) 481/479 (MNa^+, 100%); R_f 0.18 (EtOAc - hexane, 1:2).

4.1.2.5. 5,7-Dihydro-1,2,3,9-tetramethoxy-8-(methoxymethoxy)dibenz[c,e]oxepine (34)

In an adaptation of the procedure described by Fagnou *et al.*,[30] the ether **32** (276.2 mg, 0.604 mmol), anhydrous potassium carbonate (powdered, 167 mg, 1.21 mmol), DavePhos **33** (23.6 mg, 0.06 mmol) and palladium acetate (13.5 mg, 0.06 mmol) were placed in a round-bottomed flask. The flask was purged with nitrogen for 10 min and DMA (12 mL) was added. The solution was then heated, darkening above 130 ˚C to black at 145 ˚C. TLC (EtOAc - hexane, 1:2) after 21 h at 145 ˚C suggested that the reaction was incomplete. Heating was continued for 67 h, after which the DMA was evaporated *in vacuo*. The residue was diluted with EtOAc and the solution filtered through a plug of silica gel, eluting with more EtOAc. Evaporation of the eluate and chromatography of the residue, eluting with acetone - hexane (1:4), provided the *title compound* **34** (127 mg, 56%) as colourless crystals, m.p. 112–114 ˚C (MeOH) (Found: C, 64.04; H, 6.47. $C_{20}H_{24}O_7$ requires C, 63.82; H, 6.43%); ν_{max}/cm^{-1} 2937, 2855, 1599, 1579, 1482, 1462, 1436, 1401, 1370, 1333, 1304, 1274, 1242, 1225, 1196, 1154, 1116, 1089, 1060, 991, 968, 798, 734; δ_H (400 MHz, $CDCl_3$) 7.43 (1 H, d, *J* 8.6 Hz, 1-H), 7.00 (1 H, d, *J* 8.6 Hz, 2-H), 6.75 (1 H, s, 8-H), 5.22 (1 H, br d, *J* 5.6 Hz, OC*H*O), 5.18 (1 H, br d, *J* 5.6 Hz, OC*H*O), 5.10 (1 H, d, *J* 11.2 Hz, 5-H), 4.39 (1 H, d, *J* 11.3 Hz, 7-H), 4.04 (1 H, d, *J* 11.2 Hz, 7-H), 3.94 (3 H, s, OMe), 3.92 (3 H, s, OMe), 3.91 (3 H, s, OMe), 3.83 (1 H, d, *J* 11.2 Hz, 5-H), 3.66 (3 H, s, OMe), 3.64 (3 H, s, OMe); δ_C (100 MHz, $CDCl_3$) 56.0 (CH_3), 56.2 (CH_3), 57.8 (CH_3), 60.3 (CH_2), 61.0 (CH_3), 61.2 (CH_3), 67.9 (CH_2), 99.6 (CH_2), 108.8 (CH), 111.9 (CH), 125.8 (CH), 126.4 (C), 129.4 (C), 130.5 (C), 131.1 (C), 142.7 (C), 144.0 (C), 150.7 (C), 151.6 (C), 152.9 (C); *m/z* (ES^+) 399 (MNa^+, 100); R_f 0.21 (acetone - hexane, 1:4) [**1** has R_f 0.16 (acetone - hexane, 1:4)].

4.1.2.6. 5,7-Dihydro-3,9,10,11-tetramethoxybenz[c,e]oxepin-4-ol (1)

A solution of **34** (127 mg, 0.34 mmol) in MeOH (3 mL) and 2 M hydrochloric acid (1 mL, 2 mmol) was heated to 50–55 ˚C for 1.5 h, after which TLC (acetone - hexane 1:3) indicated that no **34** remained. The solution was diluted with water (5 mL) and extracted with dichloromethane (3 x 5 mL). The combined organic extract was washed with brine (10 mL), dried and evaporated. Chromatography of the residue, eluting with hexane - EtOAc (2:1), gave the title compound **1** (90 mg, 80%), identical (TLC, ^{1}H NMR) to that obtained from **27** as described above.

4.1.3. Preparative route to 15

4.1.3.1. 5,7-Dihydro-3,9,10,11-tetramethoxydibenz[c,e]oxepin-4-yl bis(phenylmethyl) phosphate (35)

The method of Silverberg *et al.*[33] was adapted thus: A three-necked flask fitted with a thermometer, nitrogen inlet and magnetic stirrer was charged with **1** (1.460 g, 4.39 mmol, 1.0 eq.), *N*,*N*-dimethylaminopyridine (60 mg, 0.49 mmol, 0.11 eq.) and anhydrous acetonitrile (25 mL). The resulting solution was cooled to an internal temperature of –10 ˚C (cooling bath of acetone, water and solid CO_2 pellets) and treated with anhydrous tetrachloromethane (2.1 mL, 3.35 g, 22 mmol, 5 eq.) followed by diisopropylethylamine (1.6 mL, 1.19 g, 9.2 mmol, 2.1 eq.). The mixture was stirred for 1 min and then treated dropwise with dibenzyl phosphite (1.4 mL, 1.66 g, 6.3 mmol, 1.44 eq.), keeping the mixture at or below –10 ˚C. The mixture was then stirred at –10 ˚C for a further 40 min, at which point TLC indicated the consumption of the organic starting materials. The mixture was quenched at –10 ˚C by the dropwise addition of a solution of potassium dihydrogen phosphate (0.68 g) in water (10 mL), allowed to warm to room temperature, and then extracted with EtOAc (3 x 30 mL). The combined organic phase was washed with water (40 mL) and brine (40 mL), dried and concentrated. The residue was purified by chromatography (silica gel preconditioned with EtOAc - hexane - Et_3N 50:50:1), eluting with EtOAc - hexane (1:1 to 3:2), which gave the *title compound* **35** (2.06 g, 79%) as a white crystalline solid, m.p. 132–133 ˚C

(EtOH) (Found: C, 64.88; H, 5.38; P, 5.18. $C_{32}H_{33}O_9P$ requires C, 64.86; H, 5.61; P, 5.23%) (M+H^+, 593.1943. $C_{32}H_{34}O_9P$ requires 593.1940); ν_{max}/cm^{-1} 2943, 2858, 1482, 1461, 1278; δ_H (400 MHz, $CDCl_3$) 7.52 (1 H, dd, *J* 8.6, 1.2 Hz, 1-H), 7.40–7.29 (10 H, m, ArH), 7.04 (1 H, d, *J* 8.6 Hz, 2-H), 6.75 (1 H, s, 8-H), 5.28–5.20 (4 H, m, OCH_2Ph), 5.12 (1 H, d, *J* 11.4 Hz, 5-H), 4.39 (1 H, d, *J* 11.3 Hz, 7-H), 4.04 (1 H, d, *J* 11.3 Hz, 7-H), 3.95 (3 H, s, OMe), 3.92 (3 H, s, OMe), 3.86 (3 H, s, OMe), 3.84 (1 H, d, *J* 11.4 Hz, 5-H), 3.66 (3 H, s, OMe); δ_C (100 MHz, $CDCl_3$) 56.1 (CH_3), 56.2 (CH_3), 60.1 (5-CH_2), 61.0 (CH_3), 61.2 (CH_3), 67.9 (7-CH_2), 69.80 (Ph*C*H$_2$), 69.86 (Ph*C*H$_2$), 108.8 (8-CH), 112.2 (2-CH), 125.9 (C), 127.1 (two peaks, 1-CH), 127.9 (Ph 2,6- or 3,5-CH), 128.2 (C), 128.2 (C), 128.5 (Ph 4-H), 128.6 (Ph 2,6- or 3,5-CH), 130.5 (C), 131.1 (C), 138.3 (C), 138.4 (C), 142.7 (C), 150.3 (C), 150.3 (C), 150.7 (C), 153.1 (C); δ_P (162 MHz, $CDCl_3$) –5.77 (quin, *J* 7.5 Hz); *m/z* (CI, NH_3) 593 (*M*H$^+$, 10%); R_f 0.22 (EtOAc - petroleum ether 60–80˚ 1:1).

4.1.3.2. 5,7-Dihydro-3,9,10,11-tetramethoxydibenz[c,e]oxepin-4-ol 4-(dihydrogen phosphate) (36)

A solution of **35** (1.481 g, 2.5 mmol) in MeOH (65 mL) and EtOAc (10 mL) containing palladium on charcoal (10% w/w; 70 mg) at room temperature was stirred under an atmosphere of hydrogen for 1 h, at which point TLC (EtOAc) indicated that the starting material had been consumed. The solution was filtered through a pad of Celite (depth 8 mm), rinsing with MeOH, and evaporated. The residue was triturated with EtOAc and the solid collected on filter, washed with EtOAc and dried *in vacuo*, giving the *title compound* **36** (984 mg, 95%) which crystallised from EtOH as colourless rosettes, m.p. >200 ˚C (dec.) (Found: C, 52.36; H, 5.20; P, 7.52. $C_{18}H_{21}O_9P$ requires C, 52.43; H, 5.13; P, 7.51%) (M+Na^+, 435.0826. $C_{18}H_{21}O_9PNa$ requires 435.0821); ν_{max}/cm^{-1} 2930, 2858, 1590, 1107; δ_H (400 MHz, CD_3OD) 7.46 (1 H, dd, *J* 8.6, 1.2 Hz, 1-H), 7.16 (1 H, d, *J* 8.6 Hz, 2-H), 6.89 (1 H, s, 8-H), 5.15 (1 H, d, *J* 11.1 Hz, 5-H), 4.41 (1 H, d, *J* 11.1 Hz, 7-H), 3.96 (1 H, d, *J* 11.1 Hz, 7-H), 3.93 (3 H, s, OMe), 3.91 (3 H, s, OMe), 3.89 (3 H, s, OMe), 3.81 (1 H, d, *J* 11.1 Hz, 5-H), 3.61 (3 H, s, OMe); δ_C (100 MHz, CD_3OD) 56.5 (CH_3), 56.6 (CH_3), 61.0 (5-CH_2), 61.3 (CH_3), 61.5 (CH_3), 68.4 (7-CH_2), 110.1 (CH), 113.3 (CH), 127.3 (C), 127.8 (CH), 129.2 (C), 131.4 (C), 132.2 (C), 140.0 (C), 140.1 (C), 144.1 (C), 151.8 (C), 152.3 (C), 154.5 (C); δ_P (162 MHz, CD_3OD) –4.81 (s); *m/z* (ES) 435 (MNa^+, 80%).

4.1.3.3. 5,7-Dihydro-3,9,10,11-tetramethoxydibenz[c,e]oxepin-4-ol 4-(disodium phosphate) (15)

A stirred solution of the dihydrogen phosphate **36** (731 mg, 1.773 mmol) in MeOH (12 mL) was treated with methanolic sodium methoxide (0.3984 M, 8.90 mL, 3.546 mmol) [prepared by dissolving freshly cut sodium (2.29 g, 99.6 mmol) in anhydrous MeOH (250 mL)]. The mixture was stirred for 2 min, then concentrated by rotary evaporation. The residue was triturated with ethanol - hexane (1:1) and dried *in vacuo*, giving the *title compound* **15** (802 mg, 99%) as a white powder, m.p. 208–215 ˚C (darkens above 180 ˚C) (Found: C, 45.50; H, 4.81; Na, 8.35; P, 6.39. $C_{18}H_{19}Na_2O_9P$ requires C, 47.38; H, 4.20; Na, 10.08; P, 6.79%);* (400 MHz, D_2O) 7.13 (1 H, dd, *J* 8.6, 1.0 Hz, 1-H), 7.05 (1 H, d, *J* 8.6 Hz, 2-H), 6.87 (1 H, s, 8-H), 5.29 (1 H, d, *J* 11.1 Hz, 5-H), 4.31 (1 H, d, *J* 11.1 Hz, 7-H), 3.84 (3 H, s, OMe), 3.83 (3 H, s, OMe), 3.81 (3 H, s, OMe), 3.76–3.69 (2 H, m, 5-H and 7-H), 3.58 (3 H, s, OMe); δ_C (100 MHz, D_2O) 55.7 (CH_3), 56.0 (CH_3), 59.9 (5-CH_2), 61.1 (CH_3), 61.2 (CH_3), 66.5 (7-CH_2), 109.3 (CH), 112.4 (CH), 124.5 (CH), 126.3 (C), 127.8 (C), 129.1 (C), 130.6 (C), 135.9 (C), 140.9 (C), 141.6 (C), 149.3 (C), 151.5 (C), 152.1 (C); δ_P (162 MHz, D_2O) –0.45 (s).

* The elemental analysis result corresponds to a solvate with a w/w distribution of **15** (93.0%), water (3.7%), methanol (3.3%); compound **15** is hygroscopic.

4.1.4. Preparative route to 18

4.1.4.1. 5,7-Dihydro-3,9,10,11-tetramethoxydibenz[c,e]oxepin-4-yl trifluoromethanesulfonate (18)

To a 5 mL flask containing the dibenzoxepinol **1** (83.2 mg, 0.25 mmol, 1.0 eq.) and anhydrous pyridine (0.28 mL, 274 mg, 3.46 mmol, 13.8 eq.) in dry dichloromethane (0.3 mL) under argon was added triflic anhydride (0.053 mL, 89 mg, 0.315 mmol, 1.26 eq.) dropwise at 0 ˚C over a period of 2–3 min. After stirring the mixture at this temperature for 30 min, TLC indicated the consumption of starting material. The mixture was transferred to a separating funnel containing dichloromethane (2 mL) and 1 M hydrochloric acid (2 mL). The organic layer was collected and washed with more 1 M hydrochloric acid (2 x 1 mL), saturated aqueous sodium hydrogen carbonate (1 mL) and brine (0.5 mL), dried and concentrated *in vacuo* to afford a dark yellow oil. Chromatography (EtOAc - petroleum, 1:2) afforded the *title compound* **18** (90.6 mg, 78%) as a white solid, m.p. 164 ˚C (*M*, 464.0748. $C_{19}H_{19}F_3O_8S$ requires 464.0753); ν_{max}/cm^{-1} 2943, 2866, 1596, 1486, 1412, 1329; δ_H (400 MHz, $CDCl_3$) 3.69 (3 H, s, OMe), 3.92 (1 H, d, *J* 11.5 Hz, 5-H), 3.93 (3 H, s, OMe), 3.95 (3 H, s, OMe), 3.98 (3 H, s, OMe), 4.00 (1 H, d, *J* 11.5 Hz, 7-H), 4.43 (1 H, d, *J* 11.5 Hz, 7-H), 4.90 (1 H, d, *J* 11.5 Hz, 5-H), 6.76 (1 H, s, 8-H), 7.12 (1 H, d, *J* 8.7 Hz, 2-H), 7.67 (1 H, d, *J* 8.7 Hz, 1-H); δ_C (100 MHz, $CDCl_3$) 56.2 (CH_3), 56.4 (CH_3), 59.9 (CH_2), 61.1 (CH_3), 61.3 (CH_3), 68.0 (CH_2), 98.5 (C), 99.7 (C), 109.0 (CH), 112.5 (CH), 125.0 (C), 129.1 (C), 130.1 (CH), 131.0 (C), 136.9 (C), 142.9 (C), 150.4 (C), 150.7 (C), 153.6 (C); δ_F (375 MHz, $CDCl_3$) –77.98; *m/z* (EI) 464 (*M*, 10%); R_f 0.35 (EtOAc - petroleum, 1:2).

4.2. Biological Evaluation

4.2.1. 1. Inhibition of tubulin assembly and K 526growth inhibition assays

Details of the procedures are described in detail elsewhere.[1]

4.2.2. 2. In vitro *screening against NCI cell lines*

Compounds **1** and **15**–**17** were submitted to the US National Cancer Institute (NIH, Bethesda, Maryland) for screening against the NCI-60 panel of human cancer cell lines, a service offered through the Developmental Therapeutics Program (DTP). Full details of the methodology for compound testing, data analysis and use of the COMPARE algorithm are available on the NCI website.[45] Compounds **1** and **15**–**17** were tested more than once in NCI-60 5-dose assays, and the average data were used in COMPARE analyses. All of these were run with the GI_{50} values as the target-set endpoints and the default settings: Minimum correlation 0.2; count results to return 50; minimum count common cell lines, 40; minimum standard deviation, 0.05.

The test results for **1** and **15**–**17** were subjected to a matrix COMPARE analysis[42] together with the colchicinoids **2**–**4** and the combretastatins **6** and **7**. In this type of analysis, the profile of antiproliferative activity of the 'seed' compound against the panel of cancer cell lines in the NCI-60 *in vitro* assays is compared with that of the 'target' compound in the same assays. The NSC numbers used to retrieve the data for this analysis were: **1**, NSC 756015; **15**, NSC 756016; **16**, NSC 756013; **17**, NSC 756014. Data for **2**–**4**, **6** and **7** are available in the NCI collection. The results provided the source data for Tables 3a and 3b.

Using the standard COMPARE protocol, the antiproliferative activity profiles of the **1** and **15**–**17** were compared with those of the NCI standard agents collection of anticancer agents. For perspective, the analysis was also carried out with **2**–**4**, **6** and **7** as the seeds. The results provided the source data for Table 3c.

All of the relevant data, including the complete Table 2, are provided in the *Supplementary Material*.

4.2.3. 3. In vivo antivascular effects of 15

Female Balb/C immunodeficient nude mice (Harlan UK Ltd., Blackthorn, UK) aged 6-12 weeks were kept in cages housed in isolation cabinets in an air-conditioned room with regular alternating cycles of light and darkness. They received Teklad 2018 diet (Harlan) and water *ad libitum*. Accurately weighed amounts of **15** or **21** were dissolved in sterile water and administered within 15 minutes of addition of solvent. To determine the MTD, **15** was administered intravenously on days 0, 2 and 4 at 200 or 400 mg kg^{-1} to groups of 2 mice, with a control group remaining untreated. Mice were frequently weighed and monitored for any visible deleterious effects for 14 d following administration. Percentage bodyweight compared to bodyweight on day 0 was determined. No major loss in bodyweight or other deleterious effects were observed at either of the concentrations of **15** administered. A persistent reduction in percentage bodyweight to 85% of starting weight would be considered toxic. Tumours were excised from a donor animal, placed in sterile physiological saline containing penicillin and streptomycin and cut into small fragments of approximately 2 mm^3. Under brief general isoflurane inhalation anaesthesia, DLD-1 fragments were implanted in both the left and right flanks of each mouse using a trocar. Once tumours had reached a volume of approximately 150 mm^3 (as measured by callipers), to ensure that an established tumour vascular network was in place, the mice were allocated into groups of three by restricted randomisation to keep group mean tumour size variation to a minimum.

Vascular shutdown: Seven groups of tumour-bearing mice (n=3 per group) were used to assess the effects of treatment with the compounds on the functional vasculature in DLD-1 tumours. Once tumours had reached a volume of approximately 150 mm^3, to ensure that an established tumour vascular network was in place, mice were treated with a single 400 mg kg^{-1} intravenous dose of **15** or **21** (three groups per compound). An untreated group was maintained as a control (one group). At 1, 4 or 24 h following treatment (n=3 per group), vascular shutdown was assessed as follows: Hoechst 33342 dye was dissolved in sterile saline and injected intravenously by the tail vein at 40 mg kg^{-1}. One minute after injection the mice in the relevant treatment group were sacrificed by cervical dislocation and the tumours carefully and rapidly excised. One tumour from each mouse was then wrapped in aluminium foil, immediately immersed in liquid nitrogen and stored at –80 °C until ready for ultracryotomy. The other tumour was immersion fixed in 10% neutral buffered formalin for 24 h and processed for paraffin embedding. The control group were processed at the same time as the 24 h time-point. Frozen sections of 10 μm thickness were taken at approximately 100 μm intervals through the tumour, with each tumour being attributed a random number so that examination was done blind. Up to five fields from each of 10 random sections were examined for each tumour under UV illumination using a Leica DMRB microscope, with images captured digitally through a JVC 3-CCD camera and processed using AcQuis (Synoptics, Cambridge, UK) software. Functional vasculature was assessed by placing a cm^2 grid over the captured digital image and counting the number of points on the grid which overlay fluorescently stained cells. The percentage functional vasculature was then calculated by taking the total number of fluorescence-positive points for each field and dividing by the total number of points. An average percentage for each animal was calculated. Comparisons were made between percentage vasculature in control and treated tumours. Statistical analysis of shutdown was carried out using a two-tailed Student's t-Test. The results are shown in Figure 1.

Tumour necrosis: For each animal, 5 μm thick paraffin sections were taken and stained with haematoxylin and eosin to assess for necrosis. Each tumour was attributed a random number so that examination was done blind. Digital images were captured using the same system as above but with bright-field illumination. Percentage necrosis was assessed by placing a cm^2 grid over the captured digital image and counting the number of points on the grid which overlay necrotic cells. The percentage necrosis was calculated by taking the total number of necrosis-positive points for each field and dividing by the total number of points. An average percentage for each animal was then calculated. Statistical analysis of shutdown was carried out using a two-tailed Student's t-Test. The results are shown in Figure 2.

See Figures 3 and 4 for sample images and *Supplementary Material* for further data.

4.2.4. 4. In vivo antitumour effects of 1

Calu-6 human lung carcinoma cells (American Type Culture Collection, Manassas, VA, USA) were cultured in RPMI supplemented with 10% FCS and 2 mmol/L glutamine. Cells were harvested in exponential phase growth and prepared at a concentration of 2×10^7 cells/mL in a 1:1 mix of serum-free RPMI and Matrigel (phenol red-free; BD Biosciences, Erembodegem, Belgium).

To initiate tumour xenografts, 0.1 mL of cell suspension was implanted at an approximate depth of 1 mm under the skin 1 cm from the tail base of female *nu*/*nu* CBA mice aged 10 to 12 wk. Palpable tumours were evident 5–7 days after cell implantation. Tumour volume was measured daily using calipers. Once a tumour volume of approximately 250 mm^3 was attained, tumours were randomised into 3 treatment groups (n=6/group): vehicle (5% DMSO in peanut oil), compound **1** at 0.5 MTD in 5% DMSO/peanut oil and compound **1** at 0.25 MTD in 5% DMSO/peanut oil. Compound/vehicle was administered IP at 0.1 mL per 10 g body weight on days 1 and 5. Mouse condition and body weight were monitored daily and the animals maintained throughout using the highest welfare standards.

All procedures had local ethics and Home Office approval and were conducted under PPL 40/2328.

4.2.5. 5. Dynamic 3D-solution structure of 1

Details of this analysis, which utilised the methodology of Blundell *et al.*,[51] are provided in the *Supplementary Material*.

Acknowledgments

We are grateful to The University of Manchester Intellectual Property (UMIP) for funding this work, the TINHAT project, through a Proof-of-Principle award, and we warmly thank Dr Richard Price and Dr Sunita Jones of UMIP for their constant support, guidance and encouragement. We also thank Prof. Ludwig Neyses and Dr Elizabeth Cartwright (Institute of Cardiovascular Sciences, University of Manchester), Dr Ian Crocker (Institute of Human Development, University of Manchester), Prof. Alan McGown (University of Salford) and Dr Charles Blundell (C4X Discovery Ltd.) for their significant contributions to this project. We are also grateful to Darren Cook (University of Salford) and Patricia Cooper (University of Bradford) for assistance with compound testing, and to the staff of the analytical services of School of Chemistry (University of Manchester), especially Gareth Smith (MS), Steve Kelly (NMR) and Martin Jennings (Microanalysis). We also wish to acknowledge the use of the EPSRC-funded Chemical Database Service at Daresbury.[59]

References and notes

1. Part 1: Edwards, D. J.; Hadfield, J. A.; Wallace, T. W.; Ducki, S. *Org. Biomol. Chem.* **2011**, *9*, 219.
2. (a) Siemann, D. W.; Chaplin, D. J.; Horsman, M. R. *Cancer* **2004**, *100*, 2491; (b) Siemann, D. W.; Bibby, M. C.; Dark, G. G.; Dicker, A. P.; Eskens, F. A. L. M.; Horsman, M. R.; Marmé, D.; LoRusso, P. M. *Clin. Cancer Res.* **2005**, *11*, 416; (c) Siemann, D. W.; Chaplin, D. J. *Expert Opin. Drug Discovery* **2007**, *2*, 1357; (d) Sebahar, P. R.; Willardsen, J. A.; Anderson, M. B. *Curr. Bioact. Compd.* **2009**, *5*, 79; (e) Horsman, M. R.; Bohn, A. B.; Busk, M. *Exp. Oncol.* **2010**, *32*, 143.
3. (a) Folkman, J. *Nat. Rev. Drug Discovery* **2007**, *6*, 273; (b) Sennino, B.; McDonald, D. M. *Nat. Rev. Cancer* **2012**, *12*, 699.
4. Ferrara, N.; Hillan, K. J.; Gerber, H.-P.; Novotny, W. *Nat. Rev. Drug Discovery* **2004**, *3*, 391.
5. (a) Tozer, G. M.; Kanthou, C.; Baguley, B. C. *Nat. Rev. Cancer* **2005**, *5*, 423; (b) Horsman, M. R.; Siemann, D. W. *Cancer Res.* **2006**, *66*, 11520; (c) Kanthou, C.; Tozer, G. M. *Int. J. Exp. Path.* **2009**, *90*, 284; (d) Schwartz, E. L. *Clin. Cancer Res.* **2009**, *15*, 2594; (e) McKeage, M. J.; Baguley B. C. *Cancer* **2010**, *116*, 1859; (f) Siemann, D. W. *Cancer Treat. Rev.* **2011**, *37*, 63.
6. Edwards, D. J.; Pritchard, R. G.; Wallace, T. W. *Acta Crystallogr., Sect. B: Struct. Sci.* **2005**, *61*, 335.
7. (a) Brossi, A. *J. Med. Chem.* **1990**, *33*, 2311; (b) Shi, Q.; Verdier-Pinard, P.; Brossi, A.; Hamel, E.; Lee, K.-H. *Bioorg. Med. Chem.* **1997**, *5*, 2277; (c) Bhattacharyya, B.; Panda, D.; Gupta, S.; Banerjee, M. *Med. Res. Rev.* **2008**, *28*, 155.
8. Kang, G. J.; Getahun, Z.; Muzaffar, A.; Brossi, A.; Hamel, E. *J. Biol. Chem.* **1990**, *265*, 10255.
9. (a) Davis, P. D.; Dougherty, G. J.; Blakey, D. C.; Galbraith, S. M.; Tozer, G. M.; Holder, A. L.; Naylor, M. A.; Nolan, J.; Stratford, M. R.; Chaplin, D. J.; Hill, S. A. *Cancer Res.* **2002**, *62*, 7247; (b) Blakey, D. C.; Westwood, F. R.; Walker, M.; Hughes, G. D.; Davis, P. D.; Ashton, S. E.; Ryan, A. J. *Clin. Cancer Res.* **2002**, *8*, 1974; (c) Beerepoot, L. V.; Radema, S. A.; Witteveen, E. O.; Thomas, T.; Wheeler, C.; Kempin, S.; Voest, E. E. *J. Clin. Oncol.* **2006**, *24*, 1491.
10. (a) Gould, S.; Westwood, F. R.; Curwen, J. O.; Ashton, S. E.; Roberts, D. W.; Lovick, S. C.; Ryan, A. J. *J. Natl. Cancer Inst.* **2007**, *99*, 1724; (b) LoRusso, P. M.; Gadgeel, S. M.; Wozniak, A.; Barge, A. J.; Jones, H. K.; DelProposto, Z. S.; DeLuca, P. A.; Evelhoch, J. L.; Boerner, S. A.; Wheeler, C. *Invest. New Drugs* **2008**, *26*, 159.
11. For reviews, see (a) Mita, M. M.; Sargsyan, L.; Mita, A. C.; Spear, M. *Expert Opin. Investig. Drugs* **2013**, *22*, 317; (b) Kretzschmann, V. K.; Fürst, R. *Phytochem. Rev.* **2014**, *13*, 191.
12. Mooney, C. J.; Nagaiah, G.; Fu, P.; Wasman, J. K.; Cooney, M. M.; Savvides, P. S.; Bokar, J. A.; Dowlati, A.; Wang, D.; Agarwala, S. S.; Flick, S. M.; Hartman, P. H.; Ortiz, J. D.; Lavertu, P. N.; Remick, S. C. *Thyroid* **2009**, *19*, 233.
13. (a) Rustin, G. J.; Shreeves, G.; Nathan, P. D.; Gaya, A.; Ganesan, T. S.; Wang, D.; Boxall, J.; Poupard, L.; Chaplin, D. J.; Stratford, M. R. L.; Balkissoon, J.; Zweifel, M. *Br. J. Cancer* **2010**, *102*, 1355; (b) Ng, Q.-S.; Mandeville, H.; Goh, V.; Alonzi, R.; Milner, J.; Carnell, D.; Meer, K.; Padhani, A. R.; Saunders, M. I.; Hoskin, P. J. *Ann. Oncol.* **2012**, *23*, 231; (c) Nathan, P.; Zweifel, M.; Padhani, A. R.; Koh, D.-M.; Ng, M.; Collins, D. J.; Harris, A.; Carden, C.; Smythe, J.; Fisher, N.; Taylor, N. J.; Stirling, J. J.; Lu, S.-P.; Leach, M. O.; Rustin G. J. S.; Judson, I. *Clin. Cancer Res.* **2012**, *18*, 3428.
14. Patterson, D. M.; Zweifel, M.; Middleton, M. R.; Price, P. M.; Folkes, L. K.; Stratford, M. R. L.; Ross, P.; Halford, S.; Peters, J.; Balkissoon, J.; Chaplin, D. J.; Padhani, A. R.; Rustin, G. J. S. *Clin. Cancer Res.* **2012**, *18*, 1415.
15. (a) Eskens, F. A. L. M.; Tresca, P.; Tosi, D.; Van Doorn, L.; Fontaine, H.; Van der Gaast, A.; Veyrat-Follet, C.; Oprea, C.; Hospitel, M.; Dieras, V. *Br. J. Cancer* **2014**, *110*, 2170; (b) Bahleda, R.; Sessa, C.; Del Conte, G.; Gianni, L.; Capri, G.; Varga, A.; Oprea, C.; Daglish, B.; Hospitel, M.; Soria, J.-C. *Invest. New Drugs* **2014**, *32*, 1188.
16. (a) Rischin, D.; Bibby, D. C.; Chong, G.; Kremmidiotis, G.; Leske, A. F.; Matthews, C. A.; Wong, S. S.; Rosen, M. A.; Desai, J. *Clin. Cancer Res.* **2011**, *17*, 5152; (b) Nowak, A. K.; Brown, C.; Millward, M. J.; Creaney, J.; Byrne, M. J.; Hughes, B.; Kremmidiotis, G.; Bibby, D. C.; Leske, A. F.; Mitchell, P. L. R.; Pavlakis, N.; Boyer, M.; Stockler, M. R. *Lung Cancer*, **2013**, *81*, 422.
17. (a) Mita, M. M.; Spear, M. A.; Yee, L. K.; Mita, A. C.; Heath, E. I.; Papadopoulos, K. P.; Federico, K. C.; Reich, S. D.; Romero, O.; Malburg, L.; Pilat, M.; Lloyd, G. K.; Neuteboom, S. T. C.; Cropp, G.; Ashton, E.; LoRusso, P. M. *Clin. Cancer Res.* **2010**, *16*, 5892; (b) Yamazaki, Y.; Sumikura, M.; Hidaka, K.; Yasui, H.; Kiso, Y.; Yakushiji, F.; Hayashi,Y. *Bioorg. Med. Chem.* **2010**, *18*, 3169; (c) Millward, M.; Mainwaring, P.; Mita, A.; Federico, K.; Lloyd, G. K.; Reddinger, N.; Nawrocki, S.; Mita, M.; Spear, M. A. *Invest. New Drugs* **2012**, *30*, 1065.
18. (a) Lickliter, J. D.; Francesconi, A. B.; Smith, G.; Burge, M.; Coulthard, A.; Rose, S.; Griffin, M.; Milne, R.; McCarron, J.; Yeadon, T.; Wilks, A.; Cubitt, A.; Wyld, D. K.; Vasey, P. A. *Br. J. Cancer* **2010**, *103*, 597; (b) Burge, M.; Francesconi, A. B.; Kotasek, D.; Fida, R.; Smith, G.; Wilks, A.; Vasey, P. A.; Lickliter, J. D. *Invest New Drugs* **2013**, *31*, 126.
19. Gramza, A. W.; Balasubramaniam, S.; Tito Fojo, A.; Ward, J.; Wells, S. A. *J. Clin. Oncol.* **2013**, *31* (May 20 supplement); ASCO meeting abstract 6074.
20. (a) Ravelli, R. B. G.; Gigant, B.; Curmi, P. A.; Jourdain, I.; Lachkar, S.; Sobel, A.; Knossow, M. *Nature* **2004**, *428*, 198; (b) Gigant, B.; Wang, C.; Ravelli, R. B. G.; Roussi, F.; Steinmetz, M. O.; Curmi, P. A.; Sobel, A.; Knossow, M. *Nature* **2005**, *435*, 519; (c) Dorléans, A.; Gigant, B.; Ravelli, R. B. G.; Mailliet, P.; Mikol, V.; Knossow, M. *Proc. Natl. Acad. Sci. USA* **2009**, *106*, 13775.
21. (a) Lampidis, T. J.; Kolonias, D.; Savaraj, N.; Rubin, R. W. *Proc. Natl. Acad. Sci. USA* **1992**, *89*, 1256; (b) Webster, D. R. *Cardiovasc. Toxicol.* **2002**, *2*, 75; (c) Motlagh, D.; Alden, K. J.; Russell, B.; García, J. *J. Physiol.* **2002**, *540.1*, 93.
22. Mikaelian, I.; Buness, A.; de Vera-Mudry, M.-C.; Kanwal, C.; Coluccio, D.; Rasmussen, E.; Downing, J. C.; Char, H. W.; Hilton, H.; Funk, J.; Hoflack, J.-C.; Fielden, M.; Herting, F.; Suter-Dick, L. *Toxicol. Sci.* **2010**, *117*, 144.
23. (a) Cooney, M. M.; Radivoyevitch, T.; Dowlati, A.; Overmoyer, B.; Levitan, N.; Robertson, K.; Levine, S. L.; DeCaro, K.; Buchter, C.; Taylor, A.; Stambler, B. S.; Remick, S. C. *Clin. Cancer Res.* **2004**, *10*, 96; (b) Varterasian, M.; Fingert, H.; Agin, M.; Meyer, M. *Clin. Cancer Res.* **2004**, *10*, 5967; (c) Ke, Q.; Bodyak, N.; Rigor, D. L.; Hurst, N. W.; Chaplin, D. J.; Kang, P. M. *Vascul. Pharmacol.* **2009**, *51*, 337.
24. (a) Van Heeckeren, W. J.; Bhakta, S.; Ortiz, J.; Duerk, J.; Cooney, M. M.; Dowlati, A.; McCrae, K.; Remick, S. C. *J. Clin. Oncol.* **2006**, *24*, 1485; (b) Strevel, E. L.; Ing, D. J.; Siu, L. L. *J. Clin. Oncol.* **2007**, *25*, 3362; (c) Subbiah, I. M.; Lenihan, D. J.; Tsimberidou, A. M. *The Oncologist* **2011**, *16*, 1120.
25. (a) Colombel, V.; Joncour, A.; Thoret, S.; Dubois, J.; Bignon, J.; Wdzieczak-Bakala, J.; Baudoin, O. *Tetrahedron Lett.* **2010**, *51*, 3127; (b) Colombel, V.; Baudoin, O. *J. Org. Chem.* **2009**, *74*, 4329; (c) Joncour, A.; Décor, A.; Thoret, S.; Chiaroni, A.;

Baudoin, O. *Angew. Chem. Int. Ed.* **2006**, *45*, 4149; (d) Nicolaus, N.; Strauss, S.; Neudörfl, J.-M.; Prokop, A.; Schmalz, H.-G. *Org. Lett.* **2009**, *11*, 341.
26. Joncour, A.; Liu, J.-M.; Décor, A.; Thoret, S.; Wdzieczak-Bakala, J.; Bignon, J.; Baudoin, O. *ChemMedChem* **2008**, *3*, 1731.
27. Suzuki, H.; Nakamura, K.; Goto, R. *Bull. Chem. Soc. Jpn.* **1966**, *39*, 128.
28. Brown, E.; Robin, J.-P.; Dhal, R. *Tetrahedron* **1982**, *38*, 2569.
29. Ritter, T.; Stanek, K.; Larrosa, I.; Carreira, E. M. *Org. Lett.* **2004**, *6*, 1513.
30. (a) Campeau, L.-C.; Parisien, M.; Leblanc, M.; Fagnou, K. *J. Am. Chem. Soc.* **2004**, *126*, 9186; (b) Leblanc, M.; Fagnou, K. *Org. Lett.* **2005**, *7*, 2849.
31. (a) Campeau, L.-C.; Fagnou, K. *Chem. Commun.* **2006**, 1253; (b) Lafrance, M.; Lapointe, D.; Fagnou, K. *Tetrahedron* **2008**, *64*, 6015; (c) Gorelsky, S. I.; Lapointe, D.; Fagnou, K. *J. Org. Chem.* **2012**, *77*, 658.
32. Cheetham, C. A.; Massey, R. S.; Pira, S. L.; Pritchard, R. G.; Wallace, T. W. *Org. Biomol. Chem.* **2011**, *9*, 1831.
33. Silverberg, L. J.; Dillon, J. L.; Vemishetti, P. *Tetrahedron Lett.* **1996**, *37*, 771.
34. Lawrence, N. J.; McGown, A. T.; Ducki, S.; Hadfield, J. A. *Anti-Cancer Drug Des.* **2000**, *15*, 135.
35. Woods, J. A.; Hadfield, J. A.; Pettit, G. R.; Fox, B. W.; McGown, A. T. *Br. J. Cancer* **1995**, *71*, 705.
36. (a) Edmondson, J. M.; Armstrong, L. S.; Martinez, A. O. *J. Tissue Cult. Methods* **1988**, *11*, 15; (b) Mosmann, T. *J. Immunol. Methods* **1983**, *65*, 55.
37. Nakagawa-Goto, K.; Jung, M. K.; Hamel, E.; Wu, C.-C.; Bastow, K. F.; Brossi, A.; Ohta, S.; Lee, K.-H. *Heterocycles* **2005**, *65*, 541.
38. Boyd, M. R.; Paull, K. D. *Drug Dev. Res.* **1995**, *34*, 91.
39. Shoemaker, R. H. *Nat. Rev. Cancer* **2006**, *6*, 813.
40. Watanabe, T.; Naito, M.; Kokubu N.; Tsuruo, T. *J. Natl. Cancer Inst.* **1997**, *89*, 512.
41. Loganzo, F.; Discafani, C. M.; Annable, T.; Beyer, C.; Musto, S.; Hari, M.; Tan, X.; Hardy, C.; Hernandez, R.; Baxter, M.; Singanallore, T.; Khafizova, G.; Poruchynsky, M. S.; Fojo, T.; Nieman, J. A.; Ayral-Kaloustian, S.; Zask, A.; Andersen, R. J.; Greenberger, L. M. *Cancer Res.* **2003**, *63*, 1838.
42. (a) Paull, K. D.; Shoemaker, R. H.; Hodes, L.; Monks, A.; Scudiero, D. A.; Rubinstein, L.; Plowman, J.; Boyd, M. R. *J. Natl. Cancer. Inst.* **1989**, *81*, 1088; (b) Zaharevitz, D. W.; Holbeck, S. L.; Bowerman, C.; Svetlik, P. A. *J. Mol. Graphics Modell.* **2002**, *20*, 297.
43. Pettit, G. R.; Singh, S. B.; Boyd, M. R.; Hamel, E.; Pettit, R. K.; Schmidt, J. M.; Hogan, F. *J. Med. Chem.* **1995**, *38*, 1666.
44. Paull, K. D.; Lin, C. M.; Malspeis, L.; Hamel, E. *Cancer Res.* **1992**, *52*, 3892.
45. DTP Human Tumour Cell Line Screen, COMPARE methodology: https://dtp.cancer.gov/databases_tools/docs/compare/compare_methodology.htm (last accessed 02/05/2016).
46. (a) Bai, R.; Paull, K. D.; Herald, C. L.; Malspeis, L.; Pettit, G. R.; Hamel, E. *J. Biol. Chem.* **1991**, *266*, 15882; (b) Paull, K. D.; Lin, C. M.; Malspeis, L.; Hamel, E. *Cancer Res.* **1992**, *52*, 3892; (c) Kuo, S.-C.; Lee, H.-Z.; Juang, J.-P.; Lin, Y.-T.; Wu, T.-S.; Chang, J.-J.; Lednicer, D.; Paull, K. D.; Lin, C. M.; Hamel, E.; Lee, K.-H. *J. Med. Chem.* **1993**, *36*, 1146.
47. (a) Hamel, E. *Pharmac. Ther.* **1992**, *55*, 31; (b) Jordan, M. A.; Wilson, L. *Nat. Rev. Cancer* **2004**, *4*, 253; (c) Gigant, B.; Cormier, A.; Dorléans, A.; Ravelli, R. B. G.; Knossow, M. *Top. Curr. Chem.* **2009**, *286*, 259; (d) Elie-Caille, C.; Severin, F.; Helenius, J.; Howard, J.; Muller, D. J.; Hyman, A.A. *Curr. Biol.* **2007**, *17*, 1765.
48. (a) Broady, S. D.; Golden, M. D.; Leonard, J.; Muir, J. C.; Maudet, M. *Tetrahedron Lett.* **2007**, *48*, 4627; (b) Broady, S. D.; Golden, M. D.; Leonard, J.; Muir, J. C.; Billard, A.; Murray, K. WO 2006/067411 A2.
49. For examples, see (a) Gourdeau, H.; Leblond, L.; Hamelin, B.; Desputeau, C.; Dong, K.; Kianicka, I.; Custeau, D.; Boudreau, C.; Geerts, L.; Cai, S.-X.; Drewe, J.; Labrecque, D.; Kasibhatla, S.; Tseng, B. *Mol. Cancer Ther.* **2004**, *3*, 1375; (b) Smith, N. R.; James, N. H.; Oakley, I.; Wainwright, A.; Copley, C.; Kendrew, J.; Womersley, L. M.; Jürgensmeier, J. M.; Wedge, S. R.; Barry, S. T. *Mol. Cancer Ther.* **2007**, *6*, 2198.
50. Gaukroger, K.; Hadfield, J. A.; Lawrence, N. J.; Nolan, S.; McGown, A. T. *Org. Biomol. Chem.* **2003**, *1*, 3033.
51. (a) Blundell, C. D.; Packer, M. J.; Almond, A. *Bioorg. Med. Chem.* **2013**, *21*, 4976; (b) Blundell, C. D.; Nowak, T.; Watson, M. J. *Prog. Med. Chem.* **2016**, *55*, 45.
52. Lessinger, L.; Margulis, T. N. *Acta Cryst.* **1978**, *B34*, 578.
53. Gottlieb, H. E.; Kotlyar, V.; Nudelman, A. *J. Org. Chem.* **1997**, *62*, 7512.
54. Perrin, D. D.; Armarego, W. L. F.; Perrin, D. R. *Purification of Laboratory Chemicals, 2nd Edition*, Pergamon, Oxford, 1980.
55. Still, W. C.; Kahn, M.; Mitra, A. *J. Org. Chem.* **1978**, *43*, 2923.
56. Cotterill, A. S.; Moody, C. J.; Roffey, J. R. A. *Tetrahedron* **1995**, *51*, 7223.
57. Pettit, G. R.; Grealish, M. P.; Herald, D. L.; Boyd, M. R.; Hamel, E.; Pettit, R. K. *J. Med. Chem.* **2000**, *43*, 2731.
58. (a) Azzena, U.; Dettori, G.; Idini, M. V.; Pisano, L.; Sechi, G. *Tetrahedron* **2003**, *59*, 7961; (b) Imperio, D.; Pirali, T.; Galli, U.; Pagliai, F.; Cafici, L.; Canonico, P. L.; Sorba, G.; Genazzani, A. A.; Tron, G. C. *Bioorg. Med. Chem.* **2007**, *15*, 6748.
59. Fletcher, D. A.; McMeeking, R. F.; Parkin, D. *J. Chem. Inf. Comput. Sci.* **1996**, *36*, 746.

Supplementary Material

Tubulin-binding dibenz[*c*,*e*]oxepines. Part 2.[1] Structural variation and biological evaluation as tumour vasculature disrupting agents

Steven B. Rossington,[a] John A. Hadfield,[b] Steven D. Shnyder,[c] Timothy W. Wallace*[a] and Kaye J. Williams[d]

[a]School of Chemistry, University of Manchester, Oxford Road, Manchester M13 9PL, UK

[b]School of Environment and Life Sciences, University of Salford, Salford M5 4WT, UK

[c]Institute of Cancer Therapeutics, University of Bradford, Richmond Road, Bradford BD7 1DP, UK

[d]Manchester Pharmacy School, University of Manchester, Oxford Road, Manchester M13 9PT, UK

*Corresponding author; e-mail: tim.wallace@manchester.ac.uk; fax +44 (0) 161 275 4939

Contents

General Experimental Information

Melting points were determined using Buchi 512 or Stuart Scientific SMP10 equipment and are uncorrected. Unless otherwise indicated, IR spectra were recorded for neat thin films on NaCl plates, using Perkin-Elmer FT-IR Spectrum RX1 or BX spectrometers. NMR spectra were measured using a Bruker Avance III 400 spectrometer and are calibrated by reference to signals from the solvent ($CDCl_3$ at 77.16 ppm and CD_3OD at 49.00 ppm for ^{13}C spectra; residual protium in $CDCl_3$ at 7.26 ppm, CD_3OD at 3.31 ppm and D_2O at 4.79 ppm for ^{1}H spectra).[53] Chemical shifts for ^{19}F and ^{31}P spectra are quoted relative to $CFCl_3$ and 85% H_3PO_4 at 0 ppm respectively. Coupling constants (*J* values) are given in Hz; multiplicities are given as singlet (s), doublet (d), triplet (t), quartet (C), quintet (qn) or multiplet (m). NMR spectra were assigned with the aid of COSY, HMBC, HMQC and DEPT spectra where appropriate. Low-resolution mass spectra were recorded on a Micromass Trio 2000 instrument using the electrospray ionisation method; data for peaks of intensity <20% of that of the base peak are omitted. High-resolution (accurate mass) data were recorded using a Thermo Finnigan MAT95XP instrument. Elemental analyses were carried out by the University of Manchester microanalytical service.

Reactions were routinely carried out under nitrogen. Most reagents and solvents were used as supplied commercially. Anhydrous THF was distilled from sodium - benzophenone ketyl immediately before use.[54] Organic solutions were dried using anhydrous magnesium sulfate and concentrated by rotary evaporation. Analytical thin layer chromatography (TLC) was carried out using Macherey-Nagel Polygram SIL G/UV_{254} plates and the chromatograms were routinely visualised using UV light (254 nm) and alkaline aq. $KMnO_4$. Preparative column (flash) chromatography was carried out on 60H silica gel (Merck 9385) using the flash technique.[55] Compositions of solvent mixtures are quoted as ratios of volume. 'Ether' refers to diethyl ether. 'Petroleum' refers to a fraction of light petroleum, b.p. 60–80 ˚C, unless indicated otherwise.

Section 4.1.5. Preparation of 19 and 20

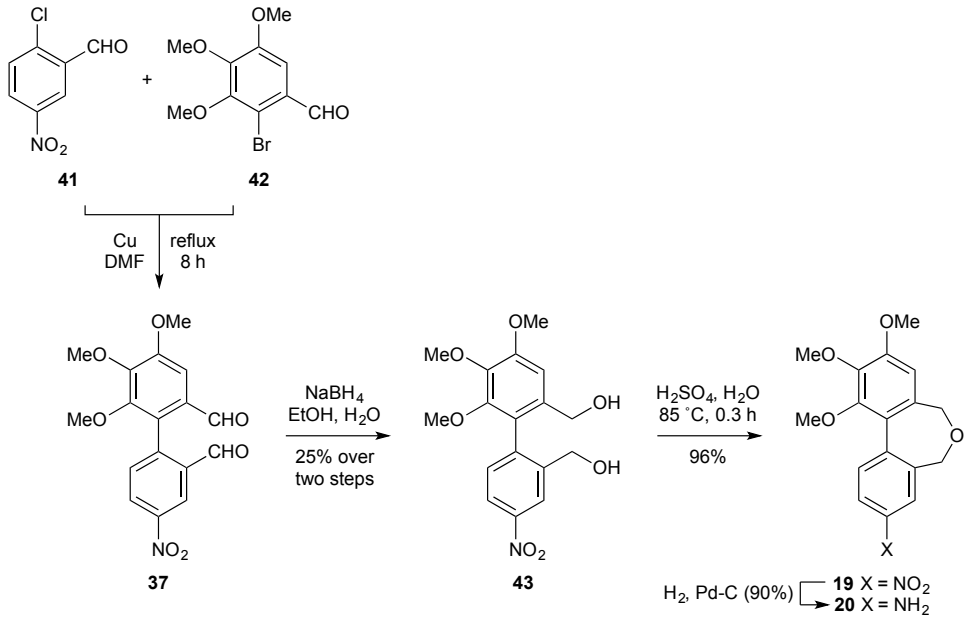

4,5,6-Trimethoxy-4'-nitro-1,1'-biphenyl-2,2'-dimethanol **43**

A mixture of 2-chloro-5-nitrobenzaldehyde **41** (Aldrich; 241.9 mg, 1.30 mmol) and 2-bromo-3,4,5-trimethoxybenzaldehyde **42**[28] (1.00 g, 3.64 mmol) in dry DMF (2 mL) was added to a stirred, boiling suspension of copper bronze (0.91 g, 14.3 mmol) in dry DMF (5 mL) over a period of 30 min. After 8 h TLC (EtOAc - petroleum, 1:4) indicated the consumption of the starting materials. The mixture was cooled, passed through a Celite plug and diluted with toluene, which was distilled off to afford a dark oil. Chromatography (EtOAc - petroleum, 1:2) afforded a sample of 4,5,6-trimethoxy-4'-nitrobiphenyl-2,2'-dicarbaldehyde **37** (259 mg, 57%) containing traces of an unidentified second compound. This sample of **37** (≤0.75 mmol) was dissolved in ethanol (5 mL) and treated with a solution of sodium borohydride (0.2 g, 5.3 mmol) in water (1.5 mL). After stirring for 40 min the mixture was added to 1 M aqueous HCl (20 mL). The precipitated product was collected on a filter, washed with water and recrystallised from ethanol, which gave the *title compound* **43** (113 mg, 25% over two steps) as a white powder which was used directly in the next step.

5,7-Dihydro-1,2,3-trimethoxy-9-nitrodibenz[*c*,*e*]oxepine **19**

4,5,6-Trimethoxy-4'-nitro-1,1'-biphenyl-2,2'-dimethanol **43** (43.7 mg, 0.125 mmol) in 50% v/v aqueous H_2SO_4 (1 mL) was heated in an oil bath of temperature 85 ˚C for 20 min. The mixture was cooled, quenched with ice (6 g) and extracted into chloroform (4 x 2 mL). The extract was dried and concentrated *in vacuo*, giving a dark tan solid. Chromatography (EtOAc - petroleum, 1:2) afforded the *title compound* **19** (39.6 mg,

96%) as a tan solid, m.p. 161 ˚C (MH^+, 332.1122. $C_{17}H_{18}NO_6$ requires 332.1129); ν_{max}/cm^{-1} 2935, 2856, 1597, 1518; δ_H (400 MHz, $CDCl_3$) 3.71 (3 H, s, OMe), 3.95 (3 H, s, OMe), 3.96 (3 H, s, OMe), 3.97–4.03 (1 H, br s, 5-H or 7-H), 4.14–4.23 (1 H, br s, 7-H or 5-H), 4.39–4.48 (1 H, br s, 5-H or 7-H), 4.55–4.64 (1 H, br s, 7-H or 5-H), 6.80 (1 H, s, 4-H), 7.89 (1 H, d, *J* 8.2 Hz, 11-H), 8.28–8.32 (2 H, m, 8-H and 10-H); δ_C (100 MHz, $CDCl_3$) 56.3 (CH_3), 61.28 (CH_3), 61.31 (CH_3), 67.1 (CH_2), 67.7 (CH_2), 109.1 (CH), 123.1 (CH), 124.4 (C), 124.8 (CH), 131.0 (CH), 131.7 (C), 136.4 (C), 142.9 (C), 144.3 (C), 146.9 (C), 151.0 (C), 154.6 (C); *m/z* (CI) 349 (*M*+18, 100%), 332 (*M*+H, 17), 319 (20), 302 (41), 272 (44); R_f 0.54 (EtOAc - petroleum, 1:2).

5,7-Dihydro-9,10,11-trimethoxydibenz[*c*,*e*]oxepin-3-amine **20**
5,7-Dihydro-1,2,3-trimethoxy-9-nitrodibenz[*c*,*e*]oxepine **19** (85.4 mg, 0.258 mmol, 1.0 eq.) in EtOAc (4 mL) containing palladium on charcoal (10% w/w; 7 mg) was stirred under a hydrogen balloon for 24 h until TLC indicated the consumption of starting material. The mixture was passed through a plug of neutral alumina (0.5 cm depth in a Pasteur pipette) and concentrated *in vacuo* to afford the *title compound* **20** (70 mg, 90%) as a yellow crystalline solid, m.p. 145 ˚C (*M*, 301.1305. $C_{17}H_{19}NO_4$ requires 301.1314); ν_{max}/cm^{-1} 3461, 3361, 2938, 2852, 1607, 1482; δ_H (400 MHz, $CDCl_3$) 3.66 (3 H, s, OMe), 3.78 (2 H, br s, NH_2), 3.91 (3 H, s, OMe), 3.94 (3 H, s, OMe), 4.03–4.18 (2 H, br s, 5-H or 7-H), 4.30–4.44 (2 H, br s, 5-H or 7-H), 6.74 (1 H, s, 8-H), 6.745 (1 H, d, *J* 2.5 Hz, 4-H), 6.78 (1 H, dd, *J* 8.2, 2.5 Hz, 2-H), 7.51 (1 H, d, *J* 8.2 Hz, 1-H); δ_C (100 MHz, $CDCl_3$) 56.2 (CH_3), 60.9 (CH_3), 61.2 (CH_3), 67.8 (CH_2), 67.9 (CH_2), 108.8 (CH), 115.0 (CH), 115.9 (CH), 126.9 (C), 127.2 (C), 130.7 (CH), 131.1 (C), 136.3 (C), 142.8 (C), 150.7 (C), 152.5 (C) (1 C unresolved); *m/z* (ES) 301 (*M*, 20%); R_f 0.32 (EtOAc - petroleum, 3:2).

Section 4.2.2. *In vitro* screening against NCI cell lines

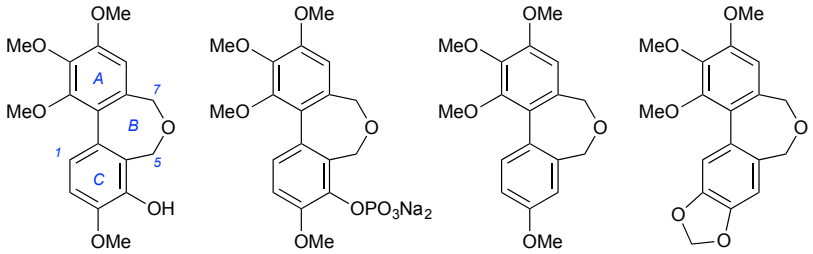

1 **15** **16** **17**

Compounds **1** and **15**–**17** were submitted to the US National Cancer Institute (NIH, Bethesda, Maryland) for screening against the NCI-60 panel of human cancer cell lines, a component of the Developmental Therapeutics Program (DTP). Full details of the methodology for compound testing, data analysis and use of the COMPARE algorithm are available in print[38] and on the NCI website.[45]

Testing: Three dose response parameters are calculated for each compound under test: (i) Growth inhibition of 50% (GI_{50}) is the drug concentration resulting in a 50% reduction in the net protein increase (as measured by sulforhodamine B staining) in control cells during the drug incubation. (ii) The TGI is the drug concentration resulting in total growth inhibition. (iii) The LC_{50} is the concentration of drug resulting in a 50% reduction in the measured protein at the end of the drug treatment, as compared to that at the beginning, indicating a net loss of cells following treatment. Values are calculated for each of these three parameters if the designated level of activity is reached. If the effect is not reached or is exceeded, the value for that parameter is expressed as greater or less than the maximum or minimum concentration tested.

Compounds **1** and **15**–**17** were tested more than once in NCI-60 5-dose assays, and the average data were used in COMPARE analyses. All of these were run with the GI_{50} values as the target-set endpoints and the default settings: Minimum correlation 0.2; count results to return 50; minimum count common cell lines, 40; minimum standard deviation, 0.05. The test results are provided in the complete version of Table 2 which follows.

Table 2. *In vitro* cell growth inhibition data for dibenzoxepines against the NCI-60 panel of human cancer cell lines.

		Cell growth inhibition (GI_{50}, μM)[a]			
Panel	*Cell line*	**1**	**15**	**16**	**17**
Leukaemia	CCRF-CEM	0.04	0.29	0.08	0.35
	HL-60(TB)	0.03	0.32	0.04	0.39
	K-562	0.04	0.28	0.04	0.21
	MOLT-4	0.06	0.40	0.09	0.47
	RPMI-8226	0.32	0.46	0.33	0.50
	SR	0.04	0.19	0.04	0.17
Non-small cell lung	A549/ATCC	0.35	0.42	0.13	0.44
	EKVX	*ND*	0.68	0.60	0.78
	HOP-62	0.63	0.79	1.12	0.69
	HOP-92	0.59	*ND*	>100	7.08
	NCI-H226	3.47	2.82	1.58	2.75
	NCI-H23	0.76	0.71	0.44	0.79
	NCI-H322M	0.52	1.32	2.04	2.00
	NCI-H460	0.31	0.36	0.17	0.38
	NCI-H522	0.04	0.30	0.28	0.39
Colon	COLO205	0.50	0.62	0.11	0.34
	HCC-2998	0.32	0.42	0.22	0.49
	HCT-116	0.32	0.43	0.05	0.37
	HCT-15	0.08	0.44	0.08	0.48
	HT29	*ND*	*ND*	*ND*	*ND*
	KM12	0.05	0.30	0.05	0.36
	SW-620	0.05	0.40	0.05	0.40
CNS	SF-268	0.09	0.79	0.46	1.32
	SF-295	0.27	0.32	0.06	0.33
	SF-539	0.05	0.33	0.16	0.35
	SNB-19	0.14	0.51	0.98	0.68
	SNB-75	0.07	0.54	0.09	0.46
	U251	0.30	0.48	0.10	0.48
Melanoma	LOXIMVI	0.08	0.66	0.21	0.87
	M14	0.05	0.27	0.05	0.23
	MALME-3M	*ND*	2.51	>100	>100
	MDA-MB-435	0.03	0.04	0.03	0.05
	SK-MEL-2	0.26	5.37	0.10	0.56
	SK-MEL-28	1.58	0.89	0.08	*ND*
	SK-MEL-5	0.04	0.26	0.03	0.21
	UACC-257	>100	4.68	>100	3.39
	UACC-62	1.00	5.50	0.08	0.79
Ovarian	IGROV1	0.63	4.07	0.85	0.95
	NCI/ADR-RES	0.05	0.28	0.07	0.36
	OVCAR-3	0.21	0.28	0.05	0.25
	OVCAR-4	0.71	1.29	0.74	2.19
	OVCAR-5	*ND*	*ND*	*ND*	*ND*
	OVCAR-8	0.20	0.42	0.31	0.52
	SK-OV-3	0.07	0.40	0.13	0.47
Renal	786-0	0.43	0.72	0.34	0.50
	A498	3.02	18.6	0.17	0.45
	ACHN	*ND*	*ND*	*ND*	*ND*
	CAKI-1	0.83	0.79	30.2	56.2
	RXF393	0.04	0.21	0.08	0.20
	SN12C	0.21	0.72	0.83	1.05
	TK-10	>100	*ND*	>100	5.13
	UO-31	14.5	19.5	15.1	3.98
Prostate	DU-145	0.06	0.39	0.18	0.37
	PC-3	0.28	0.56	0.48	0.54
Breast	BT-549	0.26	2.24	0.20	0.54
	HS578T	0.04	0.24	0.24	0.43
	MCF7	0.07	0.40	0.04	0.40
	MDA-MB-231/ATCC	0.27	0.71	0.59	1.20
	MDA-MB-468	0.22	1.15	0.03	0.17
	T-47D	33.9	8.51	>100	25.7

[a] GI_{50}: concentration required for 50% cell growth inhibition; *ND* = not determined.

Section 4.2.2. Matrix COMPARE analysis

(i) The dibenzoxepines **1** and **15**–**17** were subjected to a matrix COMPARE analysis[42] together with the colchicinoids **2**–**4** and the combretastatins **6** and **7**. Data for **2**–**4**, **6** and **7** are available in the NCI collection. The results, shown below, provided the source data for Tables 3a and 3b.

			Target vector identity								
			220339	186052	1685	367292	323413	90731	323481	148899	98121
Seed vector identity			**1**	**15**	**16**	**17**	**2**	**3**	**4**	**6**	**7**
220339	NSC:S756015 Endpt:GI50 ExpId:AVGDATA hiConc:-4.0	**1**	**1.00**	**0.81**	**0.84**	**0.79**	**0.50**	**0.43**	**0.44**	**0.40**	**0.58**
	count cell lines seed stdDev target stdDev		60 0.82 0.82	59 0.83 0.52	60 0.82 0.89	60 0.82 0.57	57 0.83 1.04	60 0.82 0.76	59 0.76 0.58	59 0.83 1.28	58 0.84 0.87
186052	NSC:S756016 Endpt:GI50 ExpId:AVGDATA hiConc:-4.0	**15**	**0.81**	**1.00**	**0.66**	**0.73**	**0.50**	**0.48**	**0.33**	**0.43**	**0.53**
	count cell lines seed stdDev target stdDev		59 0.52 0.83	59 0.52 0.52	59 0.52 0.84	59 0.52 0.56	56 0.53 1.04	59 0.52 0.76	58 0.53 0.51	58 0.53 1.28	57 0.53 0.87
1685	NSC:S756013 Endpt:GI50 ExpId:AVGDATA hiConc:-4.0	**16**	**0.84**	**0.66**	**1.00**	**0.86**	**0.53**	**0.42**	**0.62**	**0.31**	**0.40**
	count cell lines seed stdDev target stdDev		60 0.89 0.82	59 0.84 0.52	60 0.89 0.89	60 0.89 0.57	57 0.90 1.04	60 0.89 0.76	59 0.84 0.58	59 0.89 1.28	58 0.90 0.87
367298	NSC:S756014 Endpt:GI50 ExpId:AVGDATA hiConc:-4.0	**17**	**0.79**	**0.73**	**0.87**	**1.00**	**0.52**	**0.45**	**0.45**	**0.31**	**0.38**
	count cell lines seed stdDev target stdDev		60 0.57 0.82	59 0.56 0.52	60 0.57 0.89	60 0.57 0.57	57 0.58 1.04	60 0.57 0.76	59 0.56 0.58	59 0.58 1.28	58 0.57 0.87
323413	NSC:S757 Endpt:GI50 ExpId:AVGDATA hiConc:-4.0	**2**	**0.50**	**0.50**	**0.53**	**0.52**	**1.00**	**0.75**	**0.22**	**0.51**	**0.49**
	count cell lines seed stdDev target stdDev		57 1.04 0.83	56 1.04 0.53	57 1.04 0.90	57 1.04 0.58	68 1.06 1.06	67 1.06 0.83	56 1.04 0.58	68 1.06 1.30	66 1.07 0.95
90731	NSC:S51046 Endpt:GI50 ExpId:AVGDATA hiConc:-4.0	**3**	**0.43**	**0.48**	**0.42**	**0.45**	**0.74**	**1.00**	**0.02**	**0.71**	**0.58**
	count cell lines seed stdDev target stdDev		60 0.76 0.82	59 0.76 0.52	60 0.76 0.89	60 0.76 0.57	67 0.83 1.06	70 0.82 0.82	59 0.76 0.58	69 0.82 1.30	67 0.81 0.96
323481	NSC:S51045 Endpt:GI50 ExpId:AVGDATA hiConc:-4.0	**4**	**0.44**	**0.33**	**0.62**	**0.45**	**0.22**	**0.02**	**1.00**	**-0.01**	**0.12**
	count cell lines seed stdDev target stdDev		59 0.58 0.76	58 0.51 0.53	59 0.58 0.84	59 0.58 0.56	56 0.58 1.04	59 0.58 0.76	59 0.58 0.58	58 0.59 1.29	57 0.59 0.87
148899	NSC:S613729 Endpt:GI50 ExpId:AVGDATA hiConc:-5.0	**6**	**0.40**	**0.43**	**0.31**	**0.31**	**0.51**	**0.71**	**-0.01**	**1.00**	**0.77**
	count cell lines seed stdDev target stdDev		59 1.28 0.83	58 1.28 0.53	59 1.28 0.89	59 1.28 0.57	68 1.30 1.06	69 1.30 0.82	58 1.29 0.59	70 1.29 1.29	68 1.25 0.95
98121	NSC:S645646 Endpt:GI50 ExpId:AVGDATA hiConc:-6.0	**7**	**0.58**	**0.53**	**0.40**	**0.38**	**0.49**	**0.58**	**0.12**	**0.77**	**1.00**
	count cell lines seed stdDev target stdDev		58 0.87 0.84	57 0.87 0.53	58 0.87 0.90	58 0.87 0.57	66 0.95 1.07	67 0.96 0.81	57 0.87 0.59	68 0.95 1.25	68 0.95 0.95

(ii) Using the standard COMPARE protocol, the antiproliferative activity profiles of the **1** and **15**–**17** were compared with those of the NCI standard agents collection of anticancer agents. The analysis was also carried out with **2**–**4**, **6** and **7** as the seeds. The results, shown below, provided the source data for Table 3c.

r value	Seed	Target	Seed vector identity	Target vector identity	Count common cell lines	Seed standard deviation	Target standard deviation
0.567	**1**	vincristine sulfate	NSC:S756015 Endpt:GI50 ExpId:AVGDATA hiConc:-4.0	NSC:S67574 Endpt:GI50 ExpId:AVGDATA hiConc:-3.0	59	0.829	0.648
0.508	**1**	paclitaxel (Taxol)	NSC:S756015 Endpt:GI50 ExpId:AVGDATA hiConc:-4.0	NSC:S125973 Endpt:GI50 ExpId:AVGDATA hiConc:-4.0	60	0.822	0.673
0.507	**1**	maytansine	NSC:S756015 Endpt:GI50 ExpId:AVGDATA hiConc:-4.0	NSC:S153858 Endpt:GI50 ExpId:AVGDATA hiConc:-3.6	47	0.749	0.674
0.502	**1**	glycoxalic acid	NSC:S756015 Endpt:GI50 ExpId:AVGDATA hiConc:-4.0	NSC:S267213 Endpt:GI50 ExpId:AVGDATA hiConc:-2.9	58	0.821	0.213
0.450	**1**	tiazofurin	NSC:S756015 Endpt:GI50 ExpId:AVGDATA hiConc:-4.0	NSC:S286193 Endpt:GI50 ExpId:AVGDATA hiConc:-2.0	58	0.821	0.727
0.444	**1**	vincristine sulfate	NSC:S756015 Endpt:GI50 ExpId:AVGDATA hiConc:-4.0	NSC:S67574 Endpt:GI50 ExpId:AVGDATA hiConc:-5.0	59	0.829	0.964
0.444	**1**	maytansine	NSC:S756015 Endpt:GI50 ExpId:AVGDATA hiConc:-4.0	NSC:S153858 Endpt:GI50 ExpId:AVGDATA hiConc:-8.6	41	0.776	1.592
0.431	**1**	vinblastine sulfate	NSC:S756015 Endpt:GI50 ExpId:AVGDATA hiConc:-4.0	NSC:S49842 Endpt:GI50 ExpId:AVGDATA hiConc:-5.6	60	0.822	0.843
0.429	**1**	rhizoxin	NSC:S756015 Endpt:GI50 ExpId:AVGDATA hiConc:-4.0	NSC:S332598 Endpt:GI50 ExpId:AVGDATA hiConc:-4.3	47	0.749	0.837
0.426	**1**	soluble Baker's Antifol	NSC:S756015 Endpt:GI50 ExpId:AVGDATA hiConc:-4.0	NSC:S139105 Endpt:GI50 ExpId:AVGDATA hiConc:-4.0	57	0.828	1.499
0.419	**1**	AT-125 (acivicin)	NSC:S756015 Endpt:GI50 ExpId:AVGDATA hiConc:-4.0	NSC:S163501 Endpt:GI50 ExpId:AVGDATA hiConc:-4.0	54	0.784	0.436
0.416	**1**	DHAD (mitoxantrone)	NSC:S756015 Endpt:GI50 ExpId:AVGDATA hiConc:-4.0	NSC:S301739 Endpt:GI50 ExpId:AVGDATA hiConc:-4.6	58	0.821	0.696
0.416	**1**	maytansine	NSC:S756015 Endpt:GI50 ExpId:AVGDATA hiConc:-4.0	NSC:S153858 Endpt:GI50 ExpId:AVGDATA hiConc:-7.0	58	0.832	0.720
0.409	**1**	CCNU	NSC:S756015 Endpt:GI50 ExpId:AVGDATA hiConc:-4.0	NSC:S79037 Endpt:GI50 ExpId:AVGDATA hiConc:-3.3	58	0.792	0.504
0.401	**1**	paclitaxel (Taxol)	NSC:S756015 Endpt:GI50 ExpId:AVGDATA hiConc:-4.0	NSC:S125973 Endpt:GI50 ExpId:AVGDATA hiConc:-6.0	60	0.822	0.533
0.400	**1**	largomycin	NSC:S756015 Endpt:GI50 ExpId:AVGDATA hiConc:-4.0	NSC:S237020 Endpt:GI50 ExpId:AVGDATA hiConc:2.6	59	0.829	0.322

0.621	**15**	vincristine sulfate	NSC:S756016 Endpt:GI50 ExpId:AVGDATA hiConc:-4.0	NSC:S67574 Endpt:GI50 ExpId:AVGDATA hiConc:-3.0	58	0.528	0.653
0.558	**15**	maytansine	NSC:S756016 Endpt:GI50 ExpId:AVGDATA hiConc:-4.0	NSC:S153858 Endpt:GI50 ExpId:AVGDATA hiConc:-3.6	46	0.469	0.681
0.535	**15**	maytansine	NSC:S756016 Endpt:GI50 ExpId:AVGDATA hiConc:-4.0	NSC:S153858 Endpt:GI50 ExpId:AVGDATA hiConc:-4.0	58	0.528	0.691
0.502	**15**	vinblastine sulfate	NSC:S756016 Endpt:GI50 ExpId:AVGDATA hiConc:-4.0	NSC:S49842 Endpt:GI50 ExpId:AVGDATA hiConc:-5.6	59	0.524	0.850
0.492	**15**	MX2 HCl	NSC:S756016 Endpt:GI50 ExpId:AVGDATA hiConc:-4.0	NSC:S619003 Endpt:GI50 ExpId:AVGDATA hiConc:-4.0	46	0.469	0.469
0.475	**15**	vinblastine sulfate	NSC:S756016 Endpt:GI50 ExpId:AVGDATA hiConc:-4.0	NSC:S49842 Endpt:GI50 ExpId:AVGDATA hiConc:-4.0	56	0.495	0.587
0.470	**15**	tiazofurin	NSC:S756016 Endpt:GI50 ExpId:AVGDATA hiConc:-4.0	NSC:S286193 Endpt:GI50 ExpId:AVGDATA hiConc:-2.0	57	0.512	0.734
0.462	**15**	maytansine	NSC:S756016 Endpt:GI50 ExpId:AVGDATA hiConc:-4.0	NSC:S153858 Endpt:GI50 ExpId:AVGDATA hiConc:-7.0	57	0.512	0.708
0.453	**15**	rhizoxin	NSC:S756016 Endpt:GI50 ExpId:AVGDATA hiConc:-4.0	NSC:S332598 Endpt:GI50 ExpId:AVGDATA hiConc:-4.3	46	0.469	0.837
0.448	**15**	paclitaxel (Taxol)	NSC:S756016 Endpt:GI50 ExpId:AVGDATA hiConc:-4.0	NSC:S125973 Endpt:GI50 ExpId:AVGDATA hiConc:-6.0	59	0.524	0.531
0.445	**15**	DON	NSC:S756016 Endpt:GI50 ExpId:AVGDATA hiConc:-4.0	NSC:S7365 Endpt:GI50 ExpId:AVGDATA hiConc:-3.6	56	0.489	0.520
0.444	**15**	vincristine sulfate	NSC:S756016 Endpt:GI50 ExpId:AVGDATA hiConc:-4.0	NSC:S67574 Endpt:GI50 ExpId:AVGDATA hiConc:-5.0	58	0.528	0.971
0.441	**15**	AT-125 (acivicin)	NSC:S756016 Endpt:GI50 ExpId:AVGDATA hiConc:-4.0	NSC:S163501 Endpt:GI50 ExpId:AVGDATA hiConc:-4.0	53	0.541	0.428
0.440	**15**	paclitaxel (Taxol)	NSC:S756016 Endpt:GI50 ExpId:AVGDATA hiConc:-4.0	NSC:S125973 Endpt:GI50 ExpId:AVGDATA hiConc:-4.6	59	0.524	0.646
0.435	**15**	S-trityl-L-cysteine	NSC:S756016 Endpt:GI50 ExpId:AVGDATA hiConc:-4.0	NSC:S83265 Endpt:GI50 ExpId:AVGDATA hiConc:-4.0	46	0.472	0.601
0.433	**15**	bispyridocarbazolium DMS	NSC:S756016 Endpt:GI50 ExpId:AVGDATA hiConc:-4.0	NSC:S366241 Endpt:GI50 ExpId:AVGDATA hiConc:-4.0	44	0.472	0.756
0.432	**15**	methotrexate	NSC:S756016 Endpt:GI50 ExpId:AVGDATA hiConc:-4.0	NSC:S740 Endpt:GI50 ExpId:AVGDATA hiConc:-3.6	59	0.524	1.150
0.429	**15**	menogaril	NSC:S756016 Endpt:GI50 ExpId:AVGDATA hiConc:-4.0	NSC:S269148 Endpt:GI50 ExpId:AVGDATA hiConc:-5.0	49	0.490	0.497
0.427	**15**	PALA	NSC:S756016 Endpt:GI50 ExpId:AVGDATA hiConc:-4.0	NSC:S224131 Endpt:GI50 ExpId:AVGDATA hiConc:-2.0	57	0.512	0.727

0.423	**15**	DHAD (mitoxantrone)	NSC:S756016 Endpt:GI50 ExpId:AVGDATA hiConc:-4.0	NSC:S301739 Endpt:GI50 ExpId:AVGDATA hiConc:-4.6	57	0.512	0.698
0.423	**15**	soluble Baker's Antifol	NSC:S756016 Endpt:GI50 ExpId:AVGDATA hiConc:-4.0	NSC:S139105 Endpt:GI50 ExpId:AVGDATA hiConc:-4.0	56	0.516	1.491
0.410	**15**	m-AMSA (amsacrine)	NSC:S756016 Endpt:GI50 ExpId:AVGDATA hiConc:-4.0	NSC:S249992 Endpt:GI50 ExpId:AVGDATA hiConc:-4.0	49	0.490	0.752
0.409	**15**	m-AMSA (amsacrine)	NSC:S756016 Endpt:GI50 ExpId:AVGDATA hiConc:-4.0	NSC:S249992 Endpt:GI50 ExpId:AVGDATA hiConc:-3.8	45	0.483	0.814
0.405	**15**	soluble Baker's Antifol	NSC:S756016 Endpt:GI50 ExpId:AVGDATA hiConc:-4.0	NSC:S139105 Endpt:GI50 ExpId:AVGDATA hiConc:-3.0	57	0.512	1.297
0.402	**15**	pyrazoloacridine	NSC:S756016 Endpt:GI50 ExpId:AVGDATA hiConc:-4.0	NSC:S366140 Endpt:GI50 ExpId:AVGDATA hiConc:-3.2	58	0.528	0.295
0.401	**15**	CCNU	NSC:S756016 Endpt:GI50 ExpId:AVGDATA hiConc:-4.0	NSC:S79037 Endpt:GI50 ExpId:AVGDATA hiConc:-3.3	57	0.488	0.508
0.400	**15**	methotrexate	NSC:S756016 Endpt:GI50 ExpId:AVGDATA hiConc:-4.0	NSC:S740 Endpt:GI50 ExpId:AVGDATA hiConc:-5.0	55	0.494	1.020
0.539	**16**	maytansine	NSC:S756013 Endpt:GI50 ExpId:AVGDATA hiConc:-4.0	NSC:S153858 Endpt:GI50 ExpId:AVGDATA hiConc:-7.0	58	0.892	0.720
0.531	**16**	vincristine sulfate	NSC:S756013 Endpt:GI50 ExpId:AVGDATA hiConc:-4.0	NSC:S67574 Endpt:GI50 ExpId:AVGDATA hiConc:-5.0	59	0.889	0.964
0.528	**16**	vincristine sulfate	NSC:S756013 Endpt:GI50 ExpId:AVGDATA hiConc:-4.0	NSC:S67574 Endpt:GI50 ExpId:AVGDATA hiConc:-3.0	59	0.889	0.648
0.488	**16**	paclitaxel (Taxol)	NSC:S756013 Endpt:GI50 ExpId:AVGDATA hiConc:-4.0	NSC:S125973 Endpt:GI50 ExpId:AVGDATA hiConc:-4.0	60	0.890	0.673
0.467	**16**	vinblastine sulfate	NSC:S756013 Endpt:GI50 ExpId:AVGDATA hiConc:-4.0	NSC:S49842 Endpt:GI50 ExpId:AVGDATA hiConc:-5.6	60	0.890	0.843
0.464	**16**	soluble Baker's Antifol	NSC:S756013 Endpt:GI50 ExpId:AVGDATA hiConc:-4.0	NSC:S139105 Endpt:GI50 ExpId:AVGDATA hiConc:-4.0	57	0.890	1.499
0.462	**16**	cyanomorpholino-ADR	NSC:S756013 Endpt:GI50 ExpId:AVGDATA hiConc:-4.0	NSC:S357704 Endpt:GI50 ExpId:AVGDATA hiConc:-7.7	59	0.889	0.412
0.445	**16**	rhizoxin	NSC:S756013 Endpt:GI50 ExpId:AVGDATA hiConc:-4.0	NSC:S332598 Endpt:GI50 ExpId:AVGDATA hiConc:-4.3	47	0.820	0.837
0.443	**16**	hydrazine sulfate	NSC:S756013 Endpt:GI50 ExpId:AVGDATA hiConc:-4.0	NSC:S150014 Endpt:GI50 ExpId:AVGDATA hiConc:-2.5	57	0.890	0.383
0.440	**16**	paclitaxel (Taxol)	NSC:S756013 Endpt:GI50 ExpId:AVGDATA hiConc:-4.0	NSC:S125973 Endpt:GI50 ExpId:AVGDATA hiConc:-4.6	60	0.890	0.653
0.439	**16**	AT-125 (acivicin)	NSC:S756013 Endpt:GI50 ExpId:AVGDATA hiConc:-4.0	NSC:S163501 Endpt:GI50 ExpId:AVGDATA hiConc:-4.0	54	0.862	0.436

0.437	**16**	paclitaxel (Taxol)	NSC:S756013 Endpt:GI50 ExpId:AVGDATA hiConc:-4.0	NSC:S125973 Endpt:GI50 ExpId:AVGDATA hiConc:-6.0	60	0.890	0.533
0.429	**16**	DUP785 (brequinar)	NSC:S756013 Endpt:GI50 ExpId:AVGDATA hiConc:-4.0	NSC:S368390 Endpt:GI50 ExpId:AVGDATA hiConc:-2.3	57	0.890	0.955
0.417	**16**	tiazofurin	NSC:S756013 Endpt:GI50 ExpId:AVGDATA hiConc:-4.0	NSC:S286193 Endpt:GI50 ExpId:AVGDATA hiConc:-2.0	58	0.883	0.727
0.413	**16**	maytansine	NSC:S756013 Endpt:GI50 ExpId:AVGDATA hiConc:-4.0	NSC:S153858 Endpt:GI50 ExpId:AVGDATA hiConc:-3.6	47	0.820	0.674
0.404	**16**	maytansine	NSC:S756013 Endpt:GI50 ExpId:AVGDATA hiConc:-4.0	NSC:S153858 Endpt:GI50 ExpId:AVGDATA hiConc:-8.6	41	0.859	1.592
0.402	**16**	methotrexate	NSC:S756013 Endpt:GI50 ExpId:AVGDATA hiConc:-4.0	NSC:S740 Endpt:GI50 ExpId:AVGDATA hiConc:-3.6	60	0.890	1.150
0.599	**17**	paclitaxel (Taxol)	NSC:S756014 Endpt:GI50 ExpId:AVGDATA hiConc:-4.0	NSC:S125973 Endpt:GI50 ExpId:AVGDATA hiConc:-4.0	60	0.568	0.673
0.563	**17**	maytansine	NSC:S756014 Endpt:GI50 ExpId:AVGDATA hiConc:-4.0	NSC:S153858 Endpt:GI50 ExpId:AVGDATA hiConc:-7.0	58	0.570	0.720
0.559	**17**	vincristine sulfate	NSC:S756014 Endpt:GI50 ExpId:AVGDATA hiConc:-4.0	NSC:S67574 Endpt:GI50 ExpId:AVGDATA hiConc:-3.0	59	0.567	0.648
0.520	**17**	rhizoxin	NSC:S756014 Endpt:GI50 ExpId:AVGDATA hiConc:-4.0	NSC:S332598 Endpt:GI50 ExpId:AVGDATA hiConc:-4.3	47	0.507	0.837
0.499	**17**	vincristine sulfate	NSC:S756014 Endpt:GI50 ExpId:AVGDATA hiConc:-4.0	NSC:S67574 Endpt:GI50 ExpId:AVGDATA hiConc:-5.0	59	0.567	0.964
0.498	**17**	paclitaxel (Taxol)	NSC:S756014 Endpt:GI50 ExpId:AVGDATA hiConc:-4.0	NSC:S125973 Endpt:GI50 ExpId:AVGDATA hiConc:-4.6	60	0.568	0.653
0.479	**17**	vinblastine sulfate	NSC:S756014 Endpt:GI50 ExpId:AVGDATA hiConc:-4.0	NSC:S49842 Endpt:GI50 ExpId:AVGDATA hiConc:-5.6	60	0.568	0.843
0.473	**17**	paclitaxel (Taxol)	NSC:S756014 Endpt:GI50 ExpId:AVGDATA hiConc:-4.0	NSC:S125973 Endpt:GI50 ExpId:AVGDATA hiConc:-6.0	60	0.568	0.533
0.472	**17**	soluble Baker's Antifol	NSC:S756014 Endpt:GI50 ExpId:AVGDATA hiConc:-4.0	NSC:S139105 Endpt:GI50 ExpId:AVGDATA hiConc:-4.0	57	0.557	1.499
0.468	**17**	vinblastine sulfate	NSC:S756014 Endpt:GI50 ExpId:AVGDATA hiConc:-4.0	NSC:S49842 Endpt:GI50 ExpId:AVGDATA hiConc:-4.0	57	0.463	0.583
0.427	**17**	maytansine	NSC:S756014 Endpt:GI50 ExpId:AVGDATA hiConc:-4.0	NSC:S153858 Endpt:GI50 ExpId:AVGDATA hiConc:-8.6	41	0.528	1.592
0.421	**17**	hydrazine sulfate	NSC:S756014 Endpt:GI50 ExpId:AVGDATA hiConc:-4.0	NSC:S150014 Endpt:GI50 ExpId:AVGDATA hiConc:-2.5	57	0.557	0.383
0.419	**17**	trimetrexate	NSC:S756014 Endpt:GI50 ExpId:AVGDATA hiConc:-4.0	NSC:S352122 Endpt:GI50 ExpId:AVGDATA hiConc:-6.0	53	0.557	1.448

0.418	**17**	paclitaxel (Taxol)	NSC:S756014 Endpt:GI50 ExpId:AVGDATA hiConc:-4.0	NSC:S125973 Endpt:GI50 ExpId:AVGDATA hiConc:-5.0	60	0.568	0.652
0.416	**17**	DUP785 (brequinar)	NSC:S756014 Endpt:GI50 ExpId:AVGDATA hiConc:-4.0	NSC:S368390 Endpt:GI50 ExpId:AVGDATA hiConc:-2.3	57	0.557	0.955
0.415	**17**	maytansine	NSC:S756014 Endpt:GI50 ExpId:AVGDATA hiConc:-4.0	NSC:S153858 Endpt:GI50 ExpId:AVGDATA hiConc:-4.0	59	0.567	0.687
0.408	**17**	methotrexate	NSC:S756014 Endpt:GI50 ExpId:AVGDATA hiConc:-4.0	NSC:S740 Endpt:GI50 ExpId:AVGDATA hiConc:-3.6	60	0.568	1.150
0.406	**17**	maytansine	NSC:S756014 Endpt:GI50 ExpId:AVGDATA hiConc:-4.0	NSC:S153858 Endpt:GI50 ExpId:AVGDATA hiConc:-3.6	47	0.507	0.674
0.404	**17**	methotrexate	NSC:S756014 Endpt:GI50 ExpId:AVGDATA hiConc:-4.0	NSC:S740 Endpt:GI50 ExpId:AVGDATA hiConc:-5.0	56	0.541	1.036
0.784	**2**	vincristine sulfate	NSC:S757 Endpt:GI50 ExpId:AVGDATA hiConc:-4.0	NSC:S67574 Endpt:GI50 ExpId:AVGDATA hiConc:-3.0	68	1.055	0.654
0.750	**2**	vinblastine sulfate	NSC:S757 Endpt:GI50 ExpId:AVGDATA hiConc:-4.0	NSC:S49842 Endpt:GI50 ExpId:AVGDATA hiConc:-5.6	68	1.055	0.836
0.738	**2**	rhizoxin	NSC:S757 Endpt:GI50 ExpId:AVGDATA hiConc:-4.0	NSC:S332598 Endpt:GI50 ExpId:AVGDATA hiConc:-4.3	54	0.92	0.933
0.546	**2**	pancratistatin	NSC:S757 Endpt:GI50 ExpId:AVGDATA hiConc:-4.0	NSC:S349156 Endpt:GI50 ExpId:AVGDATA hiConc:-6.0	49	1.021	0.135
0.543	**2**	paclitaxel (Taxol)	NSC:S757 Endpt:GI50 ExpId:AVGDATA hiConc:-4.0	NSC:S125973 Endpt:GI50 ExpId:AVGDATA hiConc:-4.6	66	1.067	0.594
0.758	**2**	maytansine	NSC:S757 Endpt:GI50 ExpId:AVGDATA hiConc:-4.0	NSC:S153858 Endpt:GI50 ExpId:AVGDATA hiConc:-9.0	54	0.92	0.96
0.806	**3**	vincristine sulfate	NSC:S51046 Endpt:GI50 ExpId:AVGDATA hiConc:-4.0	NSC:S67574 Endpt:GI50 ExpId:AVGDATA hiConc:-3.0	69	0.823	0.651
0.886	**3**	vinblastine sulfate	NSC:S51046 Endpt:GI50 ExpId:AVGDATA hiConc:-4.0	NSC:S49842 Endpt:GI50 ExpId:AVGDATA hiConc:-4.0	58	0.716	0.578
0.826	**3**	rhizoxin	NSC:S51046 Endpt:GI50 ExpId:AVGDATA hiConc:-4.0	NSC:S332598 Endpt:GI50 ExpId:AVGDATA hiConc:-4.0	68	0.721	0.464
0.400	**3**	pancratistatin	NSC:S51046 Endpt:GI50 ExpId:AVGDATA hiConc:-4.0	NSC:S349156 Endpt:GI50 ExpId:AVGDATA hiConc:-6.0	49	0.791	0.135
0.360	**3**	paclitaxel (Taxol)	NSC:S51046 Endpt:GI50 ExpId:AVGDATA hiConc:-4.0	NSC:S125973 Endpt:GI50 ExpId:AVGDATA hiConc:-4.6	68	0.827	0.653
0.873	**3**	maytansine	NSC:S51046 Endpt:GI50 ExpId:AVGDATA hiConc:-4.0	NSC:S153858 Endpt:GI50 ExpId:AVGDATA hiConc:-4.0	69	0.823	0.693
0.405	**4**	vincristine sulfate	NSC:S51045 Endpt:GI50 ExpId:AVGDATA	NSC:S67574 Endpt:GI50 ExpId:AVGDATA	58	0.586	0.97

			hiConc:-4.0	hiConc:-5.0			
0.286	**4**	vinblastine sulfate	NSC:S51045 Endpt:GI50 ExpId:AVGDATA hiConc:-4.0	NSC:S49842 Endpt:GI50 ExpId:AVGDATA hiConc:-7.6	46	0.64	0.77
0.378	**4**	rhizoxin	NSC:S51045 Endpt:GI50 ExpId:AVGDATA hiConc:-4.0	NSC:S332598 Endpt:GI50 ExpId:AVGDATA hiConc:-4.3	46	0.641	0.843
0.494	**4**	paclitaxel (Taxol)	NSC:S51045 Endpt:GI50 ExpId:AVGDATA hiConc:-4.0	NSC:S125973 Endpt:GI50 ExpId:AVGDATA hiConc:-4.6	59	0.584	0.658
0.468	**4**	maytansine	NSC:S51045 Endpt:GI50 ExpId:AVGDATA hiConc:-4.0	NSC:S153858 Endpt:GI50 ExpId:AVGDATA hiConc:-3.6	46	0.641	0.68
0.577	**6**	vincristine sulfate	NSC:S613729 Endpt:GI50 ExpId:AVGDATA hiConc:-5.0	NSC:S67574 Endpt:GI50 ExpId:AVGDATA hiConc:-3.0	70	1.292	0.647
0.643	**6**	vinblastine sulfate	NSC:S613729 Endpt:GI50 ExpId:AVGDATA hiConc:-5.0	NSC:S49842 Endpt:GI50 ExpId:AVGDATA hiConc:-4.0	58	1.239	0.578
0.635	**6**	rhizoxin	NSC:S613729 Endpt:GI50 ExpId:AVGDATA hiConc:-5.0	NSC:S332598 Endpt:GI50 ExpId:AVGDATA hiConc:-9.0	65	1.206	0.714
0.541	**6**	pancratistatin	NSC:S613729 Endpt:GI50 ExpId:AVGDATA hiConc:-5.0	NSC:S349156 Endpt:GI50 ExpId:AVGDATA hiConc:-6.0	49	1.266	0.135
0.674	**6**	maytansine	NSC:S613729 Endpt:GI50 ExpId:AVGDATA hiConc:-5.0	NSC:S153858 Endpt:GI50 ExpId:AVGDATA hiConc:-4.0	70	1.292	0.689
0.382	**6**	actinomycin D	NSC:S613729 Endpt:GI50 ExpId:AVGDATA hiConc:-5.0	NSC:S3053 Endpt:GI50 ExpId:AVGDATA hiConc:-5.6	62	1.222	0.518
0.503	**7**	vincristine sulfate	NSC:S645646 Endpt:GI50 ExpId:AVGDATA hiConc:-6.0	NSC:S67574 Endpt:GI50 ExpId:AVGDATA hiConc:-3.0	68	0.95	0.656
0.439	**7**	vinblastine sulfate	NSC:S645646 Endpt:GI50 ExpId:AVGDATA hiConc:-6.0	NSC:S49842 Endpt:GI50 ExpId:AVGDATA hiConc:-5.6	68	0.95	0.87
0.585	**7**	rhizoxin	NSC:S645646 Endpt:GI50 ExpId:AVGDATA hiConc:-6.0	NSC:S332598 Endpt:GI50 ExpId:AVGDATA hiConc:-4.0	67	0.952	0.448
0.593	**7**	pancratistatin	NSC:S645646 Endpt:GI50 ExpId:AVGDATA hiConc:-6.0	NSC:S349156 Endpt:GI50 ExpId:AVGDATA hiConc:-6.0	48	0.969	0.136
0.447	**7**	maytansine	NSC:S645646 Endpt:GI50 ExpId:AVGDATA hiConc:-6.0	NSC:S153858 Endpt:GI50 ExpId:AVGDATA hiConc:-4.0	68	0.95	0.67
0.419	**7**	maytansine	NSC:S645646 Endpt:GI50 ExpId:AVGDATA hiConc:-6.0	NSC:S153858 Endpt:GI50 ExpId:AVGDATA hiConc:-3.6	54	0.917	0.653
0.465	**7**	pancratistatin	NSC:S645646 Endpt:GI50 ExpId:AVGDATA hiConc:-6.0	NSC:S349156 Endpt:GI50 ExpId:AVGDATA hiConc:-4.0	68	0.95	0.621

[a] Correlation (*r*) values are Pearson's correlation coefficients based on a comparison of the NCI GI_{50} mean graphs for each compound.[38]

Section 4.2.3. *In vivo* antivascular effects of 15

Results: The amount of functional vascular elements (as determined by the incorporation of the Hoechst 33342 dye into the nuclei of functioning endothelial cells) was significantly affected by administration of both **15** and **21** in all animals examined 1 h after administration. This persisted throughout the 24-h study period for **21**, whereas for **15** recovery of vasculature was seen from 4 h post dose (Figure 1, Table 4.2.3.1, and the representative images in Figure 3). Whilst there is a decrease again at 24 h for **15** from 4 h, it is not to the same extent as seen for **21** at 24 h compared with 4 h. Histological evaluation of haematoxylin and eosin stained sections showed a notable increase in the amount of necrosis in the DLD-1 tumours at 24 h post-administration for both compounds (Figure 2, Table 4.2.3.2, and the representative images in Figure 4).

Conclusions
Compound **15** is well tolerated when administered intravenously at 400 mg kg^{-1} in a multiple-dose schedule. Both **15** and **21** induce vascular shutdown 1 h after treatment when administered as a single intravenous dose of 400 mg kg^{-1}, with tumour necrosis evident after 24 h.

Table 4.2.3.1 Summary of % vascular element counts seen in DLD-1 human colon adenocarcinoma xenografts following a single intravenous dose of **15** or **21** at 400 mg kg^{-1} (data used for Figure 1).

	% vascular element counts						
		15			21		
	Untreated	1 h post-dose	4 h post-dose	24 h post-dose	1 h post-dose	4 h post-dose	24 h post-dose
Tumour 1	7.30	0.55	1.35	1.80	0.00	0.08	1.06
Tumour 2	2.20	0.41	1.52	0.91	0.02	0.22	0.10
Tumour 3	1.70	0.04	3.02	0.14	0.07	0.06	0.10
Mean ± SD	3.73 ± 3.10	0.33 ± 0.26	1.96 ± 0.92	0.95 ± 0.83	0.03 ± 0.06	0.12 ± 0.09	0.42 ± 0.55

Table 4.2.3.2 Summary of % necrotic area counts seen in DLD-1 human colon adenocarcinoma xenografts following a single intravenous dose of **15** or **21** at 400 mg kg^{-1} (data used for Figure 2)

	% necrotic area counts						
		15			21		
	Untreated	1 h post-dose	4 h post-dose	24 h post-dose	1 h post-dose	4 h post-dose	24 h post-dose
Tumour 1	8.5	33.3	24.1	73.6	28.5	18.9	78.3
Tumour 2	27.4	39.6	29.0	97.5	39.5	39.3	98.6
Tumour 3	21.2	8.4	24.9	51.1	1.6	8.6	96.2
Mean ± SD	19.0 ± 9.6	27.1 ± 16.5	26.0 ± 2.6	74.1 ± 23.2	23.2 ± 19.5	22.3 ± 15.6	91.0 ± 11.1

Section 4.2.5. Dynamic 3D-solution structure of 1

The methodology of Blundell *et al.*[51] was used to analyse the conformational dynamics of dibenzoxepine **1** in dilute aqueous solution, as described below.

(i) *Data acquisition*

Solutions of **1** (1.0 mM) in 2% (v/v) d_6-DMSO, 98% D_2O at 25 ˚C (0.3 mM d_6-DSS internal reference) were analysed by NMR spectroscopy (Bruker DRX-600, Topspin 1.3; ^1H at 600 MHz, ^{13}C at 151 MHz) using the [^1H]-1D, [^1H,^{13}C]-HSQC, [^1H,^{13}C]-HMBC and [^1H,^1H]-ROESY experiments. Comparison of the [^1H]-1D-NMR spectrum with that obtained with 0.05 mM **1** in 0.1% d_6-DMSO, 99.9% (v/v) D_2O at 25 ˚C showed no significant chemical shift differences (<0.1 ppm) due to the increase in solute concentration, indicating that no aggregation or multimerisation was occurring in the range 0.05–1.0 mM. It was concluded that the conformational properties of **1** at the higher concentration would be indistinguishable from those present under the more dilute conditions.

(ii) *Chemical shift assignments*

All of the ^1H and ^{13}C atoms in **1** were unambiguously assigned using [^1H]-1D, [^1H,^{13}C]-HSQC and [^1H,^{13}C]-HMBC spectra (Table 4.2.5.1). Broadened resonances observed in the [^1H]-1D spectra, assigned to H51, H52, H71 and H72, indicated that the oxepane ring exists as a mixture of two atropisomers (necessarily 50:50).

Table 4.2.5.1. Chemical shifts for **1**.

Atom[a]	δ_C / ppm[b]	Atom[a]	δ_H / ppm[c]
C1	123.825	H1	7.203
C2	114.924	H2	7.179
C3	149.865	H3	3.950
C3M	58.910	HO4	n/a
C4	146.038	H51/52[d]	5.096/3.827
C4A	124.080	H71/72[d]	4.491/3.987
C5	61.801	H8	7.035
C7	69.613	H9	3.943
C7A	133.669	H10	3.917
C8	112.386	H11	3.646
C9	155.300		
C9M	58.852		
C10	144.658		
C10M	64.014		
C11	152.330		
C11M	63.763		
C11A	129.112		
C11B	132.743		

[a]Refer to Figure 4.2.5.1 for atom designations.
[b]Std. error ±0.020 ppm.
[c]Std. error ±0.001 ppm.
[d]While the upfield-shifted resonance is clearly from the proton lying in the face of the adjacent aromatic ring, these protons cannot be individually assigned because the central oxepane ring is in intermediate exchange between two atropoisomers; in one form the pro-*R* proton is in the face of aromatic ring, while in the other it is the pro-*S* proton.

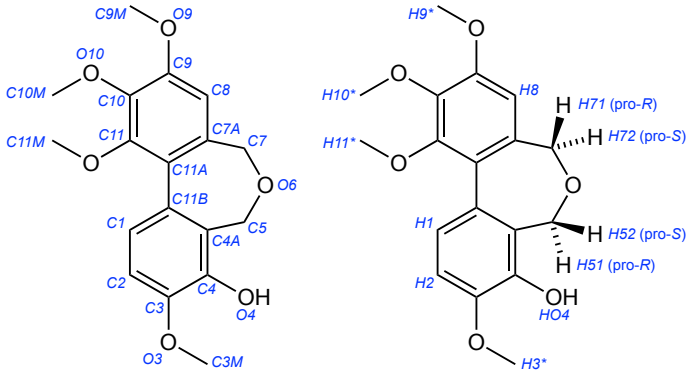

(a) Heavy atoms (b) Hydrogen atoms

Figure 4.2.5.1. Numbering system used for **1**. Degenerate hydrogen nuclei in methyl groups are indicated with an asterisk.

(iii) *Dynamic 3D-structure of **1***

The molecule **1** has five single bonds with geometry that is not predetermined by local orbitals, and whose conformations affect the overall 3D-shape of the molecule. In addition, the oxepane ring can adopt alternative puckered conformations that are rigidly defined (the broadened resonances seen for H51, H52, H71 and H72 indicates that these two ring conformations are atropoisomers). The molecule thus incorporates six degrees of freedom (Figure 4.2.5.2 and Table 4.2.5.2).

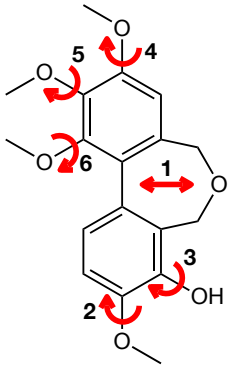

Figure 4.2.5.2. Molecular degrees of freedom within **1** that affect the conformation of the molecule. Each degree of freedom is defined as shown in Table 4.2.5.2.

Table 4.2.5.2. Definitions of molecular degrees of freedom in **1**.

Degree of freedom[a]	**Atoms defining ring puckering**
1	C4A-C5-O6-C7-C11A-C11B dihedral reported for: C7A-C11A-C11B-C4A
	Atoms defining rotatable bond dihedral angles
2	C2-C3-O3-C3M
3	C3-C4-O4-HO4
4	C8-C9-O9-C9M
5	C9-C10-O10-C10M
6	C10-C11-O11-C11M

[a]Degree of freedom numbers are as defined in Figure 4.2.5.2.

In total, 29 experimentally-determined structural restraints were used to assess the dynamic 3D-structure of **1**. Since the two atropisomers have a geometry defined by the local chemical bonds, there were therefore only 5 unknown degrees of freedom, giving a mean value of 5.8 restraints per unknown degree of freedom.

(iv) *Conformetrics*[51]

The results of the analysis of the dynamic 3D-structure of **1** in aqueous solution are given in Table 4.2.5.3. The number of conformers adopted by each rotatable bond and their relative occupancies were determined. For each adopted conformer, its mean dihedral angle and librational amplitude was measured. Notes on the behaviour of each bond are provided below.

Table 4.2.5.3. Experimentally-determined conformetrics for **1** in aqueous solution.

Degree of freedom no.[a]	Conformation[b]	Mean angle / pucker conformation	Occupancy[c]
1	1	45˚	0.50
	2	–45˚	0.50
2	1	136 ± 4˚	0.50
	2	–136 ± 4˚	0.50
3	1	108 ± 20˚	0.50
	2	–108 ± 20˚	0.50
4	1	139 ± 5˚	0.50
	2	–139 ± 5˚	0.50
5	1	142 ± 20˚	0.50
	2	–142 ± 20˚	0.50
6	1 (1-1)[e]	78 ± 3˚	0.50
	2 (1-2)[e]	–78 ± 3˚	0.50

[a]Degrees of freedom and their associated dihedral angles are as defined in Figure 4.2.5.2 and Table 4.2.5.2.

[b]Conformers are classified as distinct if rotation of the bond between the two conformers passes through a van der Waals maximum.

[c]The occupancy of each conformer is expressed as a proportion of the total for that bond.

[d]The conformation of bond 6 depends upon the oxepane ring conformation.

- *Oxepane ring conformation*: This ring is in intermediate exchange between two symmetric atropisomers. The dihedral angle is that for C4A-C11B-C11A-C7A.
- *Bonds 2, 4, 5*: Each methoxyl group can adopt two symmetrical conformers that are independent of the oxepane ring conformation and each other.
- *Bond 3*: The dihedral angle for the hydroxyl is poorly defined because the 4OH proton is not directly observable in aqueous solution. However, it clearly adopts two symmetrical conformers about the adjacent aromatic and oxepane rings.
- *Bond 6*: The conformation of this bond depends on the oxepane conformation, preferring a particular orientation for each alternative conformer.

(v) *Conformers*

Using the data from Table 4.2.5.3, it is possible to calculate the number of distinct conformers in aqueous solution that **1** naturally explores; within each of these the molecule will be seen to be librating. As shown in Table 4.2.5.3 and Figure 4.2.5.3, the dynamic 3D-structure of **1** can be considered to be a set of 32 distinct conformers, which is arrived at by the simple permutation of all the independent conformers for each bond/degree of freedom. The occupancies of these conformers are calculated to be equal. The conformational preference of bond 6 is linked to the oxepane conformation: C5 and C11M tend to be proximal.

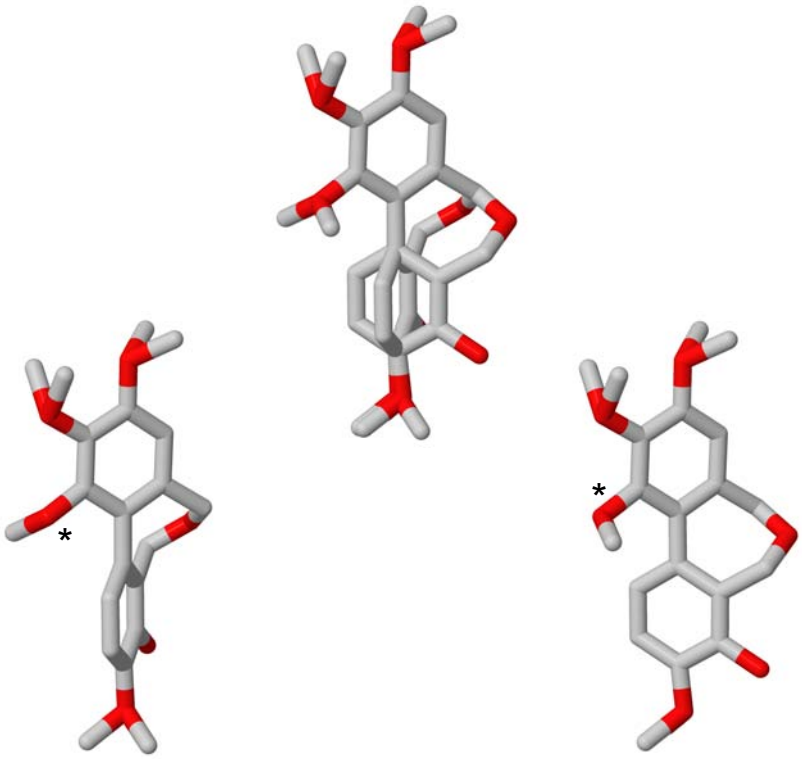

Figure 4.2.5.3. Idealised conformers adopted by **1** in aqueous solution, overlaid on atoms C11A, C8 and C10. Top: all 32 idealised conformers. Bottom: these 32 conformers can be classified into two pseudo-symmetrical sets of 16 conformers each according to the oxepane ring pucker. C atoms are shown in grey and O in red; H atoms have been omitted for clarity.

(vi) *Conformational libration of **1***

The aqueous solution structure of **1** can represented by an ensemble of 3D-structures in which the distribution of conformations accurately reflects the measured conformetrics listed in Table 4.2.5.3. This ensemble reveals conformations explored away from the mean values *via* librational motions. The ensemble representation of **1** is shown in Figure 5a.

(vii) *Overlay of **1** with DAMA-colchicine (Figure 5b)*

The DAMA-colchicine:αβ-tubulin:RB3 (1SA0) crystal structure[20a] contains two molecules of DAMA-colchicine **38**, identified as residues [CN2]700 and [CN2]701, each located within a β-subunit at the αβ-interface of a tubulin heterodimer. Comparative models with **1** bound in each of these sites in place of **38** were generated using *PyMOL*.[60] Figure 5b shows the closest matching preferred solution conformer of **1** fitted to the [CN2]701 site superimposed on the colchicinoid [CN2]701 itself, with alignment on the conserved atoms of the respective trimethoxyaryl rings. It is noted that both of the bound conformations of **38** are implausible, the tropolone rings having incorrect bond lengths and angles. Upon minimisation, O3 moves by 1.3 Å, O4 by 1.0 Å and C3M by 1.9 Å. These deviations are not trivial and suggest that the bound conformation of DAMA-colchicine **38** in 1SA0 retains some ring puckering and flexibility in the bound state.

(viii) *Overlay of **1** and **6** with colchicine **3** (Figure 5c)*

The conformation of combretastatin A-4 **6** bound to the [CN2]700 site of 1SA0 was modelled and is shown in Figure 5c as an overlay, together with **1**, on the crystal structure of colchicine **3**,[52] with alignment of the respective trimethoxyaryl rings.

REFERENCES

1. Edwards, D. J.; Hadfield, J. A.; Wallace, T. W.; Ducki, S. *Org. Biomol. Chem.* **2011**, *9*, 219.
9. (a) Davis, P. D.; Dougherty, G. J.; Blakey, D. C.; Galbraith, S. M.; Tozer, G. M.; Holder, A. L.; Naylor, M. A.; Nolan, J.; Stratford, M. R.; Chaplin, D. J.; Hill, S. A. *Cancer Res.* **2002**, *62*, 7247.
20. (a) Ravelli, R. B. G.; Gigant, B.; Curmi, P. A.; Jourdain, I.; Lachkar, S.; Sobel, A.; Knossow, M. *Nature* **2004**, *428*, 198.
28. Brown, E.; Robin, J.-P.; Dhal, R. *Tetrahedron* **1982**, *38*, 2569.
38. Boyd, M. R.; Paull, K. D. *Drug Dev. Res.* **1995**, *34*, 91.
42. (a) Paull, K. D.; Shoemaker, R. H.; Hodes, L.; Monks, A.; Scudiero, D. A.; Rubinstein, L.; Plowman, J.; Boyd, M. R. *J. Natl. Cancer. Inst.* **1989**, *81*, 1088; (b) Zaharevitz, D. W.; Holbeck, S. L.; Bowerman, C.; Svetlik, P. A. *J. Mol. Graphics Modell.* **2002**, *20*, 297.
45. DTP Human Tumour Cell Line Screen, COMPARE methodology: https://dtp.cancer.gov/databases_tools/docs/compare/compare_methodology.htm (last accessed 02/05/2016).
48. (a) Broady, S. D.; Golden, M. D.; Leonard, J.; Muir, J. C.; Maudet, M. *Tetrahedron Lett.* **2007**, *48*, 4627; (b) Broady, S. D.; Golden, M. D.; Leonard, J.; Muir, J. C.; Billard, A.; Murray, K. WO 2006/067411 A2.
51. (a) Blundell, C. D.; Packer, M. J.; Almond, A. *Bioorg. Med. Chem.* **2013**, *21*, 4976; (b) Blundell, C. D.; Nowak, T.; Watson, M. J. *Prog. Med. Chem.* **2016**, *55*, 45.
52. Lessinger, L.; Margulis, T. N. *Acta Cryst.* **1978**, *B34*, 578.
53. Gottlieb, H. E.; Kotlyar, V.; Nudelman, A. *J. Org. Chem.* **1997**, *62*, 7512.
54. Perrin, D. D.; Armarego, W. L. F.; Perrin, D. R. *Purification of Laboratory Chemicals, 2nd Edition*, Pergamon, Oxford, 1980.
55. Still, W. C.; Kahn, M.; Mitra, A. *J. Org. Chem.* **1978**, *43*, 2923.
60. The PyMOL Molecular Graphics System, Schrödinger, LLC.

NMR spectrum of 15

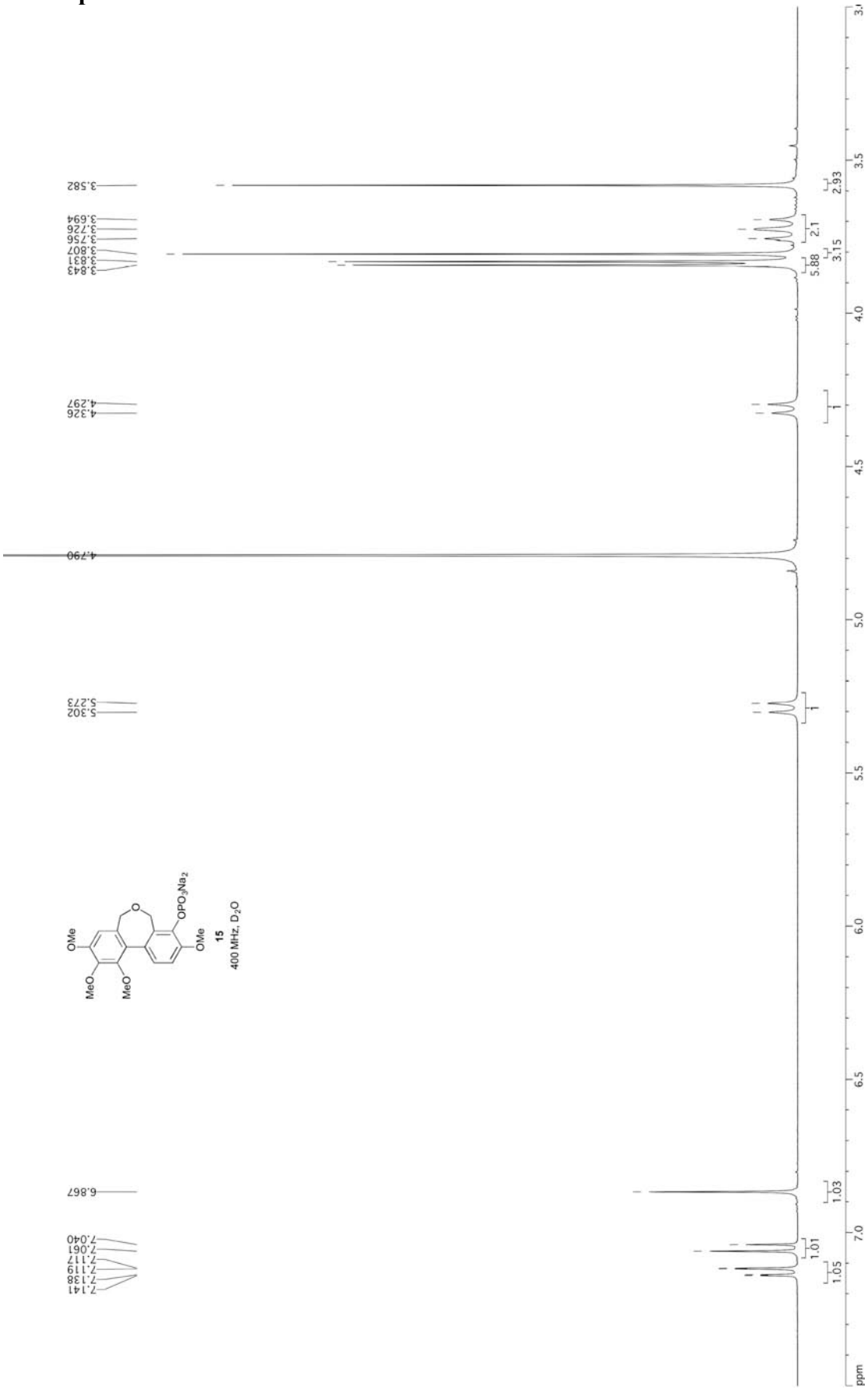

NMR spectrum of 18

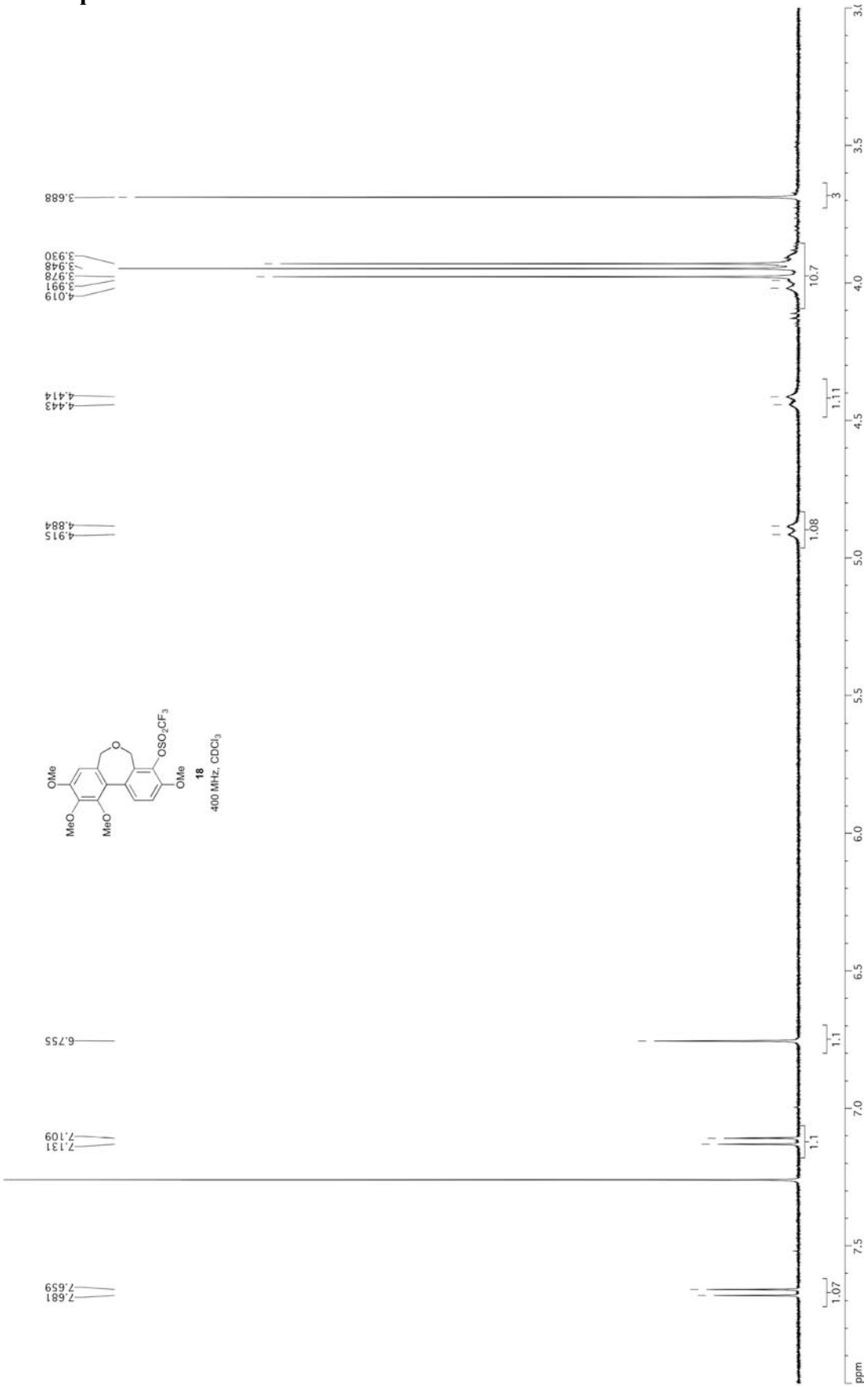

NMR spectrum of 19

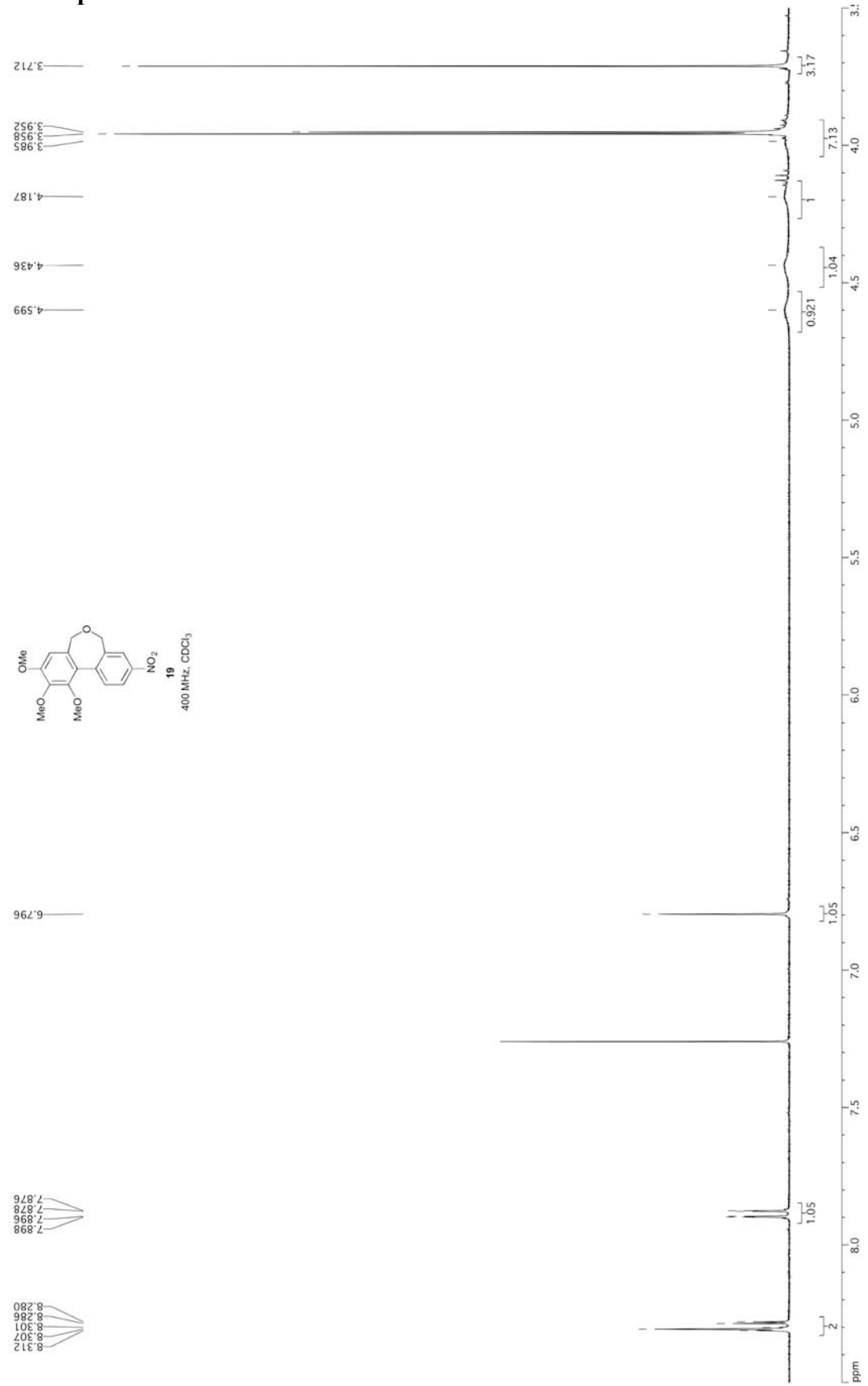

NMR spectrum of 20

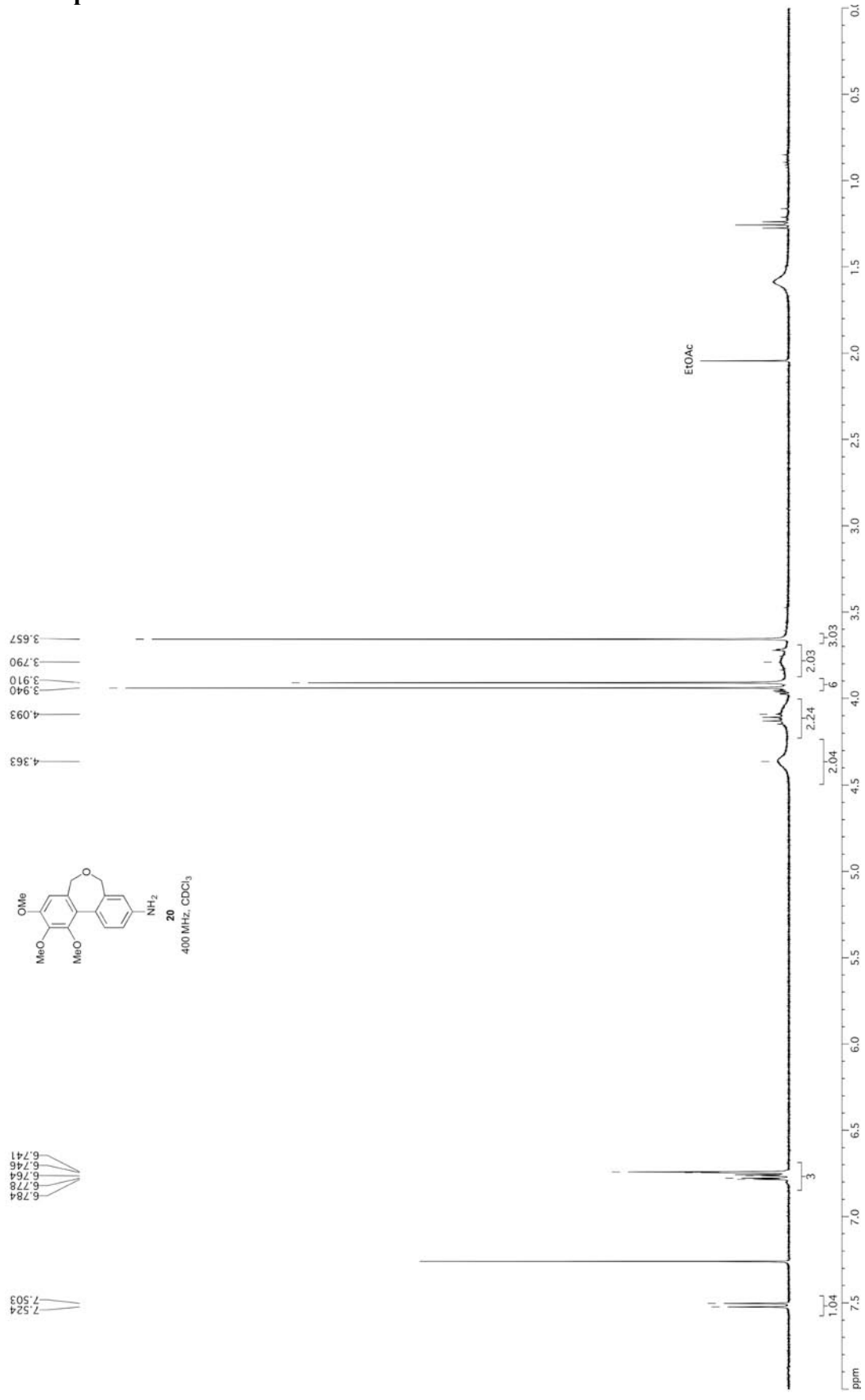

NMR spectrum of 23

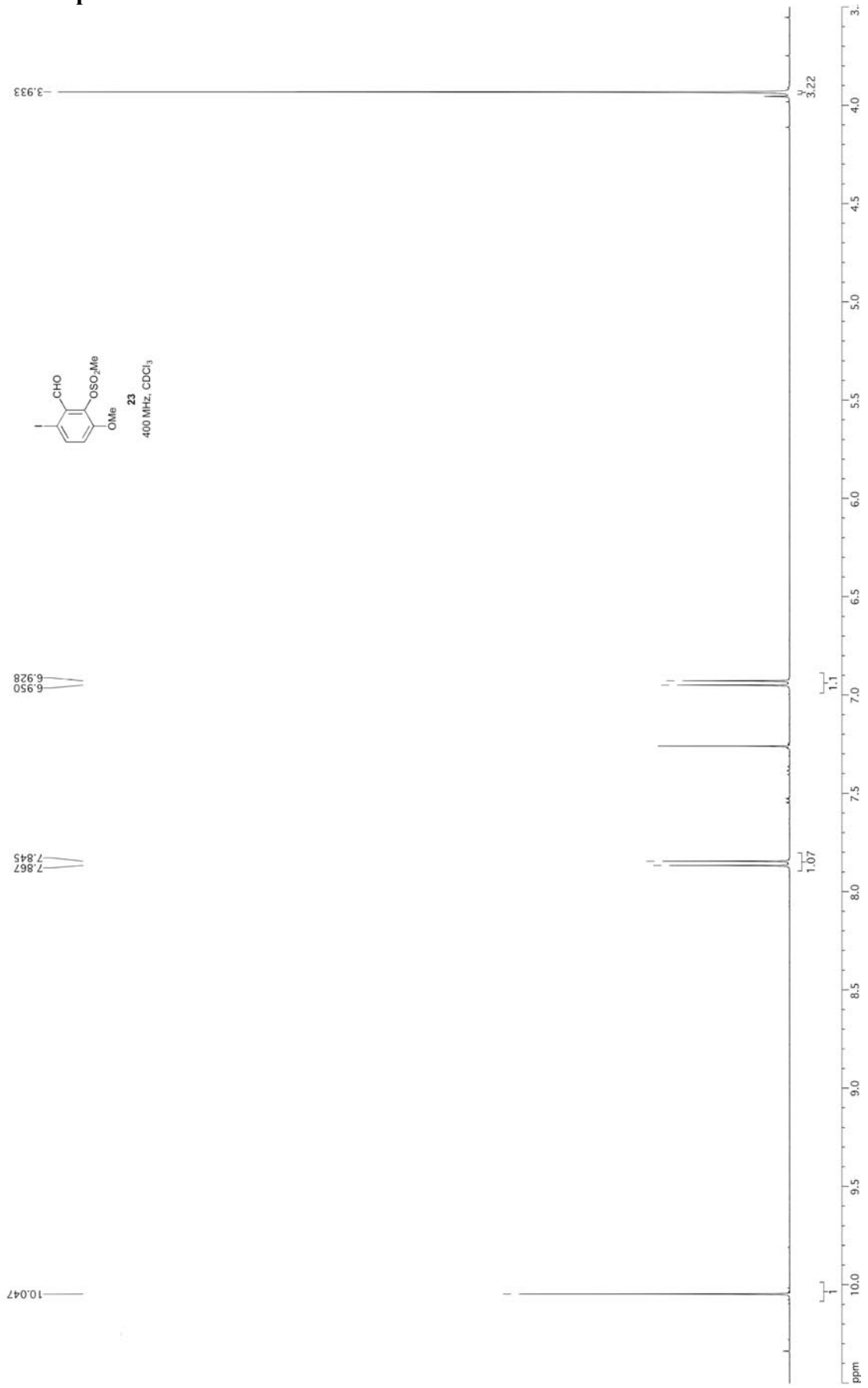

NMR spectrum of 29

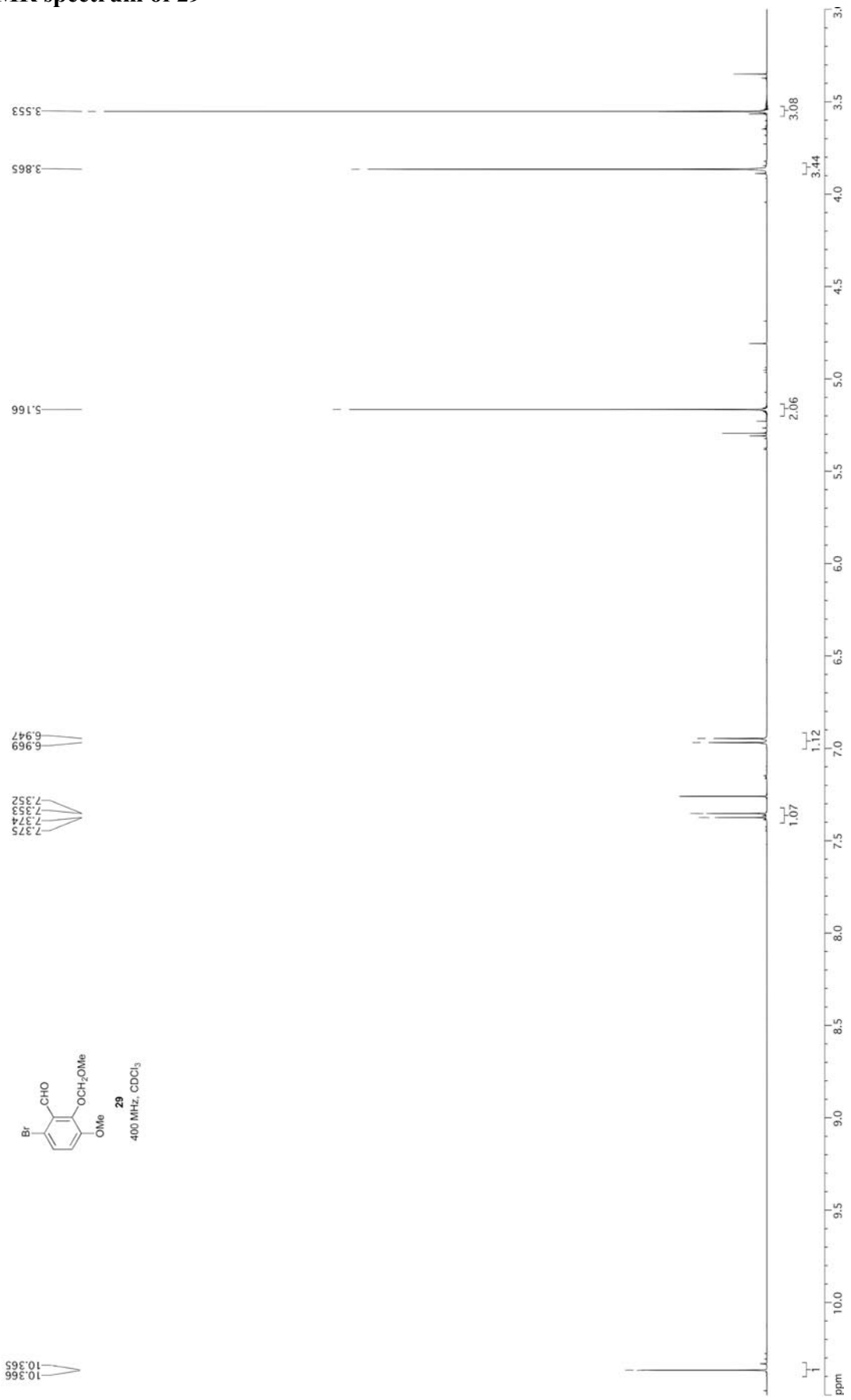

NMR spectrum of 30

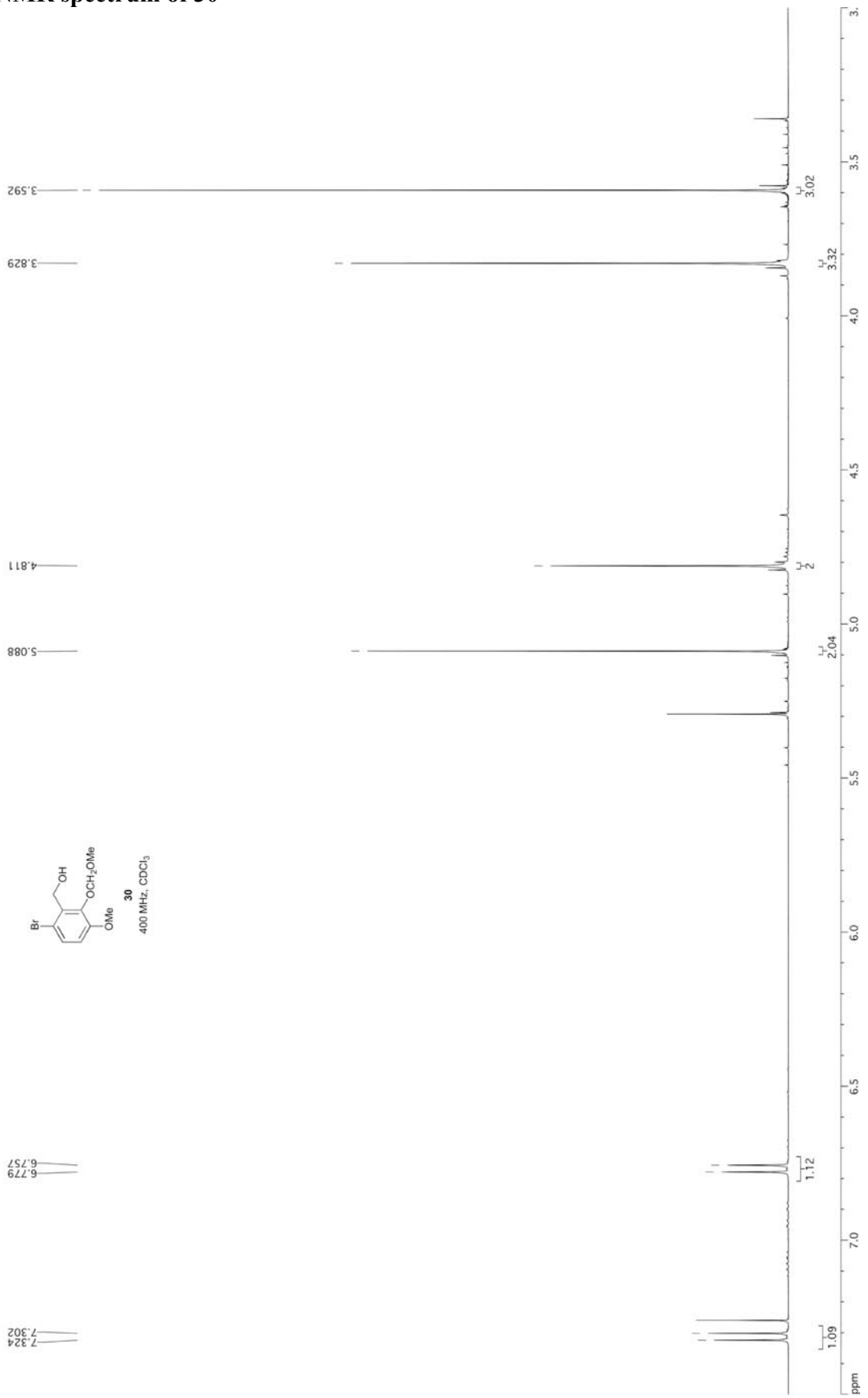

NMR spectrum of 32

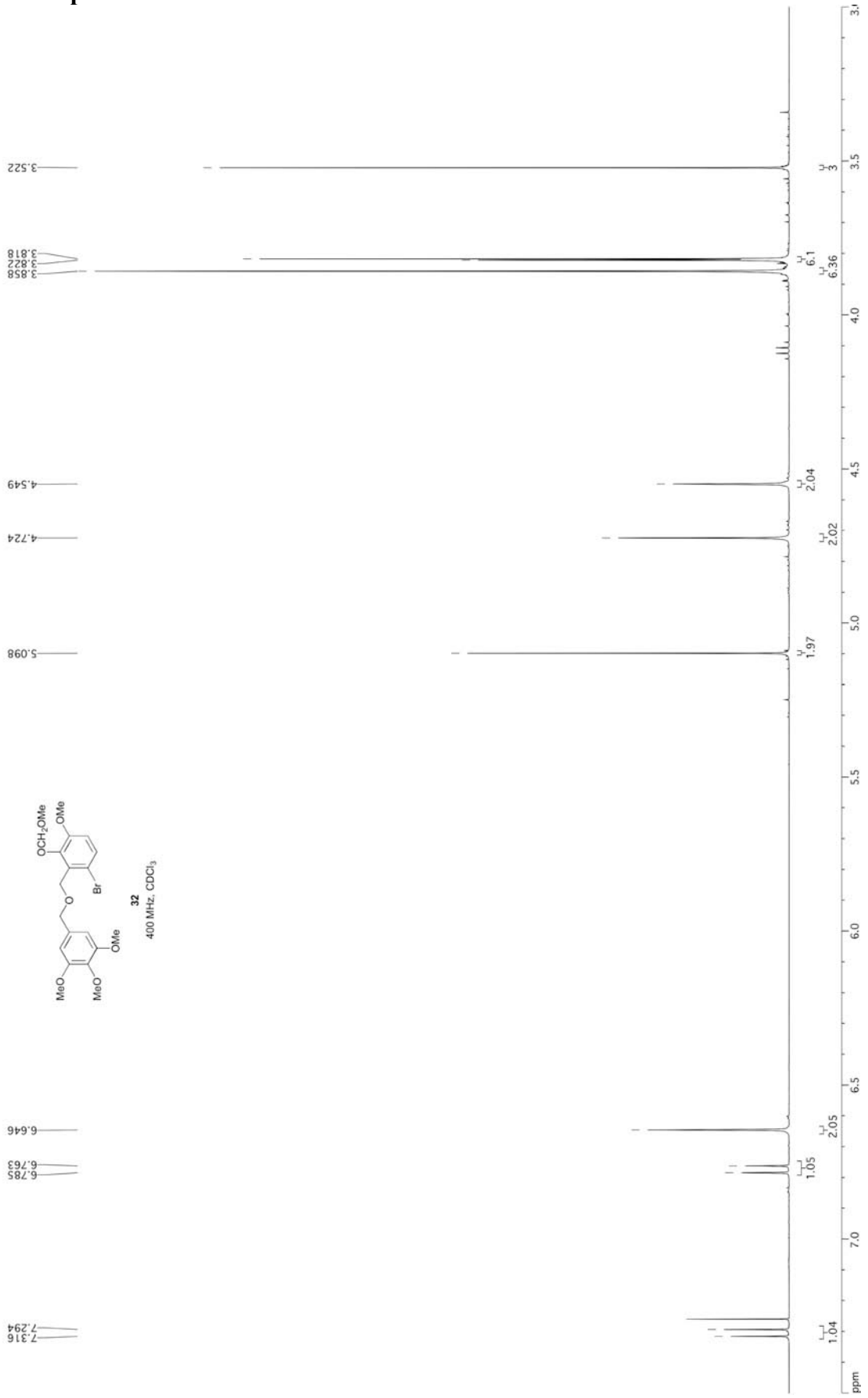

NMR spectrum of 34

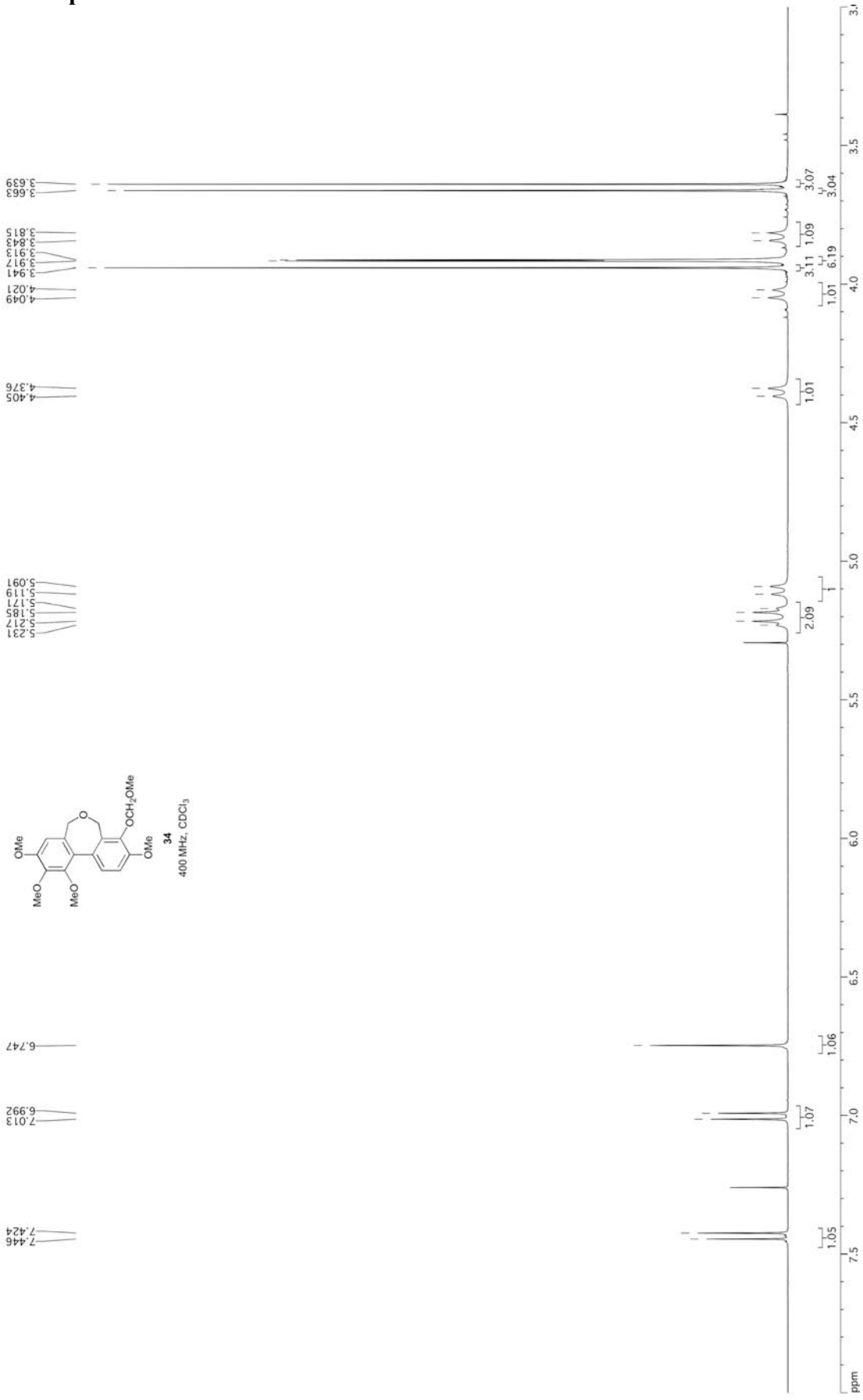

NMR spectrum of 35

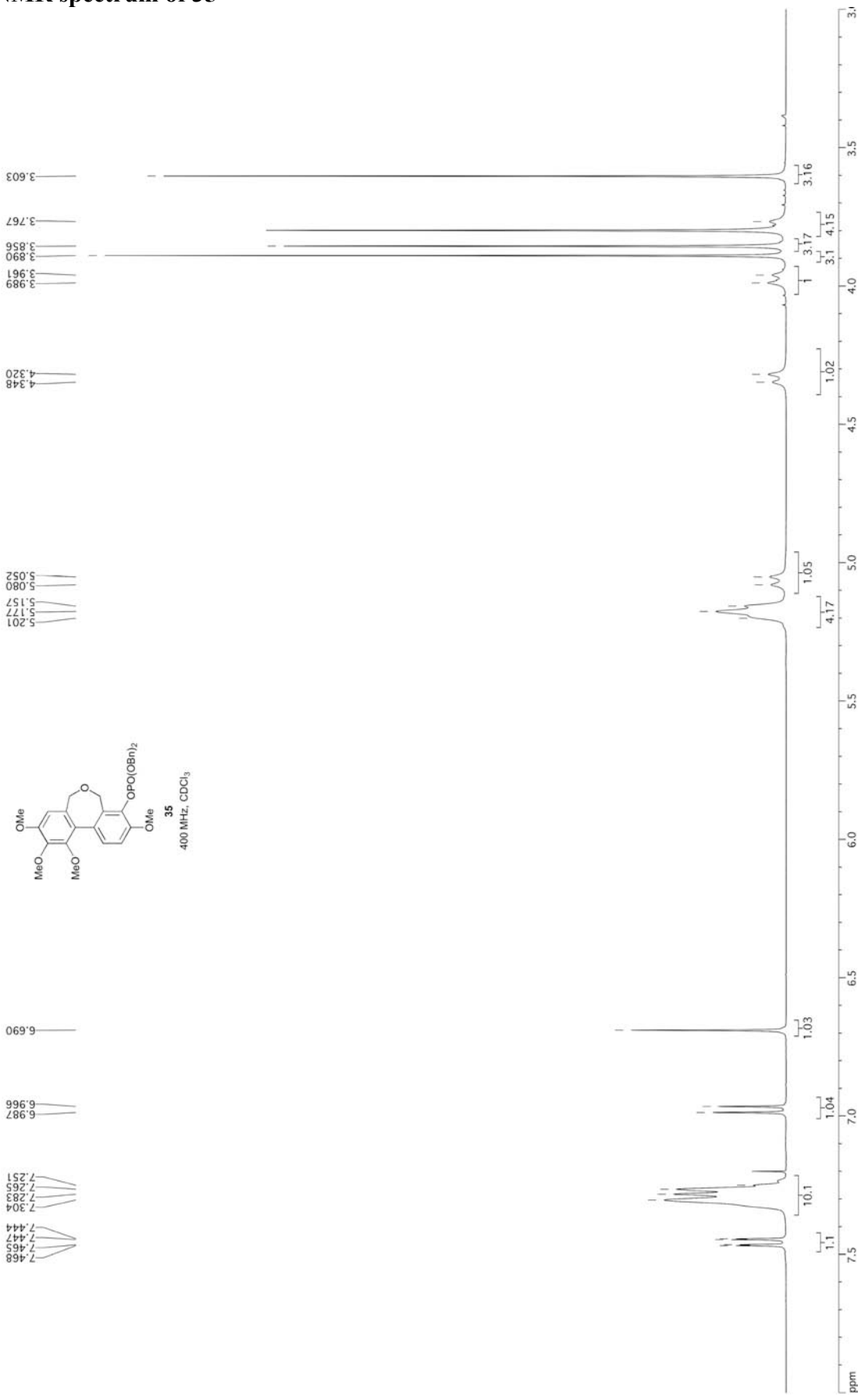

NMR spectrum of 36